QUANTUM YIELDS OF DECOMPOSITION IN THE PHOTOLYTIC OXIDATION OF METHYL MERCAPTAN, DIMETHYL SULPHIDE AND DIMETHYL DISULPHIDE

by

DONALD FREDERICK SHERATON
B.A. Sc., The University of British Columbia, 1969

91

A THESIS SUBMITTED IN PARTIAL FULFILLMENT OF
THE REQUIREMENTS FOR THE DEGREE OF
DOCTOR OF PHILOSOPHY

in

THE FACULTY OF GRADUATE STUDIES
DEPARTMENT OF CHEMICAL ENGINEERING

We accept this thesis as conforming
to the required standard

THE UNIVERSITY OF BRITISH COLUMBIA

June 1979

In presenting this thesis in partial fulfillment of the requirements for an advanced degree at The University of British Columbia, I agree that the Library shall make it freely available for reference and study. I further agree that permission for extensive copying of this thesis for scholarly purposes may be granted by the Head of my department or his representative. It is understood that copying or publication of this thesis for financial gain shall not be allowed without my written permission.

Donald F. Sheraton

Department of Chemical Engineering

The University of British Columbia
Vancouver, Canada

Date: July 3 1979

ABSTRACT

The Kraft pulping process produces vast quantities of sulphide vapours which are released to atmosphere. The major components are methyl mercaptan, hydrogen sulphide, dimethyl sulphide and dimethyl disulphide. The fate of these compounds in the atmosphere and the kinetics of their degradation processes in the atmosphere are useful in the modeling of the environment of areas proximate to Kraft pulp mills. The information may also be useful in developing pollution abatement processes.

The photolytic oxidation of methyl mercaptan, dimethyl sulphide and dimethyl disulphide was studied in a batch photolysis apparatus. Short wavelength ultra-violet light was provided by a deuterium discharge lamp and monitored by a monochromator equipped with an extended response photo-multiplier tube. Sulphide concentrations were determined on a gas chromatograph equipped with a flame photmetric detector having 365 nm sulphur response.

The rate of reaction of methyl mercaptan was found to be a linear function of the photon absorption rate and exhibited a quantum yield of decomposition of 13.9. The methyl mercaptan photo-oxidation rate was found to be unaffected by increased oxygen concentration, decreased atmospheric pressure or the presence of excess sulphur dioxide.

The quantum yield of dimethyl sulphide decomposition was found to be dependent upon atmospheric pressure. A pressure of one atmosphere gave a quantum yield of 4 and the yield increased to 8 at one-quarter atmosphere.

The quantum yield of dimethyl disulphide was found to be 1.9 at atmospheric pressure at a concentration of 7.04×10^{-5} M.

The apparatus was also operated in a configuration which allowed the detection of light emitted at 90° to the path of illumination. A slow developing emission was found for dimethyl sulphide, hydrogen sulphide and sulphur dioxide. Only slight emission was found for methyl mercaptan and dimethyl disulphide.

The emission from dimethyl sulphide was found to be linearily dependent upon the nitrogen pressure of a dry nitrogen atmosphere. The emission is attributed to aerosol formation and is due to the light scattered from particles in the reaction matrix.

TABLE OF CONTENTS

Page

ABSTRACT ii

LIST OF TABLES ix

LIST OF FIGURES x

ACKNOWLEDGMENTS xiii

Chapter

1 INTRODUCTION 1

1.1 General 1

1.2 The Primary Processes 9

1.3 The Hot Radicals Produced and Their Reactions 11

1.4 Reactions of the Hot Hydrogen Atom 13

1.5 Reactions of the Hot Methyl Radical 14

1.6 Reactions of the Methyl Thiyl Radical 17

1.7 Gas Phase Photo-oxidations 20

1.8 Photo-oxidation Reaction Sequence 22

2 EQUIPMENT 23

2.1 General System Description 23

2.2 Daily Procedure for Reaction Analysis 25

2.3 Chemical Sources 27

2.4 The Reaction Cells 29

Chapter Page

2.5 The Vacuum System. 32

2.6 The Deuterium Lamp 32

2.7 The Collimation System 33

2.8 The Reaction Cell Support System 33

2.9 The Emission Configuration 36

2.10 The Monochromator 36

2.11 The Photomultiplier System. 38

2.12 Actinometry 40

2.13 The Make-up of Potassium Ferrioxalate Crystals. 40

2.14 Preparation of the Fe^{+2} Calibration Graph 41

2.15 Deuterium Light Intensity Calibration 43

2.16 The Gravimetric Integration Method. 46

2.17 Gas Chromatography. 47

2.18 Chromatograph Calibration Procedure 51

3 EXPERIMENTAL RESULTS AND DISCUSSION OF PHOTO-OXIDATION OF SULPHIDES 56

3.1 Preliminary Experiments. 56

3.1.1 The Effect of Using Room Air 58

3.1.2 The Effect of Wet Air. 59

3.1.3 The Effect of Pure Oxygen. 59

3.2 Results Involving Quantum Yields of Removal of Sulphides 60

3.2.1 The Quantum Yield of CH_3SH Removal 60

3.2.1.1 The Initiation Reactions 63

3.2.1.2 Reactions involving H Atoms. . . . 65

Chapter | Page

3.2.1.3 Reactions involving the Methyl Thiyl Radical 68

3.2.1.4 Reactions involving the Methoxy and Methyl Peroxy Radicals. . . . 72

3.2.1.5 Reactions involving the Hydrogen Peroxy Radical 73

3.2.1.6 Reactions involving Methyl Radicals. 73

3.2.1.7 Reactions involving Atomic Oxygen Radicals 76

3.2.1.8 Reactions involving Sulphur Monoxide Radicals 77

3.2.1.9 Reactions involving Sulphydryl Radicals. 78

3.2.1.10 Reactions Eliminating Elemental Sulphur 79

3.2.2 The Chain Mechanism 79

3.2.3 The Quantum Yield of CH_3SH Oxidation as as Function of Atmospheric Pressure 82

3.2.4 The Quantum Yield of Dimethyl Sulphide Decomposition 82

3.2.5 The Quantum Yield of Dimethyl Disulphide Decomposition. 84

3.3 Other Experimental Studies. 87

3.3.1 The Effect of Added Sulphur Dioxide 87

3.3.2 A Sulphur Balance for Methyl Mercaptan Oxidation 90

3.3.3 The Quantum Yield of Product Formation for Sulphur Dioxide and Dimethyl Disulphide. 93

3.3.4 The Deposit on the inside Cell Wall 94

4 LIGHT EMISSION FROM SULPHUR-CONTAINING GAS MIXTURES 101

4.1 Observation and Time Dependence 101

Chapter Page

4.2 Possible Mechanisms to Describe the Delay of Emission 106

4.2.1 Flourescence. 106

4.2.2 Delayed Fluorescence. 106

4.2.3 Chemiluminescence 107

4.2.4 Presence of Quenching Impurity. 108

4.2.5 Photochemical Aerosol Formation 113

4.3 Concentration Dependence of Emission. 117

4.4 Pressure Dependence of Emission 117

4.5 The Emission as an Aerosol Scattering Effect. 120

4.5.1 Previous Work 120

4.5.2 Discussion of Results as a Particle Effect. 122

4.5.3 Stability of the Aerosol. 125

4.5.4 Concentration Dependence of the Aerosol . . 128

4.5.5 Pressure Dependence of the Emission 128

4.6 The Number of Particles Formed. 129

4.6.1 Attempted Optical Verficiation of Particle Size and Number. 131

5 CONCLUSIONS 132

BIBLIOGRAPHY. 134

APPENDICES

A CH_3SH Reaction Data. 139

B CH_3SSCH_3 Reaction Data 144

C CH_3SCH_3 Reaction Data. 146

D Sulphur Balance Data 147

Appendix		Page
E	Concentration Dependence of Emission from Dimethyl Sulphide Aerosol.	149
F	Dependence of Intensity of Emission from Dimethyl Sulphide Aerosol upon Atmospheric Pressure of Air.	150
G	Dependence of Intensity of Emission from M_2S Aerosol upon Atmospheric Pressure of Dry Nitrogen	153
H	Estimation of Rate Constant for Reactions (3-7) and (3-15)	155

LIST OF TABLES

Table		Page
1	Bond-Dissociation Energies of Interest	8
2	Energy Excess for Particular Bond Disruptions	9
3	The Energy Distribution of the Fragments of Methyl Mercaptan Photolysis	12
4	Photolysis Products from Long Term Dimethyl Sulphide Photolysis	21
5	Quantum Yields in CH_3SH Photolysis	62
6	Reactions Involved in the Photolytic Oxidation of Methyl Mercaptan	64
7	The Chain Mechanism	80
8	The Effect of Atmospheric Pressure on the Quantum Yield of CH_3SH Decomposition	82
9	The quantum Yield of Dimethyl Sulphide Decomposition v.s. Atmospheric Pressure	84
10	The Quantum Yield of Dimethyl Disulphide Decomposition	84
11	The Effect of Added Sulphur Dioxide	87
12	The Absorption Coefficient for CH_3SH, SO_2, CH_3SCH_3 and CH_3SSCH_3	91
13	A Sulphur Balance, Based on 25 Minutes CH_3SH Oxidation, per ml Reaction Volume	92
14	The Quantum Yields of Product Formation	93

LIST OF FIGURES

Figure		Page
1	The absorption spectrum of methyl mercaptan	2
2	The absorption spectrum of dimethyl disulphide	3
3	The absorption spectrum of dimethyl sulphide	4
4	The absorption spectrum of sulphur dioxide	5
5	Modified Jablonski diagram for photon absorption and subsequent relaxation	6
6	The apparatus as used for reaction	24
7	The reaction cells	20
8	Transmission spectrum of suprasil windows	30
9	The vacuum manifold and emission cell	31
10	Emission spectrum of deuterium light supply measured on EMI 9558 QBM operated at 800 V	34
11	The emission configuration	37
12	Spectral response of EMI 9558 QBM	39
13	Absorbance of Fe^{+2} - 1, 10-phenanthroline complex	42
14	The emission cell and actinometry cells	44
15	Transmission curve of 1.5 cm K_2 Fe $(C_2O_4)_3$ .006 M actinometric solution and of the borosilicate glass filter 1.08 mm	45

Figure		Page
16	The gas chromatograph and flame photometric detector	48
17	Carbopak BHT-100 9 ft. column retention data	49
18	Chromatograph standardizing bottles and Hamilton syringes	52
19	Typical daily calibration curve for CH_3SH.	54
20	SO_2 calibration curve.	55
21	The absorption of polychromatic u-v light by methyl mercaptan.	57
22	Molecular reaction rate of CH_3SH v.s. photon absorption rate.	61
23	The quantum yield of CH_3SCH_3 decomposition v.s. atmospheric pressure	83
24	The quantum yield of dimethyl disulphide decomposition v.s. concentration of sulphide	86
25	Reaction rate CH_3SH decomposition v.s. light absorbance with added SO_2.	88
26	Quantum yield CH_3SH decomposition v.s. % total light absorbed by SO_2.	89
27	Photomicrograph of cell deposit.	97
28	Photomicrograph of cell deposit.	98
29a	Photolysis cell deposit x100 20 kv	99
29b	Photolysis cell deposit x400 20 kv	99
29c	Photolysis cell deposit x1000 10 kv.	99
29d	Sulphur x-ray emission sources superimposed over the cell deposit at x1000 20 kv	99

Figure		Page
30	X-ray emission spectrum of cell wall deposit on end window of "zero" cell	100
31	Emission intensity of sulphur-containing compounds under polychromatic illumination v.s. wavelength.	102
32	The time dependence of CH_3SCH_3 emission	104
33a	The time dependence of SO_2 emission at 240 nm	105
33b	The time dependence of SO_2 emission at 320 nm	105
34	Emission behaviour during interrupted illumination of CH_3SCH_3.	109
35	Emission behaviour during interrupted illumination of SO_2.	110
36	Emission behaviour during interrupted illumination of SO_2.	111
37	The CH_3SCH_3 emission at 370 nm with borosilicate glass filter.	114
38	Emission of CH_3SCH_3 in air v.s. volume CH_3SCH_3 added to emission cell.	116
39	Emission from CH_3SCH_3 at 270 nm in air v.s. atmospheric pressure.	118
40	Emission from CH_3SCH_3 in dry nitrogen v.s. atmospheric pressure.	119
41	Relative importance of absorption and scattering to extinction coefficient for carbon particles	124
42	Extinction curve for the theory of Mie for particles of refractive index m = 1.5	124
43	Behaviour of the 370 nm emission during interrupted short wavelength illumination of SO_2.	127

ACKNOWLEDGMENTS

I would like to thank Dr. F.E. Murray for the opportunity to carry out this research and for his continued support throughout the project.

I would like also to thank Dr. D.G.L. James for his helpful discussions with respect to the mechanism of reaction.

The assistance of the chemical engineering workshop has been a prime factor in the completion of this work. I would like to thank Mr. John Baranowski for his helpful suggestions, Mr. Paddy Jarvis for his machining expertise and Mr. Irwin Szabo for rebuilding the electronics whenever it stopped working.

I wish also to thank Shari Haller for translating a sequence of handwritten hieroglyphics into a readable thesis.

Chapter 1

INTRODUCTION

1.1 General

The Kraft pulping process produces vast amounts of sulphide vapours which are emitted to the atmosphere. These vapours consist mostly of hydrogen sulphide (H_2S), methyl mercaptan (CH_3SH), dimethyl sulphide (CH_3SCH_3) and dimethyl disulphide (CH_3SSCH_3). The gases have odour thresholds of 5, 2, 1, and 16 ppb respectively [42].

The fate of these compounds in the atmosphere and knowledge of their breakdown by atmospheric processes would be useful in modelling the environment of areas proximate to Kraft mills. Such information may also be useful in developing pollution abatement measures.

The major mode of removal of sulphides from the atmosphere appears to be oxidation likely followed by washout through precipitation. The rate of thermal oxidation at atmospheric temperatures is rather low, however, the gases are capable of absorbing ultra-violet light which leads to the oxidation of the sulphur content to sulphur dioxide (SO_2).

Murray and Rayner [32] determined that reduced sulphides in an air atmosphere would oxidize under the influence of ultra-violet light. Short wavelength ultra-violet (2537 Å) was found to be superior to longer wavelength (3600 Å) and the order of reactivities was found to be $CH_3SH > (CH_3)_2S_2 >> (CH_3)_2S$. The oxidation of $(CH_3)_2S$ was found to be very slow.

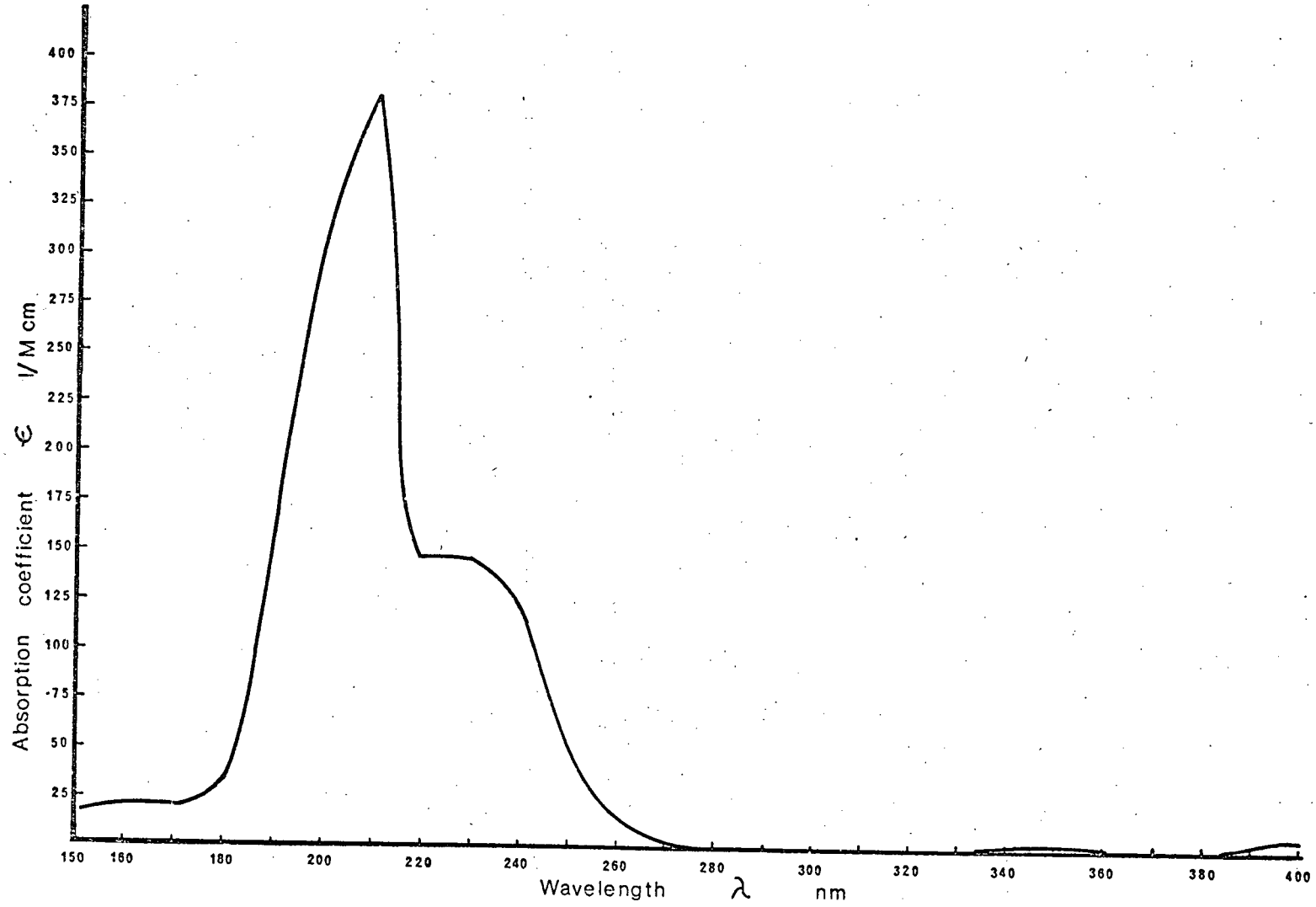

Figure 1. The absorption spectrum of methyl mercaptan.

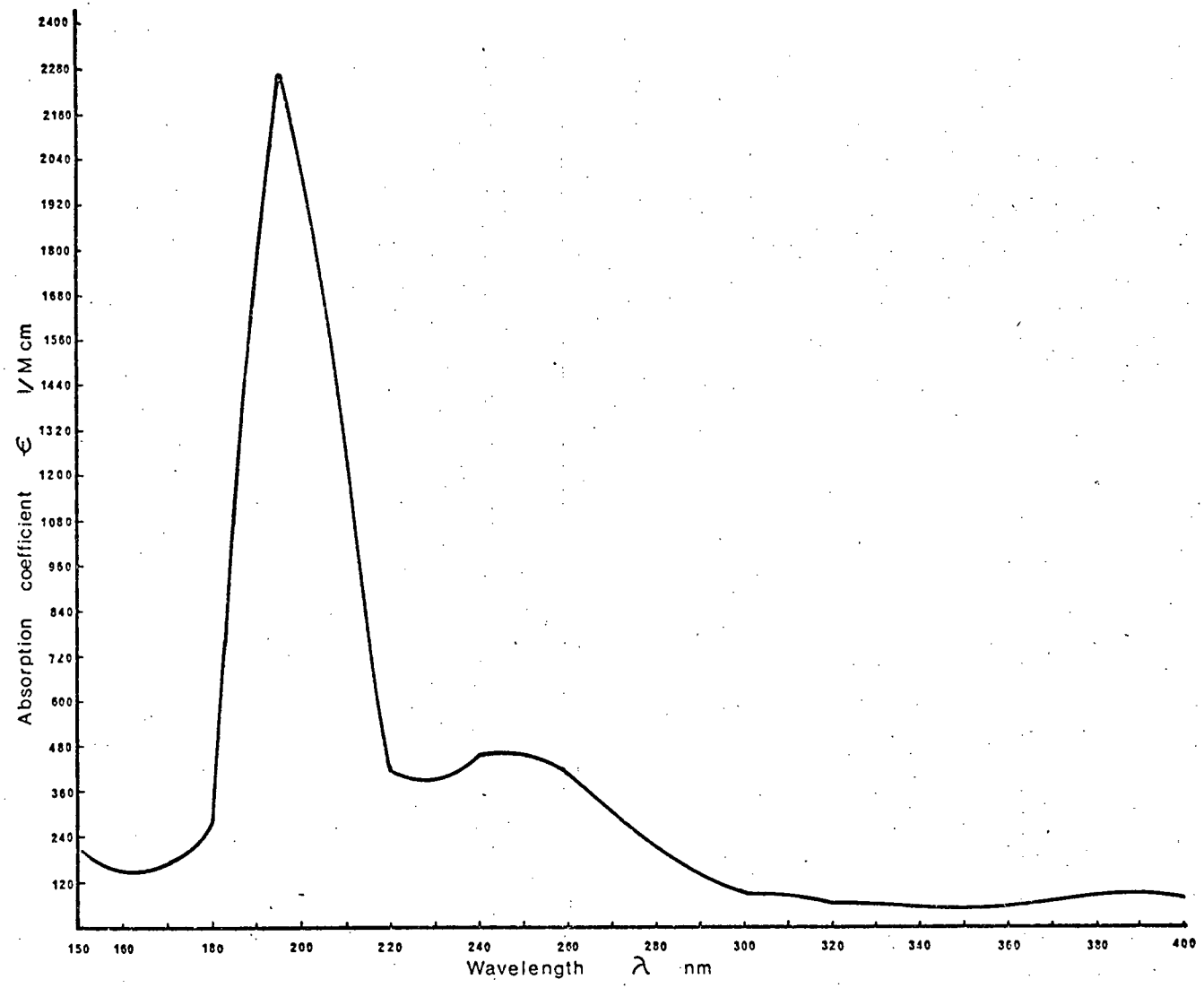

Figure 2. The absorption spectrum of dimethyl disulphide.

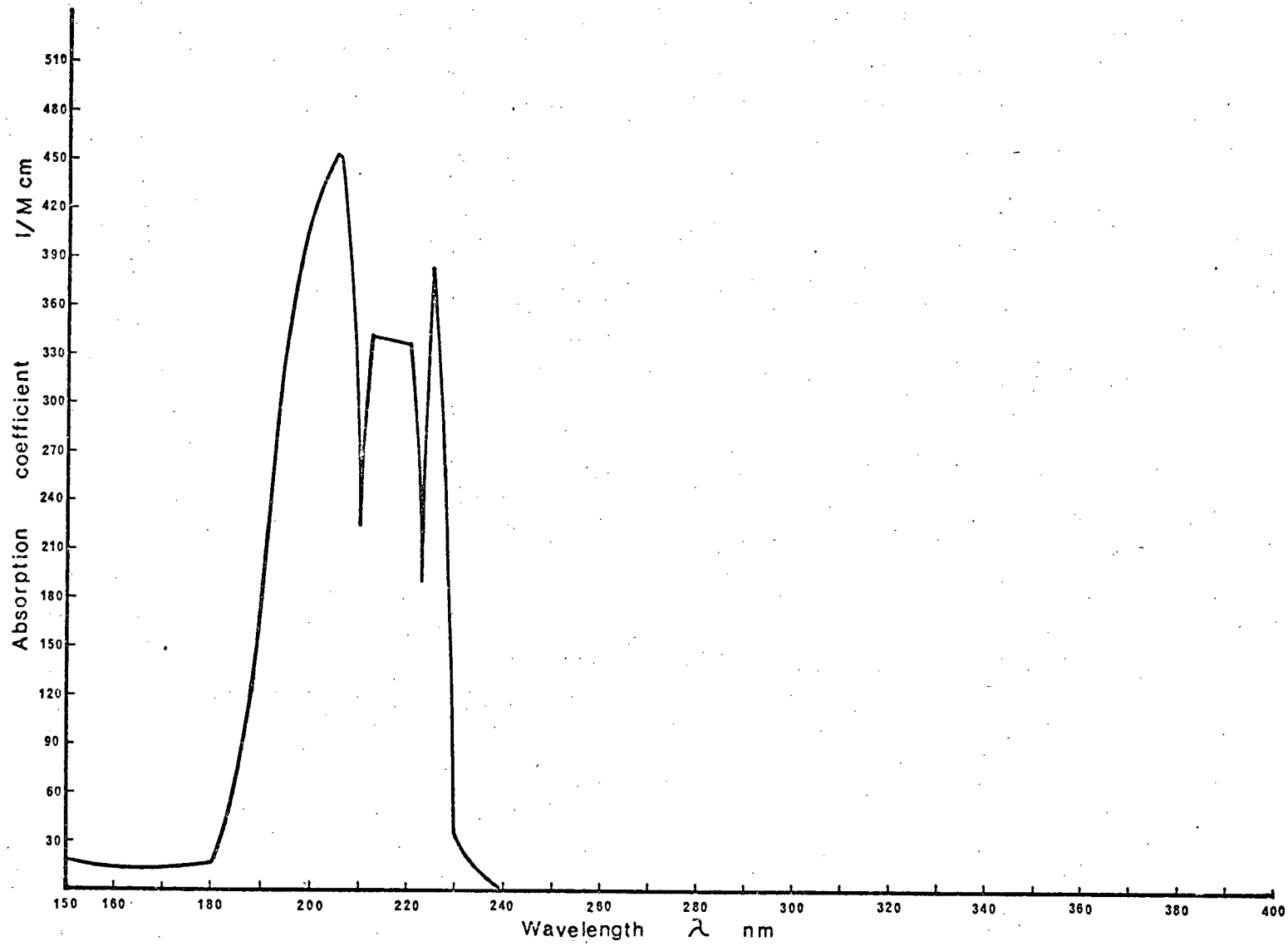

Figure 3. The absorption spectrum of dimethyl sulphide.

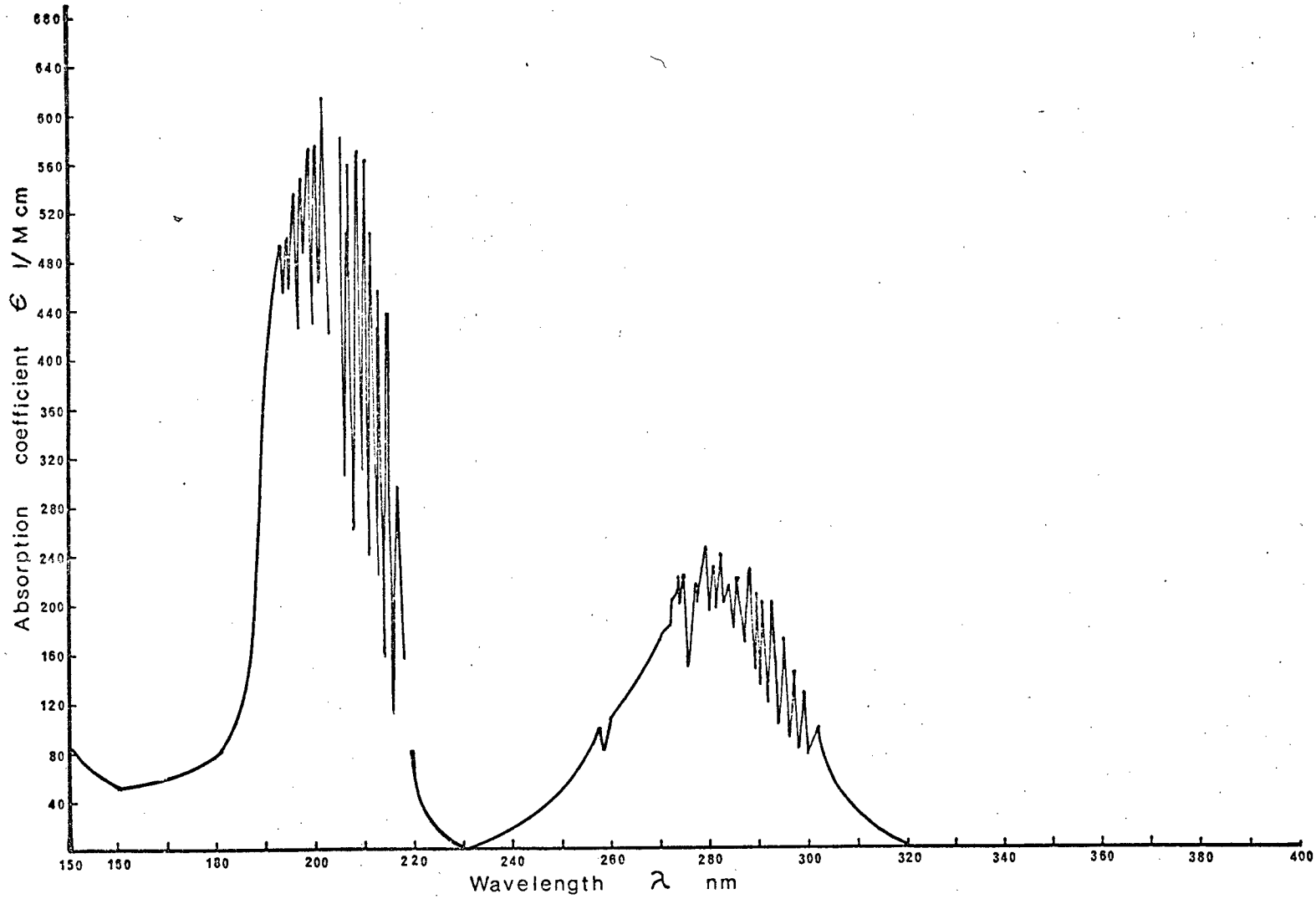

Figure 4. The absorption spectrum of sulphur dioxide.

This work describes the photolytic oxidation of the sulphides from Kraft pulp mill sources and measures the rate of disappearance of the compounds. The quantum yield (ϕ) of removal is measured in terms of the number of molecules removed per photon absorbed.

The gases studied were methyl mercaptan, dimethyl sulphide and dimethyl disulphide. These molecules are capable of absorbing ultra-violet radiation of the wavelengths shown in the absorption spectra (Figures 1, 2, 3). (This work)

The absorption of a quantum of energy results in the electronic excitation of the absorbing molecule. This energy may be distributed about the molecule and if sufficient, cause any one of a number of processes to take place. The normal photochemical processes may be illustrated by a modified Jablonski diagram (Figure 5).

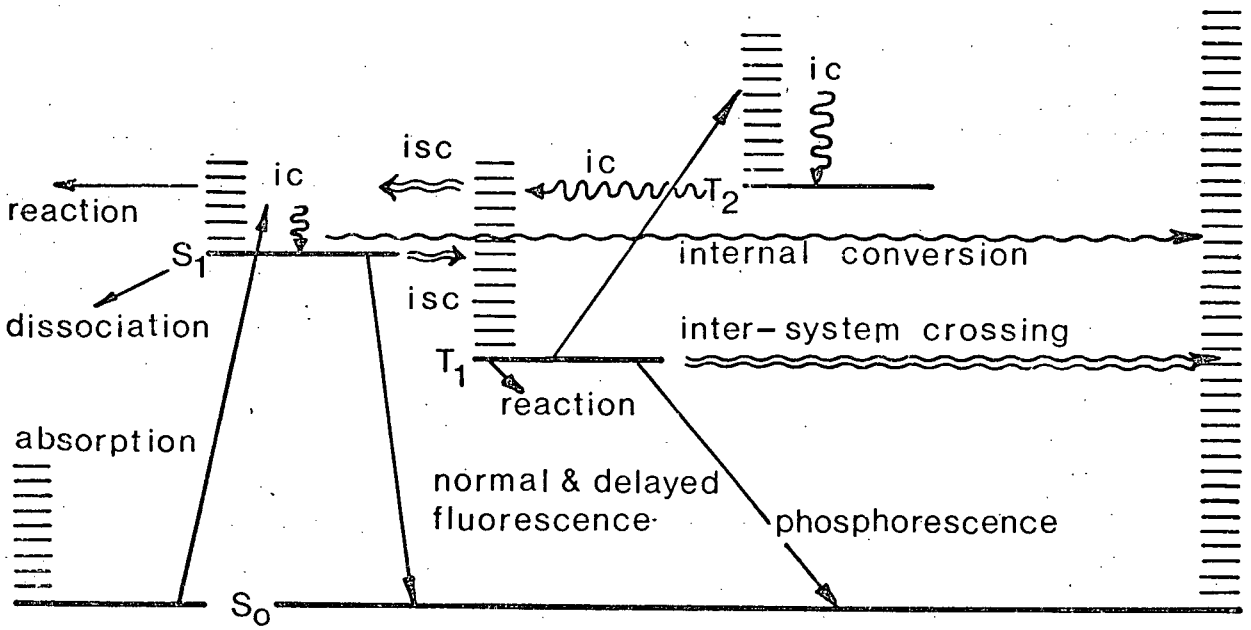

S_0 = singlet ground state
S_1 = singlet first excited manifold
T_1 = triplet first excited manifold
T_2 = second excited triplet manifold

Figure 5. Modified Jablonski diagram for photon absorption and subsequent relaxation.

The singlet state is one in which all molecular electrons are paired with opposite spins such that the multiplicity of the state [(2s + 1) where s is the net spin] is one. The triplet state results from excitation to the electronic state where not all electrons are spin paired, resulting in a net spin of one and a multiplicity of three.

The absorption of a photon will generally raise the molecule to the first excited singlet manifold due to spin conservation. If this state is repulsive, the molecule may dissociate either rapidly or slowly depending upon the degree of repulsion. Reaction of the molecular fragments produced will generally result and chain propagating steps may be involved due to reactive secondary fragments.

Should the excited singlet prove stable, other pathways exist for the removal of energy. The first of these may be reaction directly from the excited molecular singlet state with molecules in the atmosphere. Such reaction may or may not involve chain propagating steps which would result in a quantum yield greater than one.

Another pathway involves the radiationless relaxation to another excited electronic configuration. The excited singlet may internally convert to an upper vibrationally excited level of the ground state singlet. This results in a molecular heating action in which the molecule loses energy by collisional transfer to atmospheric molecules. Such a process is less likely to produce chemical reaction.

The first excited singlet may also undergo inter-system crossing and pass into the first excited triplet manifold. Molecular collision will remove the vibrational excitation and the triplet may remain in the triplet excited state for a relatively long period since return to the singlet ground

state is spin-forbidden. The triplet may react with atmospheric molecules or pick up sufficient kinetic energy through collision to return to the excited singlet state. The excited triplet may return to the ground state singlet by emitting phosphorescent radiation characteristic of the energy difference between the triplet and various vibrational levels of the ground state singlet. Similarly the excited first singlet may return to the ground state by emitting a photon of fluorescence. These transitions involving radiation do not result in chemical reaction and give a quantum yield of reaction of zero.

The incident energy in this study was provided by a deuterium discharge lamp fitted with a Suprasil, leached-sodium silica window. The emission spectrum extended to 1700 Å. The wavelength of most intense absorption for methyl mercaptan was near 2350 Å. Thus, the average energy input, from $E = h\nu$, is 121.6 kcal/einstein of photons absorbed.

The bond energies of the various species involved are listed in Table 1.

Table 1
Bond Dissociations of Interest

D(S-H) = 88.8 kcal/mol	[2, 6, 18]
D(C-S) = 75.2	[5]
D(S-S) = 67	[48]

The energy absorbed exceeds the individual bond energies of the molecules under study. There is, therefore, a high probability that the absorbing molecule will dissociate due to the energy in excess of the bond energy. The species formed will carry off this excess energy in the form

of electronic excitation as well as vibrational and rotational excitation distributed between the fragments. The excess energy for the following dissociations assuming absorption of radiation of average wavelenth 2350 Å is shown in Table 2.

Table 2

Energy Excess for Particular Bond Disruptions

$E_{h\nu}$ - D (CH_3S-H) = 32.8 kcal/mol

$E_{h\nu}$ - D (CH_3-SH) = 46.4 kcal/mol

$E_{h\nu}$ - D (CH_3S-SCH_3) 54.6 kcal/mol

Each of the fragments may carry off electronically excited or hot energy and as such may readily undergo reactions that thermalized species would not. They may exhibit unusually low apparent energies of activation in their reaction with environmental molecules [8,11,12,13,16,17,18,19,21, 22,23,25]. Dzantiev and Shishkov claim [23] that the reactions entered into by such hot atoms or radicals is determined largely by the steric factor. The hot radicals formed enter into reaction with atmospheric molecules and amongst themselves. These reactions may propagate a chain sequence thereby multiplying the effect of initiation. The reaction of the sulphur-containing radical group with oxygen is amongst the chain sequence.

1.2 The Primary Processes

The absorption of a quantum of light predominantly results in the dissociation of the absorbing molecule. The modes of decomposition of the methyl organic sulphides have been found to be the following.

$$CH_3SH + h\nu \rightarrow CH_3S + H \quad (1.1)$$

$$\rightarrow CH_3 + SH \quad (1.2)$$

[1-7,10,11,14-19,21,26-28]

$$CH_3SCH_3 + h\nu \rightarrow CH_3S + CH_3 \quad (1.3)$$

[5,12]

$$CH_3SSCH_3 + h\nu \rightarrow 2\ CH_3S \quad (1.4)$$

[2,5,8,9,20]

Dissociation of the bonds produces radicals which retain some of the excess electronic energy. There are four individual species produced:

1. The methyl thiyl radical (CH_3S)
2. The hydrogen atom (H)
3. The methyl radical (CH_3)
4. The mercaptan radical (SH)

The dissociation products share the excess energy indicated in Table 2. The primary processes above are also accompanied by either chain reactions or other primary processes which produce a yellow, oily deposit which adheres to the reaction cell walls and entrance window [1,12,16,37,41, 42]. This deposit has been found to contain sulphur and is postulated to be a mixture of thioformaldehyde and elemental sulphur [16].

The decomposition of the methyl mercaptan molecule occurs at both the C-S bond and at the S-H bond. Callear and Dickson [5] have found the ratio of S-H to C-S scission at 1950 Å flash photolysis to be 1.7 to 1. This is not what one would expect since the C-S bond is 13.6 kcal/mol lower in energy than the S-H bond. This suggests that the electronically excited

methyl mercaptan molecule (CH_3SH^*) finds a state where the S-H potential energy is repulsive. The molecule is quickly able to adjust by dissociation of the very low mass H atom. The C-S scission will be produced when the system is slower to move to the S-H dissociative state thereby more equally apportioning the energy excess over all molecular bonds before dissociation takes place. The C-S scission has been found to increase at higher incident energies (lower wavelengths). At all wavelengths in the photolysis of pure CH_3SH, the sum of quantum yields of production of H_2 and CH_4 is unity [10, 15,16]. The quantum yield of disappearance of CH_3SH approaches two. The main products in the steady-state photolysis of pure CH_3SH have been found to be CH_4, H_2 and CH_3SSCH_3 [1,3,4,6,7,10,11,15,16]. Dimethyl disulphide photolysis yields CH_3SH although much recombination takes place [8,9]. Dimethyl sulphide has been found to produce CH_3SH and disulphide [12]. It is apparent that subsequent reactions take place due to the molecular fragments produced.

1.3 The Hot Radicals Produced and Their Reactions

The molecular fragments produced by photolysis are highly energetic and initiate secondary reactions which contribute to the chain nature of the reaction sequence. The energy available to the hot H atom has been investigated by Sturm and White [26,27,28].

The photolysis of CH_3SH was carried out in the presence of deuterium (D_2) to investigate the production of HD through deuterium atom abstraction by hot H [26]. The H_2/HD ratio, found by mass spectroscopy, is a function ofthe H atom energy. The H_2/HD ratio is compared to the known H_2/HD ratios

produced from the photolysis of HBr in D_2 at various incident wavelengths. Comparison of the two ratios yields the energy of the H atom dissociated from the photolysed CH_3SH molecule. The H atom energy was found to peak at 2138 Å and to decrease both at longer and shorter wavelengths. The energies of the CH_3SH fragments found are shown in Table 3 [26].

Table 3

The Energy Distribution of the Fragments of CH_3SH Photolysis

λ	E_{max}	E_0	$E_{max}-E_0$
2537	1.05 ± .1 eV 24.21 kcal/mol	.89 eV 20.5 kcal/mol	.16 eV 3.69 kcal/mol
2288	1.57 ± .1 36.2	1.23 28.4	.34 7.84
2138	1.94 ± .1 44.7	1.40 32.3	.54 12.45
1849	2.83 ± .1 65.3	1.13 26.1	1.70 39.2

λ = wavelength incident

E_{max} = (light energy)-(bond energy)

E_0 = H atom energy

E_m-E_0= CH_3S energy

The hot H atom appears to have a maximum energy at an incident wavelength of about 2138 Å whereafter the C-S scission appears to increase in probability. The energies in both fragments are sufficient to produce further reactions.

The hot H may react with CH_3SH to abstract the sulphydryl H atom. This process appears temperature independent, thus having no apparent Arrhenius

activation energy [10]. Conversely, H atom abstraction from CH_3SCH_3 by hot CH_3S radicals was found to have an activation energy of 5.4 kcal/mol [12]. The activation energy for H atom abstraction from CH_3SSCH_3 by hot CH_3S radicals was found to be 1.5 kcal/mol [8]. The activation energy for H atom abstraction from CH_3SCH_3 by hot CH_3 radicals was found to be 2.3 kcal/mol [12].

1.4 Reactions of the Hot Hydrogen Atom

The hot H atom can possess up to 32 kcal/mol of dissociation excess energy at 2138 Å. The major reaction of the hot H atom in the presence of CH_3SH is the abstraction of the sulphydryl hydrogen atom to form H_2 and the methyl thiyl radical [3,6,10,11,15,17,18].

$$H + CH_3SH \rightarrow H_2 + CH_3S \qquad (1.5)$$

The hot H does not attack the methyl hydrogen atoms. Inaba and Darwent, in the photolysis of pure CH_3SD at 2537 Å found only D_2 and CH_3D as products [3]. This suggests a reaction sequence as shown below.

$$CH_3SD + h\nu \rightarrow CH_3S + D$$

$$D + CH_3SD \rightarrow CH_3S + D_2$$

and

$$CH_3SD + h\nu \rightarrow CH_3 + SD$$

$$CH_3 + CH_3SD \rightarrow CH_3D + CH_3S$$

No H_2 and no HD were found as products. The reaction of the H atom terminates the reactions of that radical. The CH_3S radical formed will propagate further

chain reactions from the original absorbed quantum. The original hot H may become quenched and undergo reactions of a thermal nature. The order of quenching efficiency for various gases has been found to be:

$$He > CO_2 > N_2 > C_2H_6 > C_2D_6 \quad [21]$$

Argon does not affect the quantum yield of H_2 or CH_4 and thus is not a quencher for hot H atoms.

In the presence of an appreciable quantity of oxygen the hydrogen atom will oxidize to form the hydrogen peroxy radical

$$H + O_2 \rightarrow HOO \qquad (1.6)$$

Available rate data will be discussed later in the mechanism section, however, the oxidation reaction appears to proceed at a rate somewhere between 1/3 and three times the rate of hydrogen abstraction from CH_3SH.

The hydrogen peroxy radical is capable of continuing the chain reaction by abstracting the sulphydryl hydrogen atom from CH_3SH to form hydrogen peroxide.

$$HOO + CH_3SH \rightarrow HOOH + CH_3S \qquad (1.7)$$

The chain is further continued by reactions involving the methyl thiyl radical.

1.5 Reactions of the Hot Methyl Radical

Hot methyl radicals have been found to abstract methyl hydrogen atoms from CH_3SCH_3 with an apparent activation energy of 2.3 kcal/mol [12].

$$CH_3 + CH_3SCH_3 \rightarrow CH_4 + CH_2SCH_3 \qquad (1.8)$$

They also undoubtedly abstract sulphydryl hydrogen from CH_3SH.

$$CH_3 + CH_3SH \rightarrow CH_4 + CH_3S \qquad (1.9)$$

The rate constant for reaction (1.9) has been found to be 1.8×10^4 $M^{-1}\ s^{-1}$ [54]. This rate is slower than other reactions which may occur to a methyl radical in an oxygen-containing atmosphere. A more complete discussion of rates of competing reactions will be found in Chapter 3.

In the presence of an appreciable concentration of oxygen, the major reaction of a methyl group is to oxidize to the methyl peroxy radical [61].

$$CH_3 + O_2 + M \rightarrow CH_3OO + M$$
$$k = 3.1 \times 10^8 \quad M^{-1}\ s^{-1} \qquad (1.10)$$

Adachi and James [61] developed a computer simulation of a methyl radical in an oxygen-containing atmosphere. The mechanism of mutual interaction of the methyl peroxy radical resulted in the following products:

$$2\ CH_3OO \rightarrow 2\ CH_3O + O_2$$
$$\rightarrow CH_3OH + HCHO + O_2$$
$$\rightarrow CH_3OOCH_3 + O_2$$
$$k = 3.5 \times 10^8 \quad M^{-1}s^{-1} \qquad (1.11)$$

The most notable product of this interaction is the production of the methoxy radical CH_3O.

The methoxy radical is a reactive oxidizing species which is capable of reacting with itself or with reduced species. In an oxygen-containing atmosphere, the major product of CH_3O reactions with O_2 is the formation of the hydrogen peroxy radical.

$$CH_3O + O_2 \rightarrow HCHO + HOO$$
$$k = 4 \times 10^5 \quad M^{-1}\ s^{-1} \qquad (1.12)$$

The hydrogen peroxy radical may react with reduced species or may mutually interact.

$$2\ HOO \rightarrow HOOH + O_2$$
$$k = 2 \times 10^9 \quad M^{-1}\ s^{-1} \quad [61] \qquad (1.13)$$

The Adachi-James program was employed to estimate the concentrations of CH_3OO, CH_3O and HOO in reactive atmospheres containing varying amounts of oxygen. A high O_2 concentration was chosen as 3.23×10^{-2} M (78% by vol.). The low O_2 concentration was chosen as 1×10^{-3} M (2.44% by vol.). At the high O_2 concentration 99.97% of the available CH_3 radicals form CH_3OO within 50 μs after the photo flash. The remaining 0.03% form CH_3O radicals. During the high concentration simulation the HOO concentration eventually reaches 12% of the original CH_3OO concentration. At low concentrations of O_2 96.9% of the available CH_3 radicals oxidize to CH_3OO. Only 3.1% appear as CH_3O radicals. The ultimate concentration of HOO radicals reached only 3% of the CH_3OO concentration.

Thus for free CH_3 radicals in an oxygen containing atmosphere, the predominant reaction is the formation of methyl peroxy radicals. These oxidizing species will further react with reduced species in the reaction matrix.

1.6 Reactions of the Methyl Thiyl Radical

The methyl thiyl group may possess between 3.69 kcal/mol (2537 Å) and 39.2 kcal/mol (1849 Å) excess energy after bond scission. In an oxygen-containing atmosphere the methyl thiyl radical rapidly reacts with the oxygen. Flash photolysis studies by Callear and Dickson [5] showed that 100 torr O_2 suppressed the 2185 Å absorption band attributed to the CH_3S radical. The 2000 Å flash persisted 20 μs to half intensity and the first transient spectra were recorded at 5 μs delay. The elimination of the CH_3S absorption spectrum indicates very rapid reaction with O_2.

Sulphur dioxide (SO_2) is not the initial product of the sulphur oxidation [35,36,38,40). McGarvey and McGrath photolysed hydrogen sulphide in the presence of a 3:1 ratio of O_2:H_2S and observed the very rapid appearance of SO absorption bands. The SO bands were slowly replaced by SO_2 absorption bands. The appearance of the SO bands coincided with a broad band absorption continuum extending from 2000 Å to 2500 Å. The band appeared 50 μs after flash initiation and had disappeared by 1 ms. After 1 ms the SO bands were still present although weakened and the SO_2 bands were starting to become apparent.

A flash photolysis of pure SO_2 revealed a group of bands from 1780 Å to 1840 Å. The group also appeared in O_2/H_2S flashes. The nature of the SO_2 absorption spectrum suggested the appearance of an isomeric form

of SO_2 [35]. The isomeric form was suggested since an electronically excited form would be expected to have a lifetime under 10^{-8} s and a vibrationally excited form would be expected to deactivate by collision faster than was indicated by the observed bands. The isomer probably forms from SO and rearranges to SO_2. Norrish and Zelenberg [40] found the early formation of S_2O_2 (the stable form of SO below 300°C)to precede the formation of SO_2 in the flash oxidation of H_2S.

Thus the oxidation sequence seems to follow a pattern such as

$$CH_3S + O_2 \rightarrow CH_3O + SO$$

$$\Delta H_f = -25.3 \text{ kcal/mol} \qquad (1.14)$$

$$CH_3S + O \rightarrow CH_3 + SO$$

$$\Delta H_f = -53.6 \text{ kcal/mol} \qquad (1.15)$$

This initial rapid oxidation will be followed by the slower oxidation:

$$SO + O_2 \rightarrow SO_2 + O \qquad (1.16)$$

$$SO + O \rightarrow SO_2 \qquad (1.17)$$

Methyl thiyl radicals are also able to undergo other reactions. The main fate of CH_3S radicals produced in non-oxidative atmospheres is combination to form dimethyl disulphide [5,8,9]

$$2\ CH_3S \rightarrow CH_3SSCH_3 \qquad (1.18)$$

Disulphide molecules in photolysis can directly expel elemental sulphur [5]

$$CH_3SSCH_3 + h\nu \rightarrow S_2 + 2\ CH_3 \qquad (1.19)$$

The CH_3S radical is sufficiently reactive to abstract the methyl hydrogen atom of CH_3SSCH_3 to form CH_3SH during disulphide photolyses [8].

$$CH_3S + CH_3SSCH_3 \rightarrow CH_3SH + CH_2SSCH_3 \qquad (1.20)$$

The addition of nitric oxide (NO) in gas phase photolyses scavenges the CH_3S radical to produce methyl thionitrite (CH_3SNO) [8]. The addition of NO to pure disulphide photolysis resulted in a CH_3SNO production rate twenty times that of CH_3SH [8]. This indicates the hydrogen abstraction rate to be much less favoured than is recombination. The disulphide formation is a main chain terminator and disulphide is present as a reaction product even at oxygen pressures of 150 torr. The methyl hydrogen abstraction does not take place in liquid photolyses possibly due to rapid collisional cooling of the CH_3S [9].

The photolysis of liquid mixtures of diethyl disulphide and dimethyl disulphide gave a mixed methyl-ethyl disulphide cross-product [9]. The rate of formation of the cross-product indicated a production quantum yield of 330 [9]. This indicates an attack by the methyl or ethyl thiyl radical upon the S-S bond with an average chain length of 165. In the case of CH_3S attack upon pure CH_3SSCH_3, the exchange is not detectable.

The methyl thiyl radical trap, NO, has been found to suppress the recombination of CH_3S to disulphide [7]. Nitric oxide also stops the CH_3SH formation in disulphide photolysis by trapping the CH_3S as CH_3SNO.

Photolysis of CH_3SH in the presence of NO produces very long chain lengths probably involving reactions of H and NO in the chain propagation [10]. No dark reaction was found between CH_3SH and NO. The photolytic quantum yield of H_2 formation was decreased at NO pressures above 20 torr indicating participation of hot H in reactions other than those forming H_2. The H_2 yield was unaffected at pressures below 20 torr.

The rate of appearance of CH_3SNO (8.02×10^{17} molecules/min) at the absorbed energy (9.45×10^{15} phot/min) indicates a quantum yield of 84.9 at NO pressures of 20 torr. This is a long chain length. Increased concentrations of NO up to 125 torr caused a reaction sequence which continued for 35 minutes after termination of radiation. This confirms a long chain length and CH_3SNO production rates indicate a quantum yield of 339 [10]. The hot H is involved in the chain length and Steer and Knight suggest participation of a HNO chain such as the following:

$$H + NO \rightarrow HNO \qquad (1.21)$$

$$HNO + CH_3SH \rightarrow CH_3SNO + H_2 \qquad (1.22)$$

Steer and Knight were unable to demonstrate a maximum in CH_3SNO production rate with added NO. The rate is not due to NO absorption since it is largely transparent at wavelengths greater than 1900 Å [49].

1.7 Gas Phase Photooxidations

Murray and Rayner [32] determined that photo-oxidation of sulphides took place under ultra-violet light. Sulphur dioxide was a major product.

Short wavelength (2537 Å) ultra-violet was superior to longer wavelength (3600 Å) and the order of reactivities, uncorrected for absorption, was found to be CH_3SH > CH_3SSCH_3 >> CH_3SCH_3.

R.W. Murray and S.L.J. Indall [33] found dialkyl disulphides to oxidize in O_2 saturated solution under the influence of methylene blue sensitizer.

Graham and Sie [34], however, found CH_3SH to undergo very slow photooxidation to produce SO_2 with a quantum yield about 3 to 6 x 10^{-5}. This is in conflict with other groups noting the rapid appearance of SO and SO_2 spectra upon flash photolysis in air [5,32,35,37,38,40] and with those groups noting rapid appearance of SO_2 as product.

Bentley, Douglass and Lacadie [37] photolysed CH_3SCH_3 for six hours under high intensity mercury arc (2537 Å) in the presence of oxygen. Many reaction products were found containing both methyl group photoproducts and containing the methyl thiyl group.

Table 4

Photolysis Products from Long Term CH_3SCH_3 Photolysis

1.	dimethyl sulphoxide	CH_3SOCH_3
2.	dimethyl sulphone	$CH_3SO_2CH_3$
3.	methane sulphonic acid	CH_3SO_3H
4.	dimethyl disulphide	CH_3SSCH_3
5.	methane methanethiol sulphonate	$CH_3SO_2SCH_3$
6.	sulphur dioxide	SO_2
7.	sulphur trioxide	SO_3
8.	methanol	CH_3OH
9.	formaldehyde	HCHO
10.	formic acid	HCO_2H
11.	methyl formate	HCO_2CH_3

An aerosol product was noticed shortly after the start of the reaction. This was felt to involve the water content of the air (.43 mg H_2O/ℓ) and the condensible photoproducts [37].

1.8 Photo Oxidation Reaction Sequence

In view of the previously mentioned reactions, the sequence of reactions of methyl mercaptan upon photo oxidation is probably the following.

$CH_3SH + h\nu \rightarrow CH_3S + H$	1-1
$\rightarrow CH_3 + SH$	1-2
$H + O_2 \rightarrow HOO$	1-6
$CH_3S + O_2 \rightarrow CH_3O + SO$	1-14
$CH_3S + O \rightarrow CH_3 + SO$	1-15
$CH_3 + O_2 + M \rightarrow CH_3OO + M$	1-10
$CH_3OO + C\ H_3SH \rightarrow CH_3OOH + CH_3S$	1-23
$CH_3O + CH_3SH \rightarrow CH_3OH + CH_3S$	1-24
$CH_3O + O_2 \rightarrow HCHO + HOO$	1-12
$HOO + CH_3SH \rightarrow HOOH + CH_3S$	1-7
$SO + O_2 \rightarrow SO_2 + O$	1-16
$SO + O \rightarrow SO_2$	1-17
$CH_3S + CH_3S \rightarrow CH_3SSCH_3$	1-18
$CH_3S + CH_3O \rightarrow CH_3SOCH_3$	1-25
$CH_3S + CH_3OO \rightarrow CH_3SOOCH_3$	1-26

A more detailed consideration of the reaction mechanism is to be found in the results and discussion.

Chapter 2

EQUIPMENT

2.1 General System Description

The reactions were performed in a dry-nitrogen-swept, parallel-ended, grease-free tubular reactor. The system was designed to transmit light to 180 nm. Illumination was provided by a medium pressure deuterium discharge lamp collimated by two quartz lenses. The polychromatic illumination passed through a teflon-sealed 10 cm pyrex reaction vessel fitted with suprasil windows. Transmitted light was analysed by a Jarrell-Ash 0.25 meter Ebert-type monochromator. The 0.25 nm bandwidth exit beam was measured by an EMI 9558 QBM photomultiplier tube and recorded on a chart recorder. The reactor support system could be manipulated to insert various reactor cells without altering the optical alignment of the system.

The monochromator and photomultiplier assembly could also be brought perpendicular to the optical path for use as an emission detection system. A photograph of the apparatus in reaction configuration is shown in Figure 6. Gas concentrations were monitored by a gas chromatograph equipped with a flame photometric detector. The chromatograph was calibrated daily.

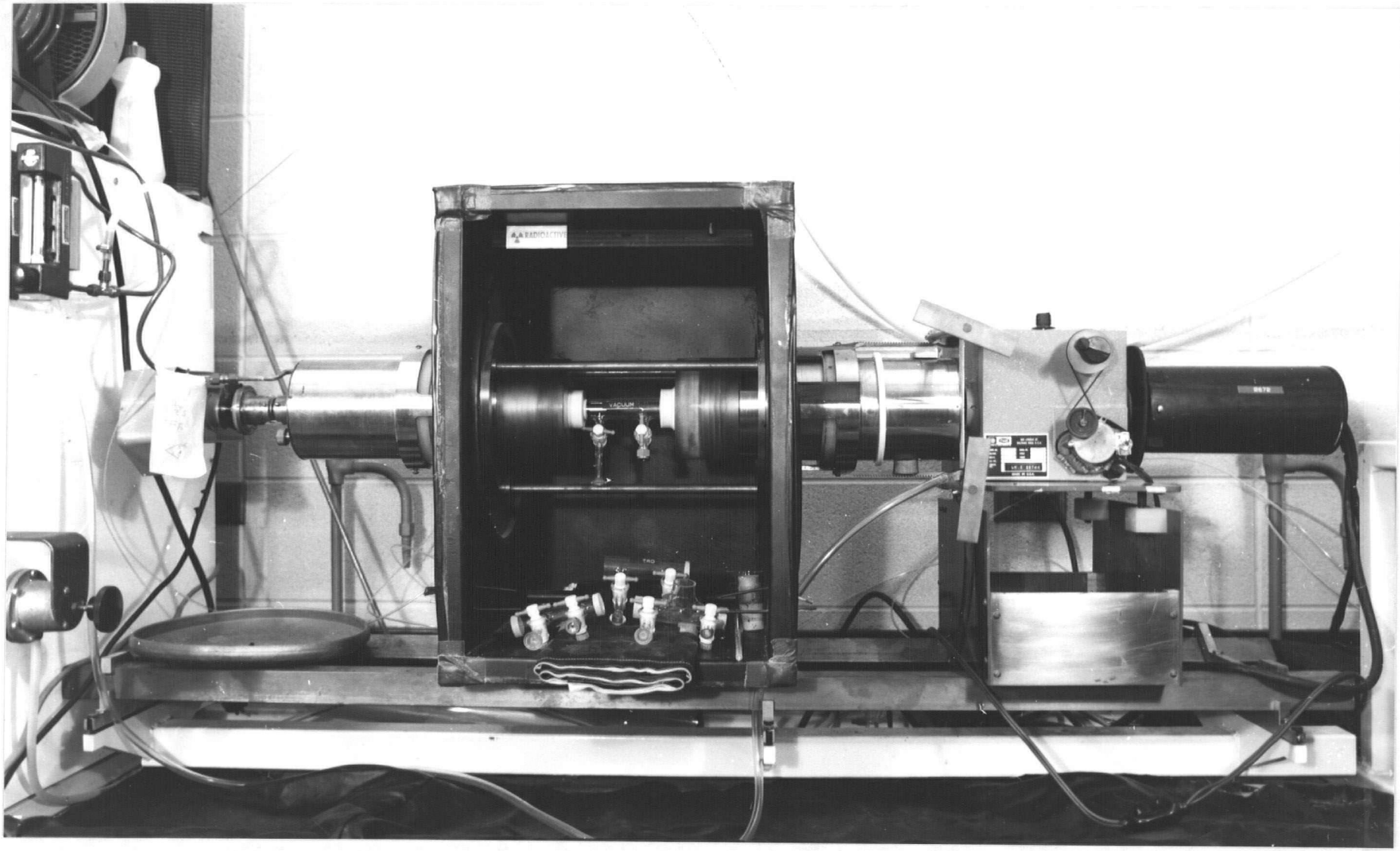

Figure 6. The apparatus as used for reaction.

2.2 Daily Procedure for Reaction Analysis

The daily process was begun by measuring the flow rate to the gas chromatograph of helium carrier gas, and air, oxygen and hydrogen flow to the flame photometric detector. Flow rates were checked using a soap-bubble gas flow meter and when correctly adjusted to 20, 20, 20 and 250 ml/min respectively, the photo-detector flame was ignited. The photo-detector was allowed to warm up for at least one hour. The deuterium lamp was ignited and allowed at least 30 minutes to reach thermal equilibrium before the first spectra were recorded. The reaction cells were swept with bottled compressed air passed through a glass tube filled with Drierite drying compound. Before entering the cell, the gas was filtered through a Whatman gama 12 grade 10, 1.0 micron particle filter which permitted passage of only .0001% of 0.6μ particles. This prevented drying compound and other foreign matter from entering the reaction cells. The optical pathway was swept with dry nitrogen at a flow rate of 1.0 cubic foot per hour (CFH) for a minimum of 12 hours before the start of a reaction sequence and this flow was continuously maintained during the series of runs.

The sample cells, filled with air, were placed in the optical path and exposed to polychromatic radiation. A transmission spectrum from 150 nm to 500 nm was recorded by the monochromator coupled to a chart recorder in order to measure the amount of light entering the reaction vessel. The area under the intensity-wavelength curve was related to the calibrated area measured with the same clear cell during the actinometric studies in order to determine the photometric energy input. Input energy curves were run for each cell each day and a continuous profile was maintained on the transmission of all cells.

The cells were filled from Matheson compressed gas cylinders using Hamilton teflon-ended "Gas-tite" syringes. Liquid samples of dimethyl sulphide and dimethyl disulphide were maintained in glass bottles and the reaction cells were filled with liquid using Hamilton micro-litre liquid syringes. The filled reaction cells were allowed to sit for one-half hour to equilibrate. The reaction cells were sampled by injecting 0.25 ml air and flushing the syringe numerous times before removing a 0.25 ml gas sample and analysing on the gas chromatograph. A 0.25 ml sample was used for many runs however higher concentration runs required the use of 0.1 ml sample volumes in order to stay in the region of maximum sensitivity of the gas chromatograph calibration curve.

The calibration of the gas chromatograph was carried out simultaneously with the filling and analysing of the reaction gas. This calibration was performed each day in order to more accurately measure the sensitivity to CH_3SH. Calibration consisted of measuring four concentrations of each sulphide in four known sample-bottle volumes. The average of three reproduceable injection peaks was taken as the best value for each concentration.

The calibrated reaction cells were placed in the optical path between the telescoping ends of the reactor support system. The dark slide was removed and the cell was exposed to polychromatic radiation for a period of one-half to one hour depending on the gas concentrations and the degree of absorbance.

Immediately after initiation of the photo reaction, a second transmission curve was run on the same sulphide-filled cell coinciding with the transmission curve of the air-filled cell. The area between these two curves is the measure of the amount of light absorbed by the sulphur-containing gas.

The spectrum required about five minutes to sweep from 150 nm to 500 nm. The monochromator was then adjusted to follow the 290 nm absorbance peak of SO_2 and a continuous measurement was recorded at 290 nm to indicate the formation of SO_2 and CH_3SSCH_3.

At the end of the reaction run, the cells were allowed to equilibrate for one-half hour and then analyzed on the gas chromatograph. All runs were analyzed for CH_3SH, CH_3SCH_3, SO_2, and H_2S at 65°C and the column was then raised in temperature to 100°C to analyse the CH_3SSCH_3 and the polysulphides trapped on the column. At the conclusion of analysis, the cells were flushed with dry, filtered, bottled air and the reactor support was closed by corks to maintain the dry nitrogen flush over night.

2.3 Chemical Sources

The sulphur-containing gases CH_3SH, SO_2 and H_2S were supplied in pressurized lecture bottles by the Matheson Company of Canada. The bottles were fitted with stainless steel valves connected to lengths of rubber tubing. The rubber tubing led to a flask of water which allowed air from the tube to be displaced by bubbling through the water. Volumes of gas were removed by piercing the rubber tube and withdrawing the appropriate amount in a Hamilton Gas-tite syringe.

The liquids CH_3SCH_3 and CH_3SSCH_3 were supplied by the Eastman Kodak Company from lots 711-1 and 702-1 respectively. The CH_3SCH_3 was transferred to a pyrex bulb fitted with a teflon stopcock and a sampling septum. The CH_3SSCH_3 was stored in a dark screw-cap bottle. All materials were analyzed for sulphur-containing contaminants and were found to be greater than 99% pure by gas chromatographic analysis and were used without further purification.

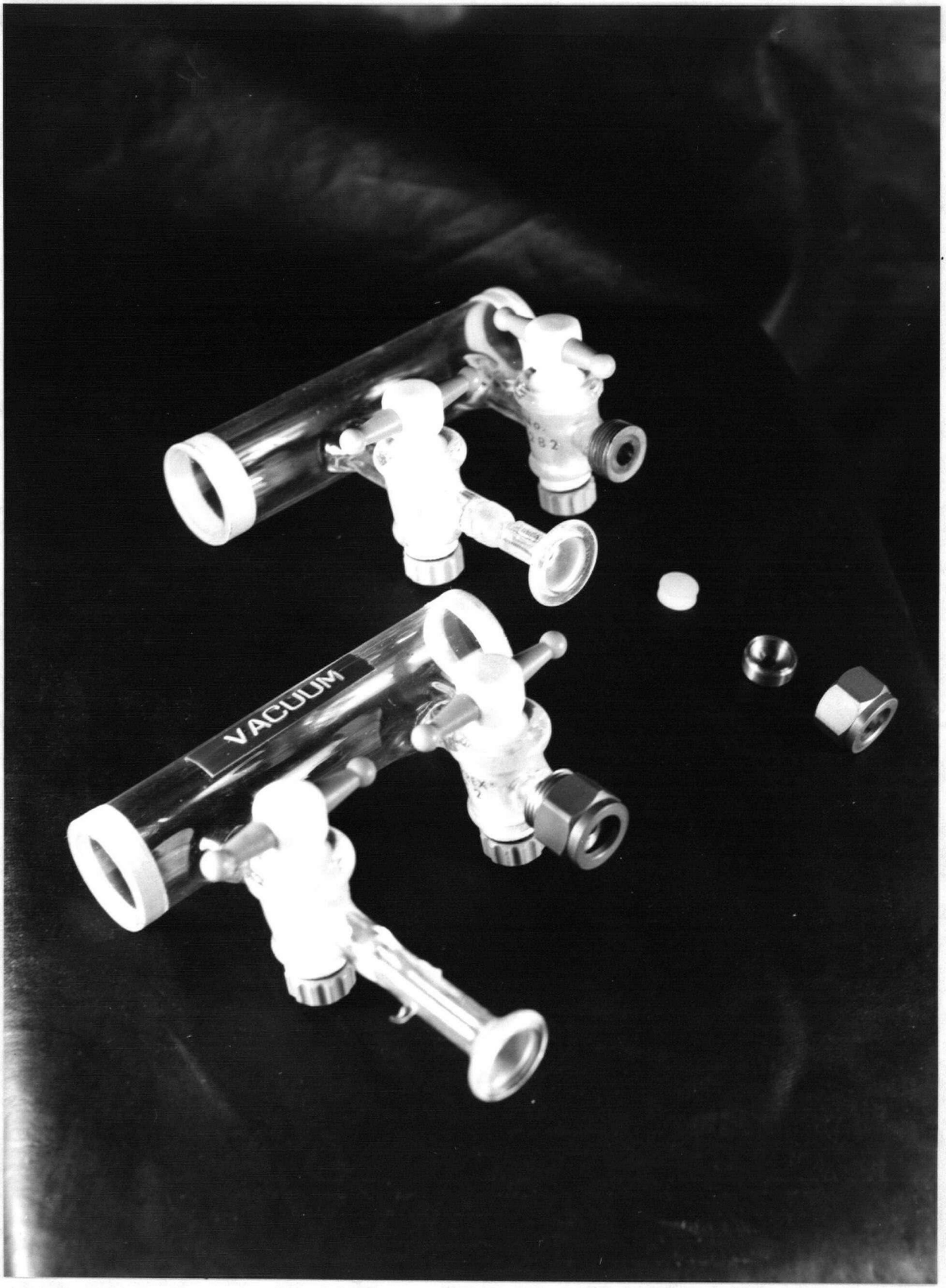

Figure 7. The reaction cells.

2.4 The Reaction Cells

The reaction cells (Figure 7) were fabricated from pyrex tubing 25.4 mm O.D. and were 10.0 cm in optical path length. The average volume was 40.05 ml. Each cell was sealed by two teflon and glass stopcocks blown into the body of the cell. One stopcock was closed by a teflon-faced silicone rubber injection septum located by a brass fitting sealed with epoxy cement to the tube of the stopcock and held in place by a cap screw. The other stopcock was fitted with a QVF vacuum ball fitting either blown in place or attached using epoxy cement. This fitting facilitated flushing the cells with dry air and allowed the evaucation of the cells on the vacuum system for those runs at reduced pressure. The cells could be sampled through the injection septum at any time during a run.

Each end of the cell was sealed by a 1.5 mm thick optical window made of the leached-sodium silica, Suprasil. This material will transmit ultra-violet light of shorter wavelengths than will pure quartz (Figure 8). The ends of the pyrex cell were ground and the inside perimeter of each window disc was ground to provide a roughened sealing surface. The windows were then sealed to the annealed cell body by Araldite 20 AC-OV epoxy resin. This resin was chosen because of its extremely low coefficient of shrinkage which permits the connecting of rigid materials such as glass.

After an initial period of condition, the cells maintained concentrations of CH_3SH, CH_3SCH_3 and CH_3SSCH_3 longer than one hour without detectable loss. Two of the cells could maintain a pressure level of one-quarter atmosphere for one-half hour without detectable change ($\frac{1}{4}$ in Hg).

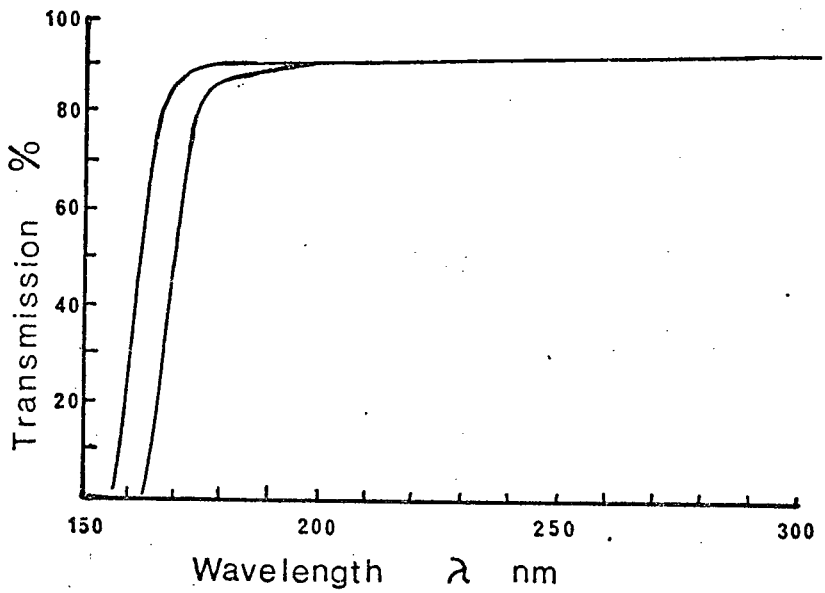

Figure 8. Transmission spectrum of suprasil windows (1 mm and 10 mm thickness).

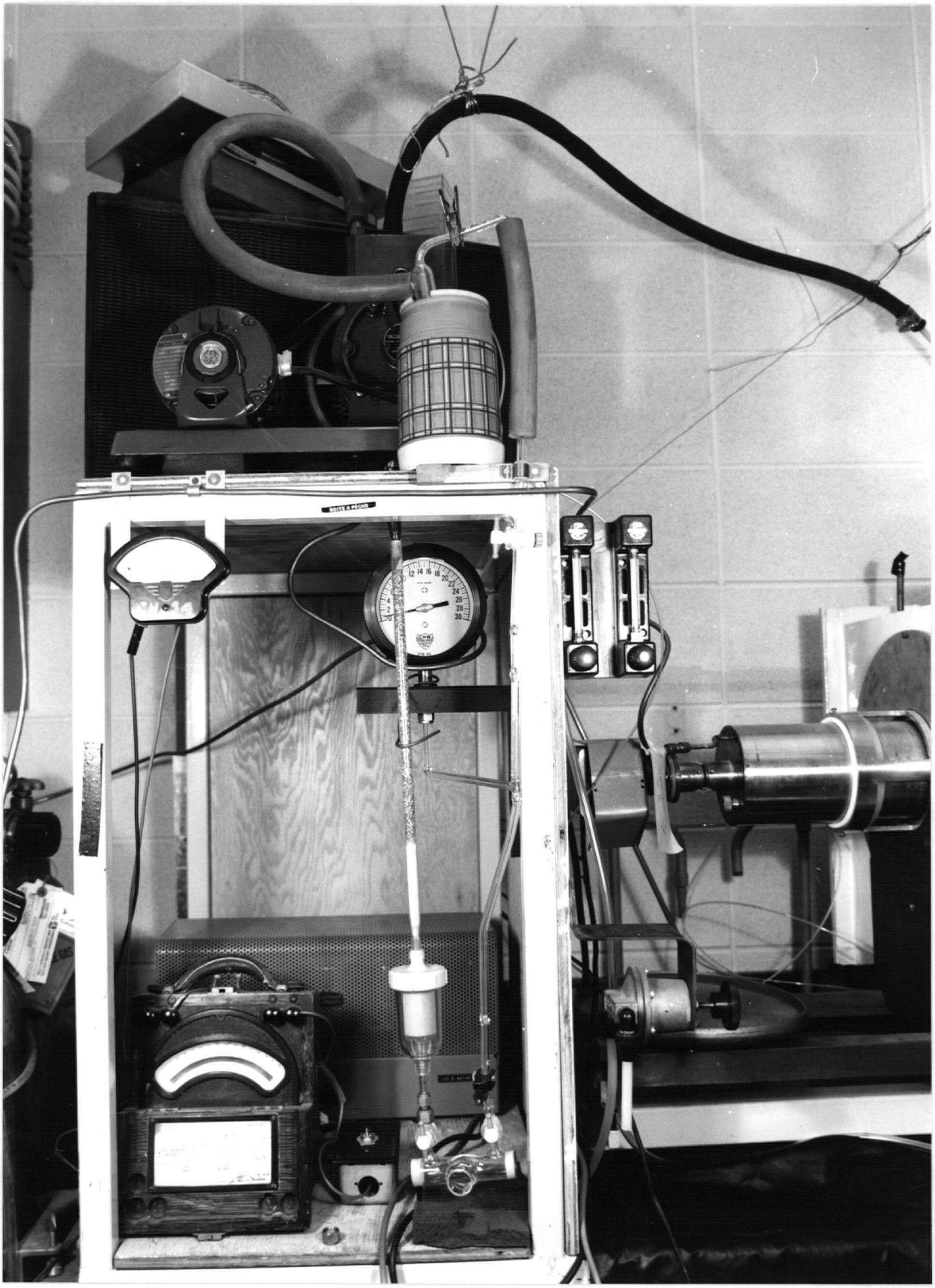

Figure 9. The vacuum manifold and emission cell.

2.5 The Vacuum System

The reaction cells were flushed and filled with bottled, compressed, medical-purpose air using a glass vacuum manifold system (Figure 9). Vacuum was created by a Welch duo-seal vacuum pump which was isolated from the system by a cold finger operated at -20°C. The grease-free, mercury-free system was closed by teflon stopcocks and was joined to the cells by QVF ball joints. The ball joints were covered by .001 inch thick teflon film stretched to cover the ball. Vacuum levels were measured on a C.P.W. Hydropoise bourdon tube vacuum gauge readable to 1/4 inch mercury. The vacuum could be maintained for one-half hour without loss.

2.6 The Deuterium Lamp

Polychromatic ultra-violet light was produced by a medium-pressure deuterium-filled electric discharge lamp rated at a nominal 30 or 60 watts. The lamp was provided with a suprasil window and was powered by a Jarrell-Ash power supply. The emission spectrum measured through a new cell by an EMI 9558 QBM photomultiplyer tube on a 1/4 meter Ebert monochromator is shown in Figure 10.

The efficiency of light production was determined by placing an ammeter in line with the lamp supply and a voltmeter across the two lamp leads. The lamp was found to draw 29.7 watts on high power setting. Assuming an average absorbed wavelength of 235 nm, the efficiency of photon production from electrical energy can be calculated. The frequency of 235 nm radiation is 1.276×10^{15} sec^{-1}. Thus the energy per photon ($E = h\nu$) is 8.464×10^{-19} Joules/photon. For one hour at 29.7 watts, there are (29.7)(60)(60)(1) =

1.069×10^5 watt seconds/hour. Since one Joule is one watt second, a 100% efficient light would produce:

$$\frac{1.069 \times 10^5 \text{ watt seconds}}{\text{hour}} \cdot \frac{1 \text{ photon}}{8.4638 \times 10^{-19} \text{ watt seconds}}$$

$$= 1.263 \times 10^{23} \text{ photons per hour}$$

From actinometric studies 2.2154×10^{18} photons of wavelength shorter than 300 nm are produced. Thus the deuterium lamp produces ultra-violet light of wavelength shorter than 300 nm with an efficiency of 1.7537×10^{-5}.

2.7 The Collimation System

Light emitted from the deuterium lamp passes through a quartz lens situated in the exit tube of the lamp housing. A further quartz lens of 100 mm focal length is placed 10 cm down the entrance tube of the reactor support to collimate the divergent beam at 2.5 cm diameter. The light passes by a 2.5 cm aperture 5 cm before the entrance window and then passes into the reactor cell.

2.8 The Reaction Cell Support System

The reaction cell is supported in teflon end caps by two telescoping tubes which maintain optical alignment of the source, reactor and detector systems. The atmosphere of the support system is swept by dry nitrogen gas in order to sweep the optical path free of oxygen. The removal of O_2 is necessary to prevent the formation of ozone in the entrance and exit areas

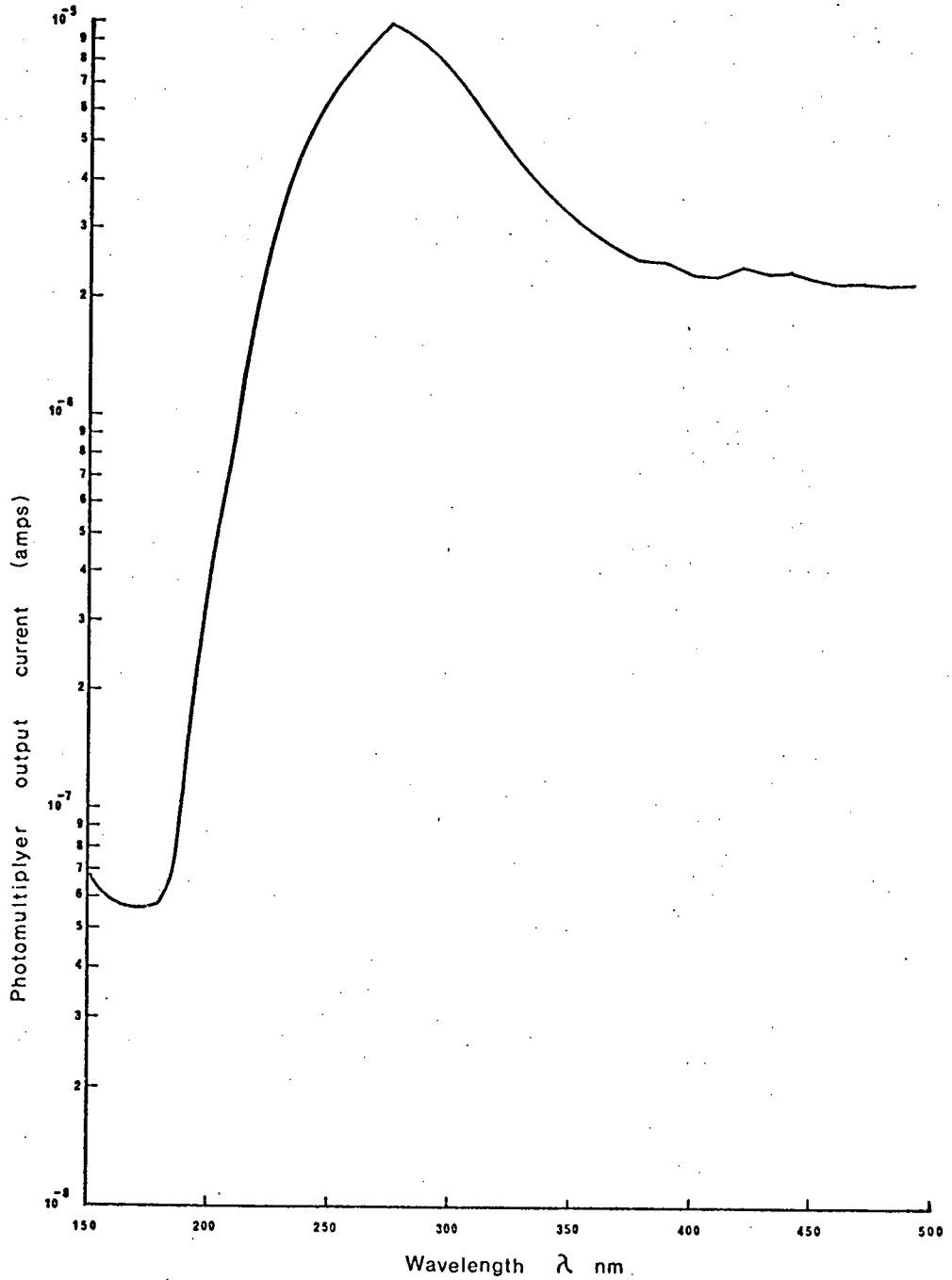

Figure 10. Emission spectrum of deuterium light supply measured on EMI9558QBM photomultiplyer at-800 V.

of the support mechanism. The absorption of very short wavelength ultra-violet light by O_2 promotes the formation of ozone as shown below:

$$O_2 + h\nu \rightarrow 2\ O$$

$$O + O_2 \rightarrow O_3$$

The ozone thus formed absorbs ultra-violet light of longer wavelengths. These are the reactions responsible for the formation of the ozone layer which shields the earth from solar ultra-violet light. The absorption by ozone of ultra-violet light at longer wavelengths breaks up the ozone molecule to molecular oxygen and the cycle begins anew.

$$O_3 + h\nu \rightarrow O_2 + O$$

The presence of O_2 in the optical path would allow this sequence to take place and would produce a variable absorbance within the optical train. This variable absorbance would be difficult to separate from reactions within the reactor cell and would lead to variations in the incident light intensity or to the intensity detected in the photomultiplier-monochromator system. The situation was avoided by dry-nitrogen purging the reactor tube support segments, the monochromator and the photomultiplier tube housing with an initial over night flow rate of 2.5 CFH and a steady-state flow of 1 CFH for long periods of time.

The light source, cell, monochromator and photomultiplier system are held in alignment by the telescoping system supported on an accurately aligned track (Figure 6). The end pistons move back and forth to accommodate

cells of varying path length from 1 cm to 25 cm. The cell diameter and radiation path diameter can be varied up to 7.6 cm by changing the end caps and the colimating lens. The reaction cell area is enclosed on five sides by a light-tight black metal box and can be blacked out completely by enclosing the sixth side with a curtain.

2.9 The Emission Configuration

The monochromator and photomultiplier may be removed from the alignment rack to provide an emission observing configuration. In this configuration, the monochromator was placed perpendicular to the reaction light axis in order to measure the visible radiation emitted by the gases under study (Figure 11). The monochromator was modified by removing the 150 micron (μ) slit arrangement and substituting a 2 mm width entrance and exit slit. The entrance of the monochromator was provided with a 10 inch long, 1½ inch diameter tubular entrance mask. The monochromator-photomultiplier combination was mounted perpendicular to the light axis on a small stand. The monochromator and photomultiplier system was enclosed in two layers of blackout cloth which joined the cell shroud in order to reduce extraneous signals. The monochromator motor drive control was operated by an external switch arrangement when in the emission configuration.

2.10 The Monochromator

The light exiting the reactor cell was chromatically analyzed by a Jarrell-Ash one-quarter meter focal length Ebert monochromator. The monochromator was fitted with two diffraction gratings which could be selected

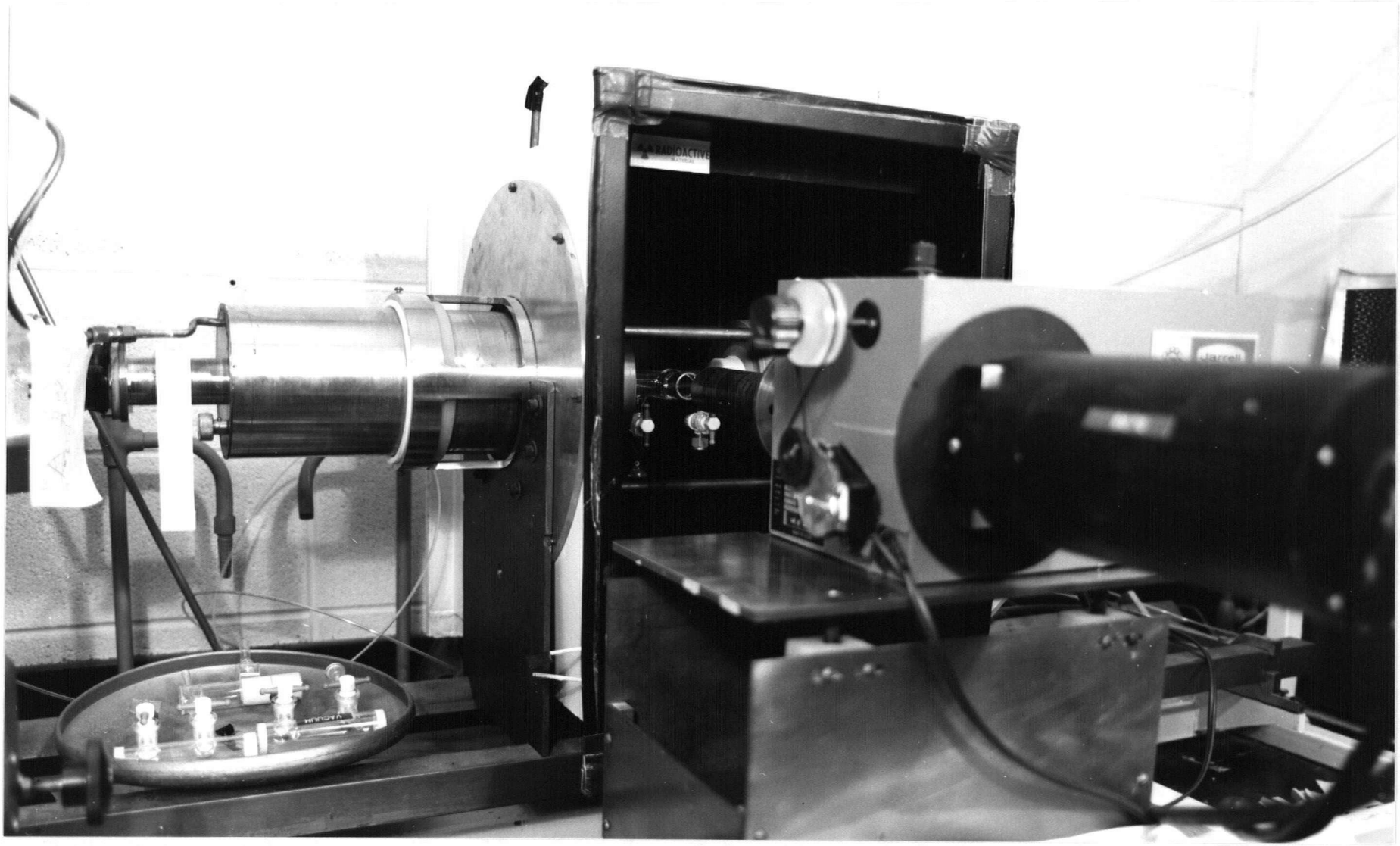

Figure 11. The emission configuration.

to cover the range 150 nm to 500 nm or 150 nm to 1000 nm. The low blaze grating was optically coated to maximize transmission at 300 nm. The diffraction gratings were scribed with 60,000 lines per inch (2360 G/mm) and 30,000 LPI (1180 G/mm). The grating dispersions of 1.65 nm/mm and 3.3 nm/mm provided a band-pass of 0.25 nm and 0.50 nm respectively for the 150 micron slit widths. During emission runs, the slits were opened to 2 mm to provide a stronger photomultiplier signal. This slit width allowed a band-pass of 3.3 nm and 6.6 nm for the low and high-blaze gratings respectively. The monochromator wavelength drive was calibrated with the 435.8 nm blue and 546.0 nm green Hg emission lines of a fluorescent tube. The wavelength drive was operated by a rubber drive belt from a synchronous motor fitted with pulleys which co-ordinated the drive rate with that of a Sargent chart recorder. The spectrum could be taken at any point in the reaction or specific wavelengths could be followed in time throughout the reaction.

2.11 The Photomultiplier Tube

Photoelectric light measurement was provided by an EMI 9558 QBM photomultiplier tube. This tube has a tri-alkali $CsNa_2KSb$ photocathode and 11 stages of amplification. The entrance window is suprasil and the tube combination has S 20 Q extended ultra-violet response. The tube manufacturers claim a spectral sensitivity shown in Figure 12. The tube was operated at -800 V cathode potential and a Jarrell-Ash Model 385 power supply and ammeter were used with a Sargent chart recorder to record light transmissions. During emission runs, the photomultiplier tube housing was modified to operate the housing at cathode potential in order to reduce the noise level. The housing was in turn housed in a polyvinyl chloride enclosure and isolated from the

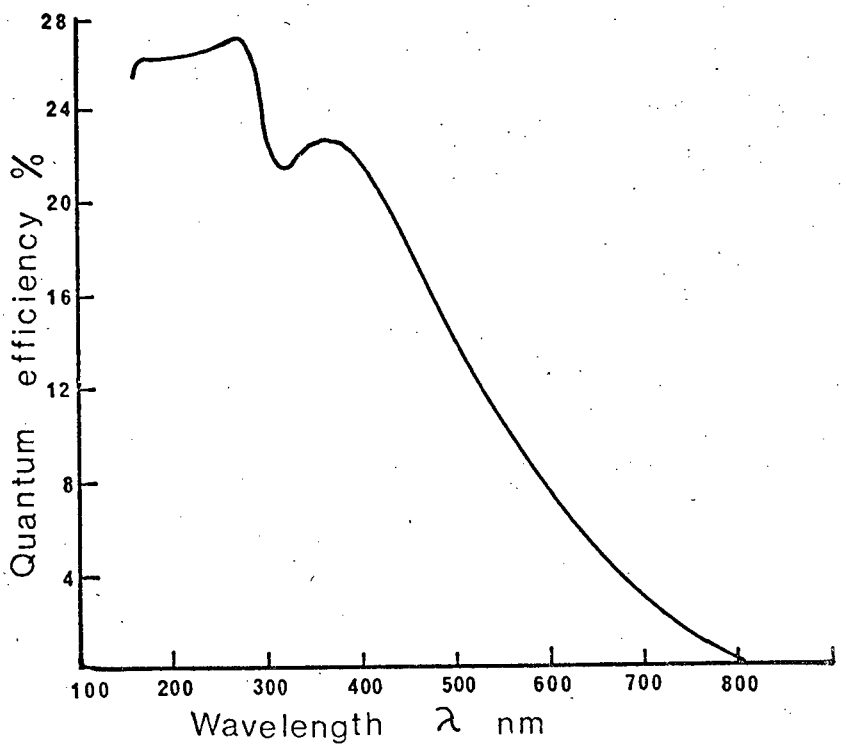

Figure 12. Spectral response of EMI9558QBM photomultiplyer (EMI).

monochromator by insulating pads and nylon screws. The photoelectric light measuring system was calibrated by use of a potassium ferrioxalate chemical actinometer system.

2.12 Actinometry

The photoelectric light measuring system was calibrated directly by use of the potassium ferrioxalate liquid chemical actinometer developed by Hatchard and Parker [50]. This method makes use of the sulphuric acid catalyzed reduction of Fe^{+3} to Fe^{+2} by ultra-violet light. The Fe^{+3} is reduced and the oxalate oxidized. The resulting Fe^{+2} is detected by the 1, 10-phenanthroline complex which forms a red dye that is analyzed using a double-beam spectrophotometer at 510 nm. Light absorption by the solution is very good at wavelengths shorter than 480 nm. The quantum yield is quite consistent over the wavelength range of interest and the sensitivity is uniform over large ranges of light intensity and reactant concentration. The solutions, when stored in the dark, are stable over a period of a few weeks.

2.13 The Make-up of Potassium Ferrioxalate Crystals

The crystals of potassium ferrioxalate were prepared by mixing three volumes of 1.5 M A.R. potassium oxalate with one volume 1.5 M A.R. ferric chloride while stirring. The brilliant green potassium ferrioxalate crystals precipitated rapidly and were separated by filtration. The crystals were recrystalized three times from warm water, filtered and dried in a stream of warm air. The crystals were stored in glass in the dark. The .006 M actinometric solution was prepared under red photographic safe-light as follows:

1. dissolve 2.947 g $K_3Fe(C_2O_4)_3 \cdot 3H_2O$ crystals in 800 ml distilled water
2. add 100 ml 1.0N H_2SO_4
3. dilute to 1 ℓ and mix well
4. store in the dark

2.14 Preparation of the Fe^{+2} Calibration Graph

The calibration of the Fe^{+2} content as a function of the 510 nm absorbance of the 1-10, phenanthroline complex was carried out using dilute solutions of Fe SO_4 in H_2SO_4. The following solutions were prepared:

1. 0.4×10^{-6} M/ml $FeSO_4$ in 0.1N H_2SO_4
2. 0.1% 1,10-phenanthroline monohydrate in water
3. Buffer Solution

   600 ml 1N Sodium Acetate

   360 ml 1 N H_2SO_4

   diluted to 1 ℓ

The calibration liquids were prepared in 50 ml volumetric flasks as follows:

1. place 1, 2, 3, 4, 5 → 10 ml of liquid (1) in flask
2. add 25 ml - volume (1) of 0.1N H_2SO_4 to make acidity equivalent to 25 ml 0.1N H_2SO_4
3. Add 5 ml 1,10-phenanthroline solution
4. Add 12.5 ml buffer solution
5. dilute to 50 ml with water and let stand one-half hour.

The optical density of the orange coloured solution was determined at the 510 nm plateau of the Fe^{+2} phenanthroline absorbing complex. The spectra were determined on a Unicam SP800B, double-beam spectrophotometer in both 1 cm

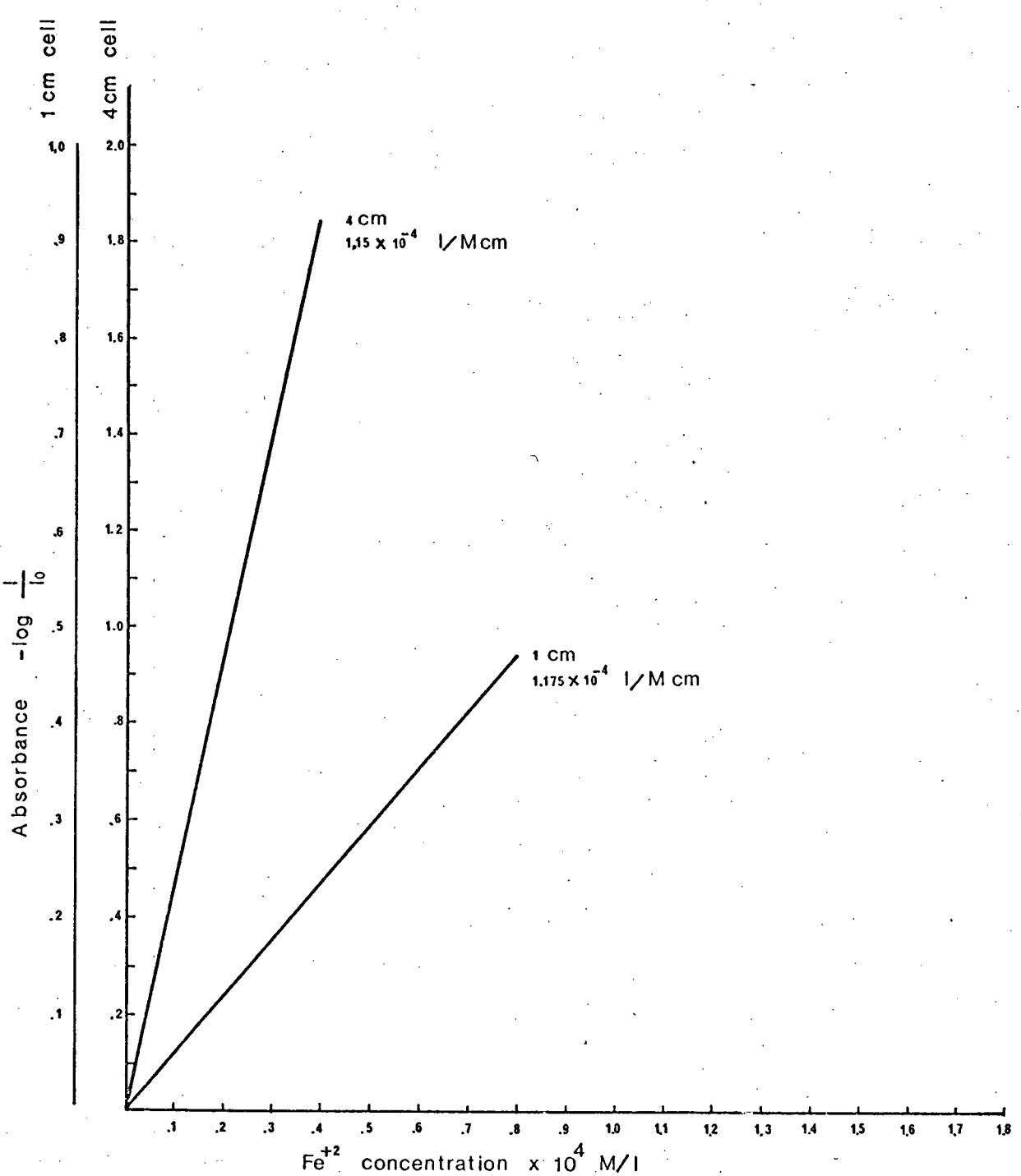

Figure 13. Absorbance of Fe^{+2} - 1, 10-phenanthroline complex at 510 nm.

and 4 cm matched cells. The calibration graph is shown in Figure 13, and the extinction coefficient was found to be 1.15×10^4 ℓ/M cm for 4 cm cells and to be 1.175×10^4 ℓ/M cm for 1 cm cells.

2.15 Deuterium Light Intensity Calibration

The intensity of the deuterium lamp was measured using a cell of 1.5 cm path length filled with .006 M $K_3Fe(C_2O_4)_3$. The actinometry cell (Figure 14) was fitted with suprasil ends and an 8.45 cm pyrex skirt which kept the photoelectric light measuring devices in positions similar to those in a reaction run. A duplicate 1.5 cm path length cell was used unilluminated as a zero device. As can be seen from Figure 15, the 1.5 cm .006 M $K_3Fe(C_2O_4)_3$ cell absorbed 98% of the light up to 400 nm. A borosilicate glass filter was used to eliminate wavelengths shorter than 300 nm (Figure 15). In this manner the photon flux shorter than 300 nm can be found from the difference between filtered and unfiltered actinometry runs.

The actinometric cells and solutions were placed in the dark room and handled under red photographic safe light. Six ml .006 M $K_3 Fe(C_2O_4)_3$ actinometer solution were pipetted into both the measuring cell and the zero cell. The zero cell was handled in an identical manner to the measurement cell except for exposure to the ultra-violet light beam. Both cells were placed in a light-proof bag and transported to the reactor in the laboratory. The reactor was enclosed in a light-proof bag fitted with elastic arm holes through which the cells could be unwrapped and placed into position for light measurement. Once in position in the reactor, the measurement cell was exposed to the full polychromatic intensity for 15 minutes by removal

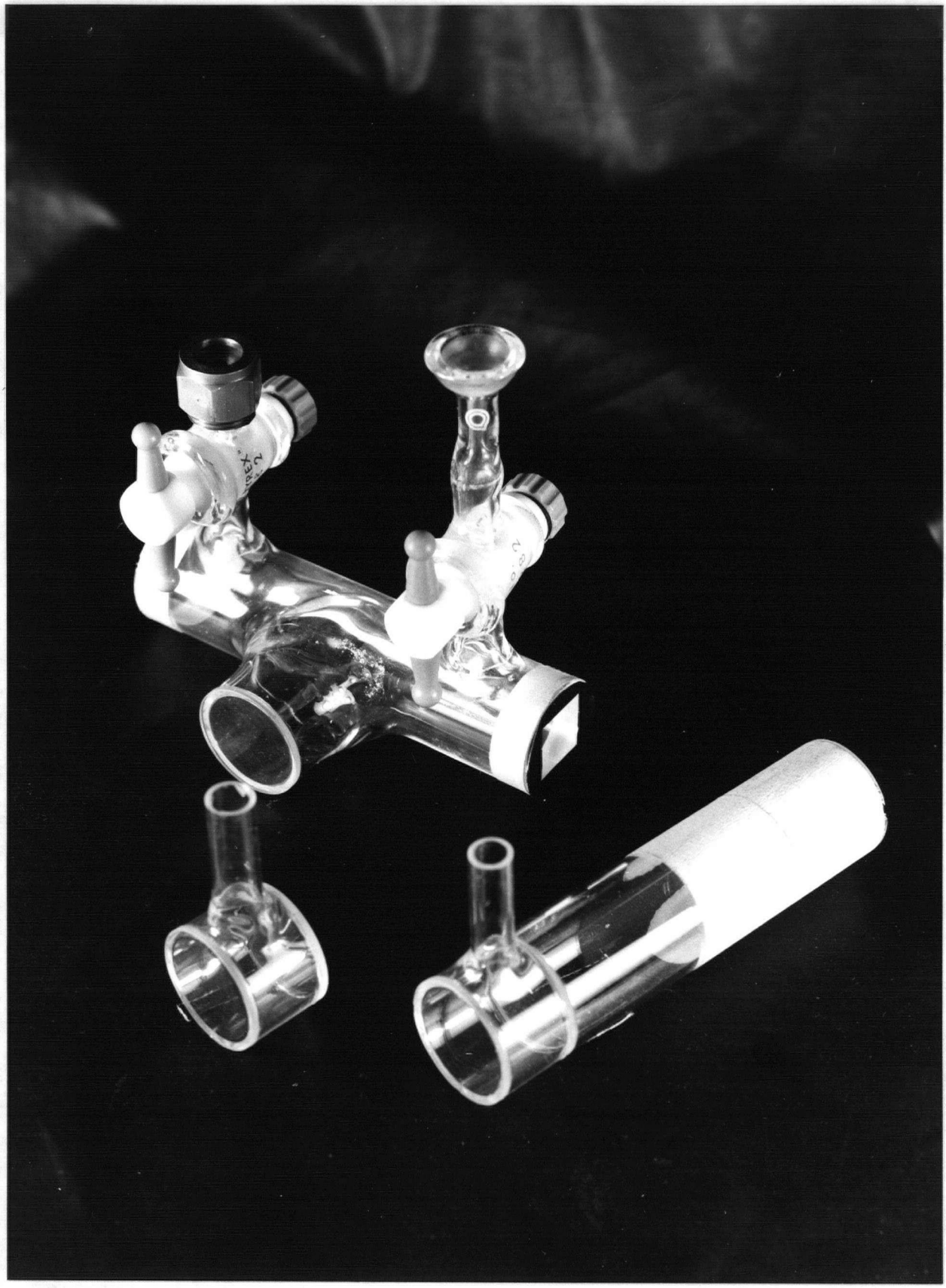

Figure 14. The emission cell and actinometry cells.

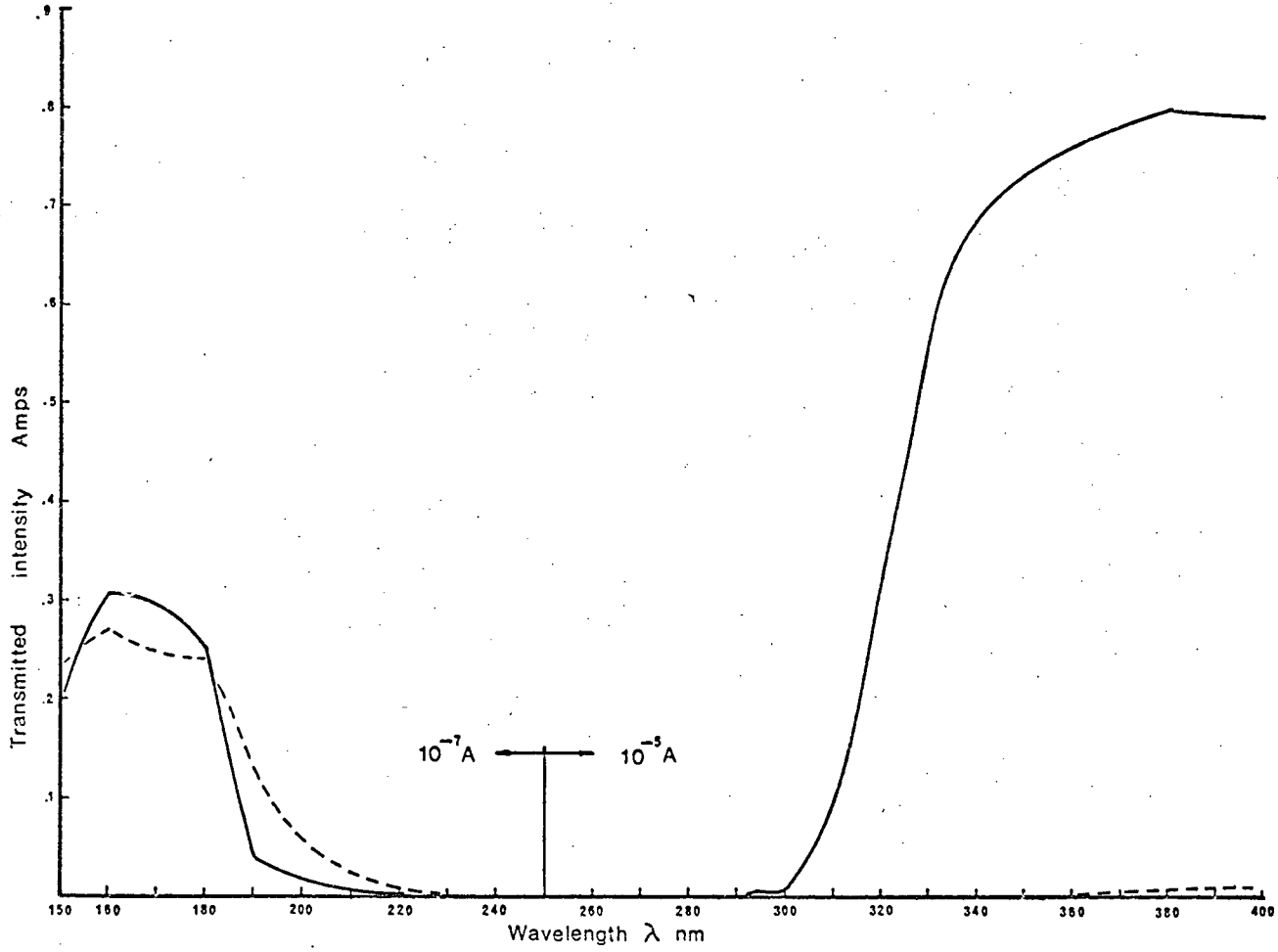

Figure 15. Transmission spectrum of ——— borosilicate glass filter (1.08 mm) and of ----- 1.5 cm $k_2F_e(C_2O_4)_3$ .006M actinometry solution.

of the dark slide. The measurement and zero cells were then wrapped in the light-proof bag and removed to the dark room.

The cells were emptied and rinsed into 25 ml volumetric flasks. Three ml of buffer solution were added as were 2 ml of 0.1% 1,10-phenanthroline solution. The cells were made up to 25 ml and let stand for one-half hour in the dark. The absorbance at 510 nm was then measured on the unicam SP800B double beam spectrophotometer with either 1 cm or 4 cm cells. The intensity of the borosilicate filtered runs was subtracted from the non-filtered runs to give the photon flux for wavelengths shorter than 300 nm.

2. 16 The Gravimetric Integration Method

Assessment of the absorbed light intensity was done by gravimetric integration of the photomultiplyer intensity v.s. wavelength chart recordings. Continuous monitoring of the photon flux through an air-filled reaction cell allowed measurement of the daily light input and made corrections for clouding of the optical window and for exhaustion of the deuterium lamp.

The intensity-wavelength curve for the mercaptan-filled cell was superimposed on that for the air-filled cell. That graph was then xeroxed twice. The sheets were corrected for paper weight variation. The analogous areas under the input and output curves were cut out, weighed, corrected for amplification and the differences interpreted as percentage of incident light absorbed by the gas. The air-filled cell reading was used as a measure of incident energy relative to that during the period of lamp actinometric calibration. Long and short wavelength cut-off points were set at 300 nm and 150 nm. The long wavelength limit was set by the cut-off frequency of

the borosilicate glass filter. No reaction was noted for runs using the borosilicate filter. The short wavelength limit was set to exceed the transmission characteristics of the quartz lens.

2.17 Gas Chromatography

The analysis of sulphur containing gases was performed on a Varian model 1400 temperature-programmed gas chromatograph. Detection of the sulphur gases was accomplished by a Meloy Laboratories model FPD100AT flame photometric detector operated by a Tracor 12001 power supply and electrometer. The detector and electrometer were mounted external to the chromatograph.

The flame photometric detector is sensitive to the light emitted from sulphur-containing compounds burned in a reducing flame. The detector was modified by providing a parabolic, front surface mirror opposite the photo multiplier tube window and 394 nm interference filter. This had the effect of increasing sensitivity. The 6 cm focal length front surface mirror was placed so that the flame would be at its focal point. The mirror was separated from the burning chamber by a pyrex window which passed the light to the phototube. The entire detector was surrounded by fiberglass wool and asbestos packing material to thermally insulate the block. The detector was mounted on the side of the gas chromatograph. Chromatograph column effluent was transferred from the column to the detector by a teflon column filled with Triton X-405 adsorbed on chromosorb W. The transfer line was electrically heated and insulated to provide a minimum impedance to passage of effluent gases. This line was maintained at 80°C.

The injection block of the chromatograph was fitted with a teflon injector liner to minimize the stainless-steel-catalyzed decomposition of CH_3SH.

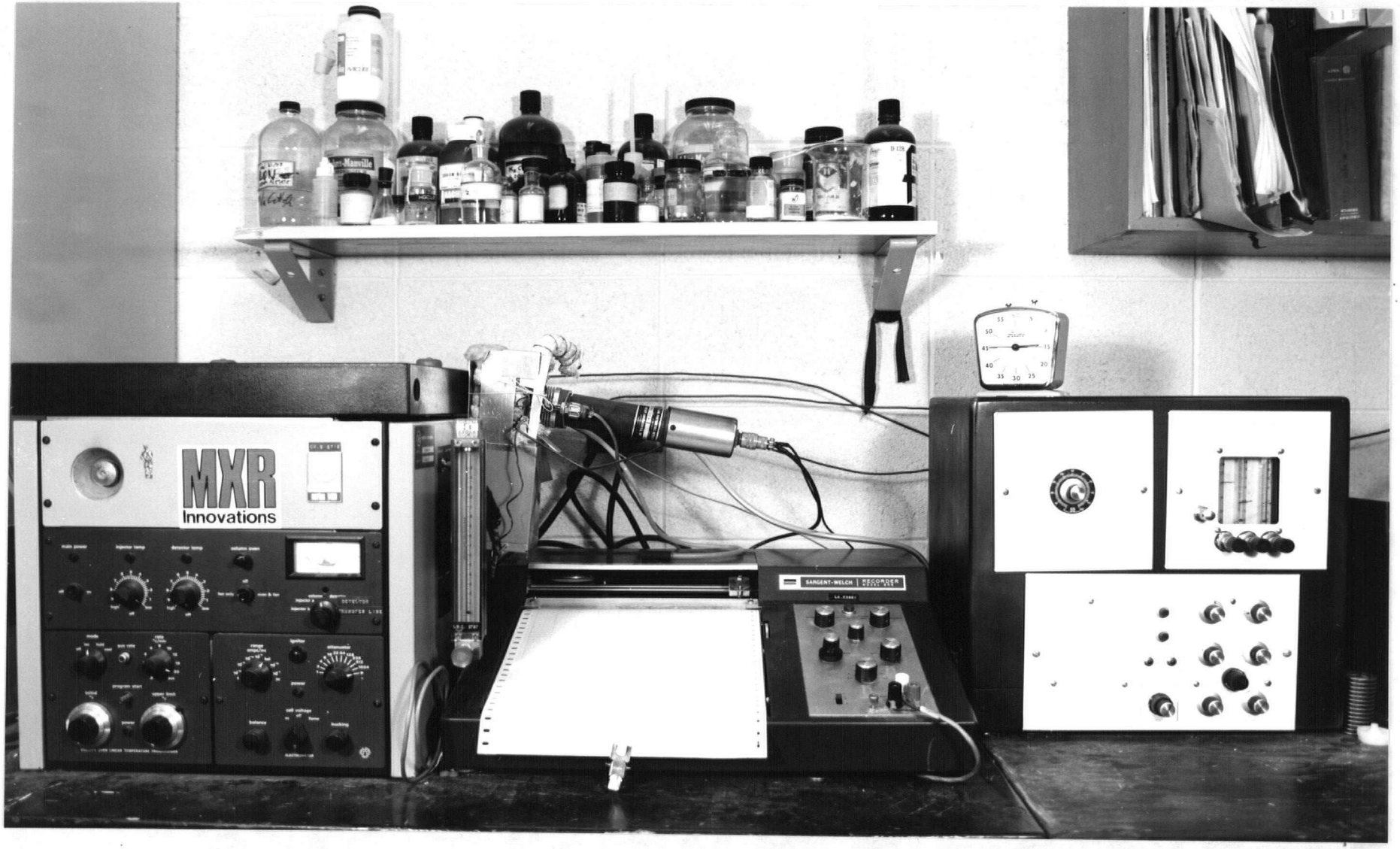

Figure 16. The gas chromatograph and flame photometric detector.

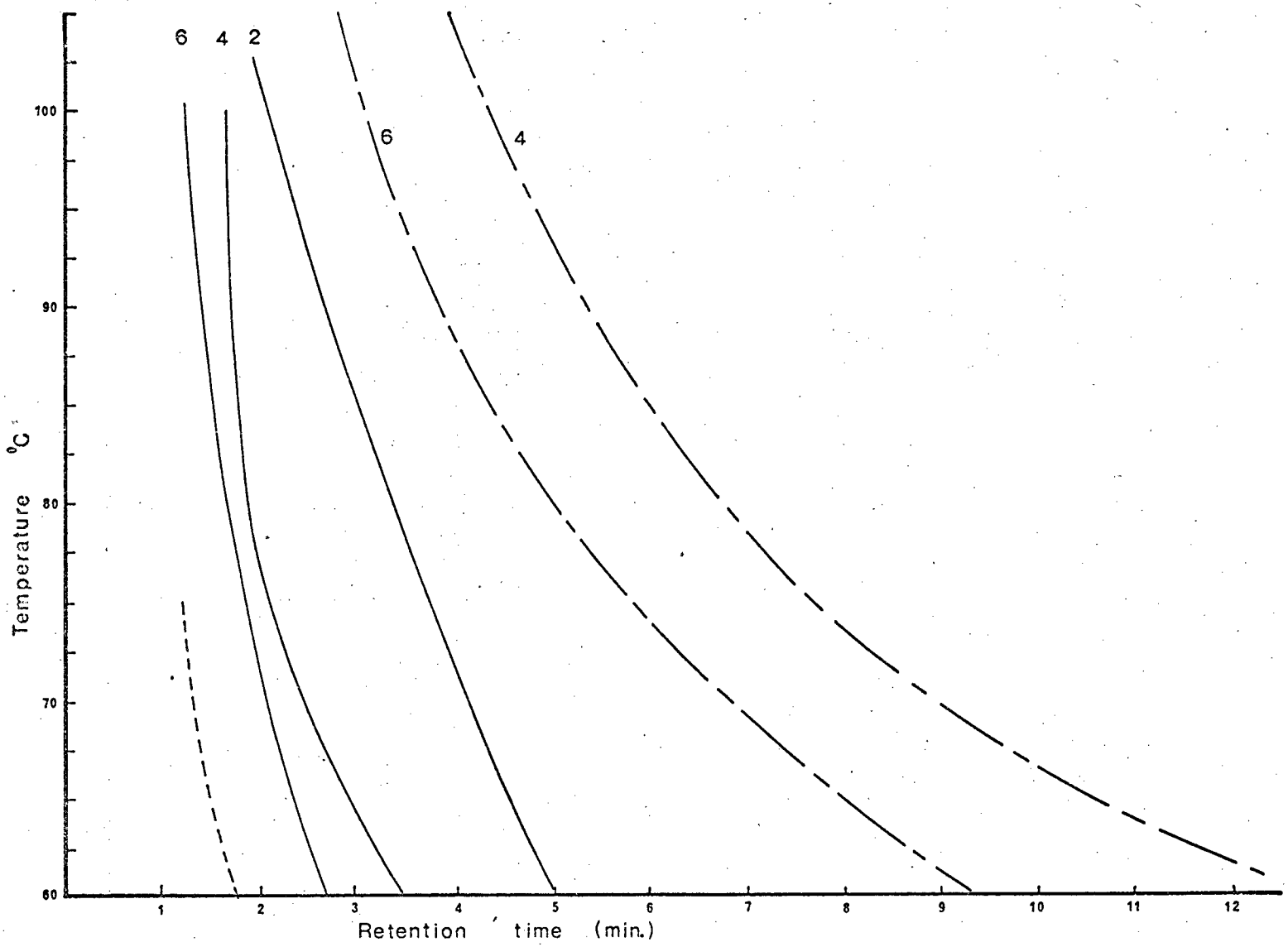

Figure 17, Carbopak BHT-100 9 ft. column retention data.
----- H_2S; ——— CH_3SH; ——— — ——— CH_3SCH_3
at various carrier gas flow rates.

The chromatograph columns were fabricated of 1/8" O.D. heavy-wall teflon tubing to minimize wall reactivity and permeation of the wall. Teflon columns were found to offer performance equal to glass, to be easier to fill and were significantly more durable. The columns were attached to the chromatograph by teflon swagelock ferrules and stainless steel swagelock caps. The tubes were prevented from collapsing by the insertion of a 1" length of 16-guage stainless tubing inside the column where the swagelock ferrule compressed it. This procedure was followed at each column joint from the injection block to the transfer line and into the detector.

Numerous columns were used during the work. These included:

silicone gum rubber SE-30 10%

Tri Cresyl Phosphate 20%

Triton X-405 20, 30, 40%

Acid Washed Deactigel 40/60 mesh

Carbopak BHT-100

The most useful column was found to be Carbopak BHT-100 in 9 feet of teflon tube. This provided excellent separation of H_2S, CH_3SH, CH_3SCH_3 and SO_2. The CH_3SSCH_3 was retained on the column at 65°C for an extended time, so temperature programming was employed. The Carbopak is a hydrogen-reduced, activated-carbon porous material with no liquid phase to desorb. The column can be run easily to 100°C and is limited mainly by the nature of the column wall material. Temperature programming was employed to remove the disulphides at the end of each day's runs. The variation of retention time with flowrate and temperature is shown in Figure 17. The conditions settled upon for operation were:

column temperature 65°C prog. to 100°C @ 20°C/min	
He	20 ml/min
O_2	20
Air	20
H_2	250
Transfer line	80°C
detector	140°C
injector	70°C

2.18 Chromatograph Calibration Procedure

The chromatograph was calibrated daily since large daily variations were noticed at essentially identical conditions. The flow rates of He carrier gas, air, O_2, and H_2 were adjusted using bubble tube flow meters at an oven temperature of 65°C with the detector flame unignited. The injection septum was a Hamilton 75804 teflon-faced silicone rubber septum. The teflon face minimized septum bleed and septum contamination. Glass sample bottles were fabricated which were closed by a teflon-faced septum held in place by modified tube fittings sealed to the glass bottles with epoxy cement (Figure 16). Hamilton teflon-tipped gas-tight syringes with Cheny adapters were used to provide a sample volume of either 0.1 ml or 0.25 ml. The sample size was chosen appropriately for the sulphur gas concentration which was to be examined in the reaction vessel. Gas concentrations in the four sample bottles were adjusted to span the range under consideration.

Samples were injected every five minutes in order to maximize reproduceability for given concentrations. A minimum of three reproduceable

Figure 18. Chromatograph standardizing bottles and Hamilton syringes.

points were taken to obtain one calibration point. A typical daily calibration is shown for CH_3SH in Figure 19 and in Figure 20 for SO_2. The intensity of response for SO_2 was much greater than that for CH_3SH. The SO_2 calibration is a straight line. The CH_3SH calibration is not a straight line and as can be seen from Figure 19 the response tends to level off at higher levels of CH_3SH. The plateau can lead to inaccurate analyses if one should carry out the entire reaction in the plateau region. For this reason the sample volumes of the syringe were adjusted to keep the analysis of varying cell concentrations in regions of adequate response sensitivity.

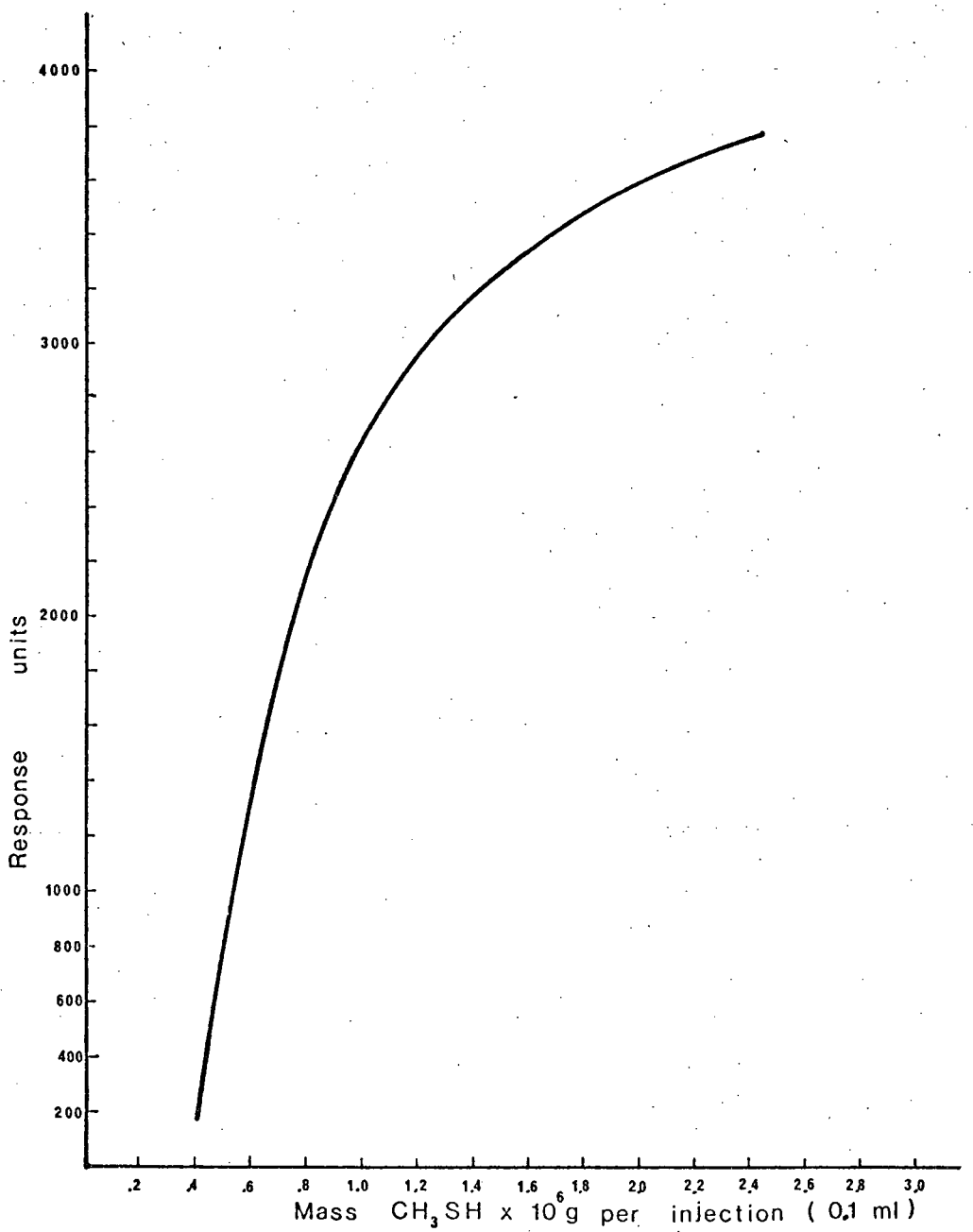

Figure 19. Typical daily calibration curve for CH_3SH (0.1 ml sample) Jan 11, 1977; Carbopak BHT 100. He = 20 ml/min.; O_2 = 20 ml/min.; Air = 20 ml/min.; H_2 = 250 ml/min.; T = 65°C.

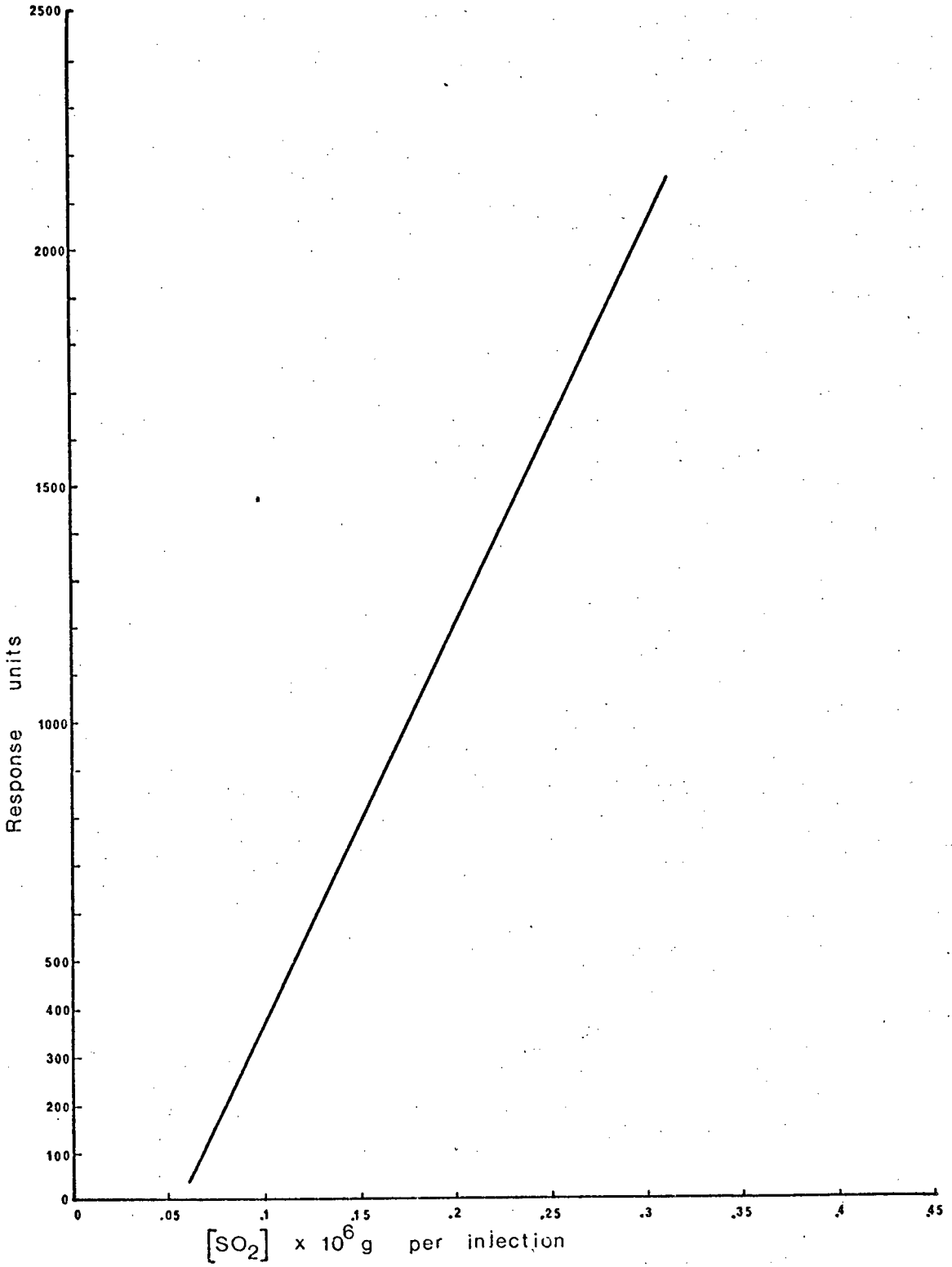

Figure 20. SO_2 calibration Dec. 18/76, Carbopak BHT-100. He = 20 ml/min.; O_2 = 20 ml/min.; Air = 20 ml/min.; H_2 = 250 ml/min.; T = 65° C.

Chapter 3

EXPERIMENTAL RESULTS AND DISCUSSION OF PHOTO-OXIDATION OF SULPHIDES

3.1 Preliminary Experiments

The photo-oxidation experiments were carried out in 40 ml pyrex reaction vessels equipped with Suprasil entrance and exit windows. The reaction cell was flushed with dry, bottled, compressed air which was passed through drierite, a bed of molecular sieve 5 Å, and a Whatman gas filter to remove water, oil vapours and particulate matter, respectively. A transmission spectrum of the air-filled cell was run before the sulphide addition in order to provide a measurement of incident light intensity and to provide a basis for the measurement of the amount of light absorbed by the added sulphur gas. A second transmission spectrum was run upon commencement of the photo-reaction in order to measure the absorbed photon rate. The absorption was found to be a function of mercaptan concentration in the reaction atmosphere. The percentage light ($\lambda < 300$ nm) absorption of the air-mercaptan mixture is shown in Figure 21 as a function of the weight of CH_3SH added to a 40 ml reaction cell. The

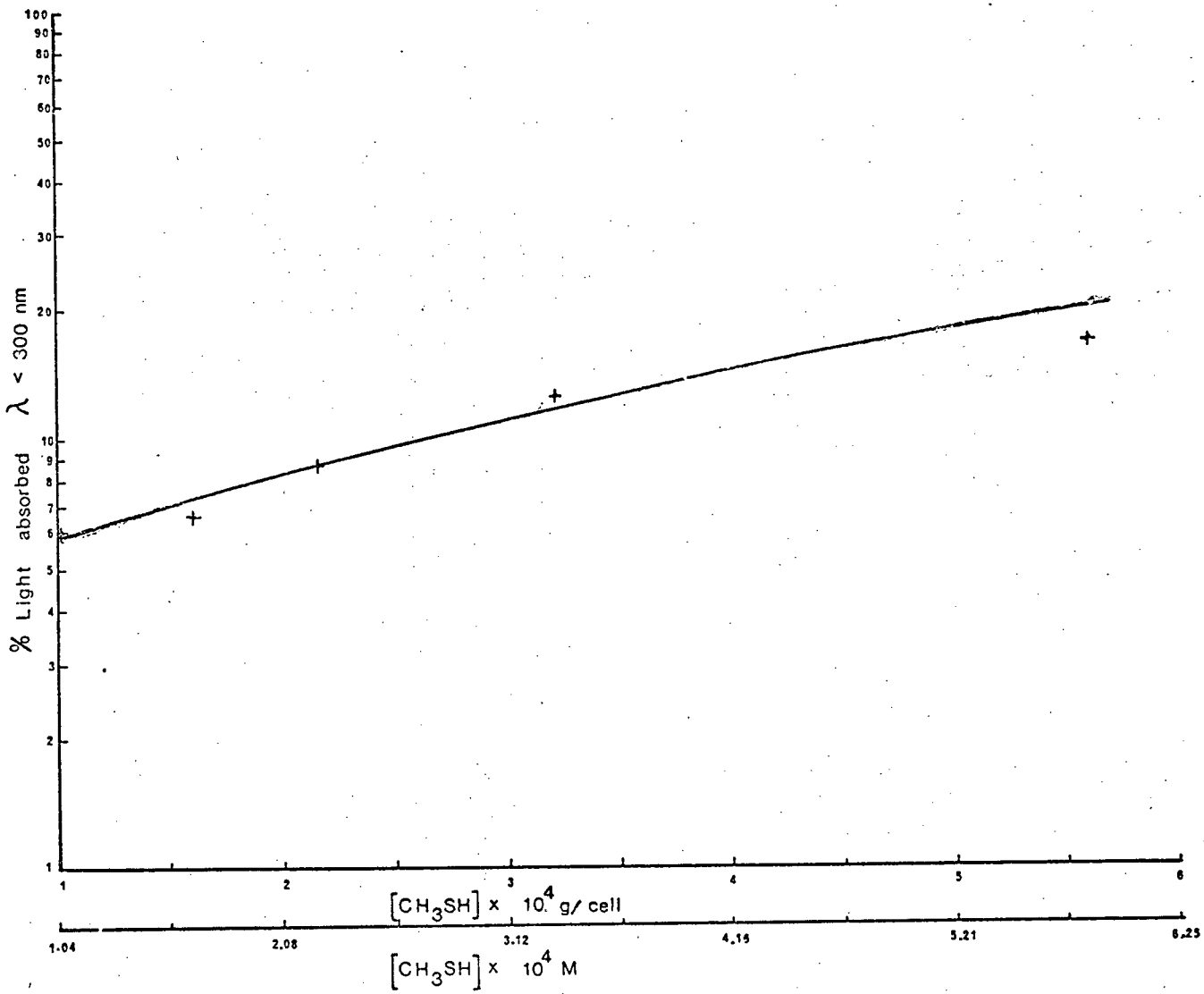

Figure 21. The absorption of polychromatic (λ < 300 nm) UV light by methyl mercaptan.

absorbance of 10 cm of air was not noticeably different from that of pure N_2. This is due to the fact that the quartz lens of the collimation system did not pass significant intensity at wavelengths shorter than 185 nm. The amount of light that one would expect air to absorb may be calculated from the absorption coefficient of O_2. At 190 nm the log of the absorption coefficient of O_2 is -2 atm^{-1} cm^{-1} [59]. Thus one would expect O_2 to absorb 4.5% of the incident energy at 190 nm. As one approaches the incident energy maximum at 220 nm, the log of the absorption coefficient of O_2 drops to -4 and the adsorbed intensity drops to 0.046% for a 0.2 atm pressure of O_2 for a 10 cm path length.

The concentration of mercaptan in the cells was measured by gas chromatography and the chromatograph was calibrated daily for CH_3SH and SO_2. During an experiment, the cell was exposed to irradiation for a 30 minute period. Immediately after the start of a run, as soon as the second absorption curve was completed, the monochromator was set to continuously monitor the transmission at 290 nm. This frequency was largely free from absorption by mercaptan and showed a linear decrease in transmission with time during the reaction . The decrease was due to the production of CH_3SSCH_3 and SO_2 which absorb at the 290 nm wavelength.

3.1.1 The Effect of Using Room Air

Early experiments were performed using air taken from the laboratory atmosphere. The rates of reaction measured from experiments performed in this way proved to be highly scattered. Traces of vapours from laboratories were responsible for interfering with the photochemical reaction. The lack of

reproduceability was reduced by using dried, filtered, bottled air to flush the reaction cells and to provide the reacting atmosphere.

3.1.2 The Effect of Wet Air

Undried atmospheric air was used for a number of initial runs. These experiments proved to be highly variant and gave a low rate of reaction. The high variation and lack of data regarding H_2O content prevent meaningful correlation of the reaction rates with water content. It is apparent from the observations, however, that water vapour inhibits the mercaptan oxidation reaction.

3.1.3 The Effect of Pure Oxygen

A series of reactions were carried out using an atmosphere containing 100% oxygen instead of air. The series was intended to reveal the role played by O_2 absorption as a photo-initiator of the reaction sequence. The five-fold increase in O_2 concentration would reveal, through an increase in reaction rate, the importance of oxygen as a rate controlling parameter. The quantum yield in air for that sequence of experiments was 11.8 ± 4.7. The quantum yield of experiments performed at identical CH_3SH concentrations in dry O_2 was 8.5 ± 2.1. These two yields are not significantly different. The lack of significant rate increase demonstrates that light absorption by O_2 is not the major initiating photo-process. Hence, one may conclude that an ozonolysis reaction with CH_3SH is not a major rate contributing reaction.

This result suggests that those reactions which involve molecular oxygen as a reaction partner are already operating at a maximum rate in the

atmospheric concentration of O_2 (8.17×10^{-3} M). Thus there is no benefit to be gained by operating in pure O_2.

3.2 Results Involving Quantum Yields of Removal of Sulphides

The major purpose of this work was to examine the photo reactions of odorous sulphides and to determine the quantum yield of removal of the sulphides CH_3SH, CH_3SCH_3 and CH_3SSCH_3. The quantum yield is defined as the number of molecules of reactant removed per photon absorbed by the gas mixture.

$$\phi = \frac{\text{no. of molecules decomposed}}{\text{no. of photons absorbed}}$$

3.2.1 The Quantum Yield of CH_3SH Removal

The molecular rate of CH_3SH removal is a linear function of the rate of photon absorption (Figure 22). This linearity would be expected of a reaction which is induced by mercaptan photon absorption. The line best fitting these points yields a slope of 13.9 which indicates an average quantum yield of 13.9 molecules of mercaptan removed per photon absorbed. The average standard deviation of the quantum yields is 4.03 (29%). The slope of 13.9 represents the data well within one standard deviation. The point 0, 0 has been included since the reaction is initiated by absorption of energy by the sulphide molecule. At 0, 0 there is no absorption, hence no reaction. The slope of the line is linear at very low concentrations since the main chain-propagating species are involved more with oxygen - and hence are interacting with a reactant at a constant concentration - than with sulphur containing species. Thus the chain effect will be operating at normal rate

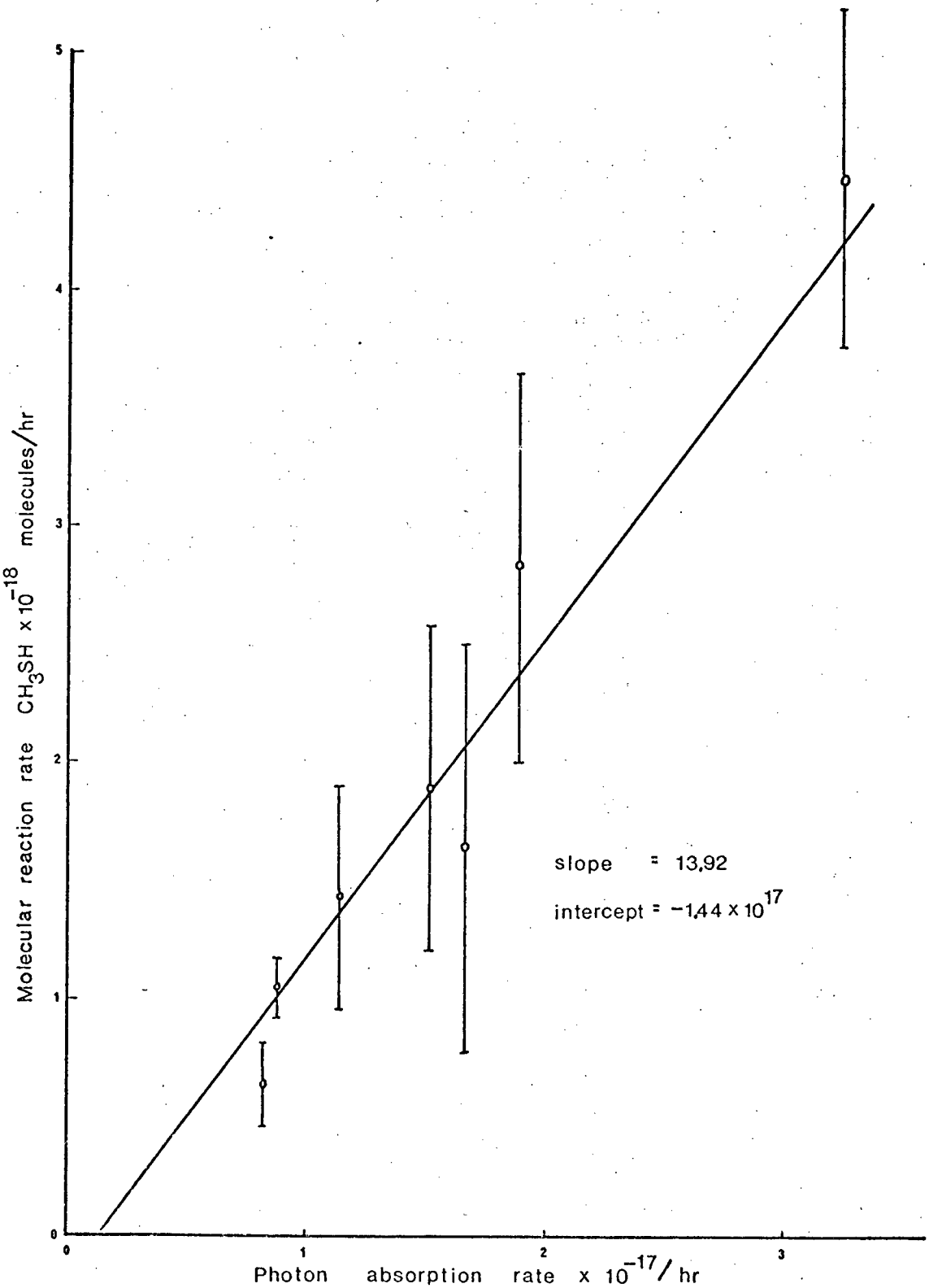

Figure 22. Molecular reaction rate of CH_3SH vs. photon absorption rate.

even at low sulphide concentration. This point will be further covered in the chain mechanism discussion.

The reaction rate can be described as a linear function of the range of CH_3SH concentrations studied (2.67×10^{-6} g/ml to 13.37×10^{-6} g/ml or 5.56×10^{-5} M to 2.78×10^{-4} M).

$$R_{-SH} = 13.9\ Ia - 1.44 \times 10^{17} \text{ molecules/hr}$$

R_{-SH} = molecular rate of CH_3SH decomposition

Ia = absorbed photon intensity

Φ_{SS} = quantum yield of CH_3SSCH_3 appearance

The major sulphur-containing products were sulphur dioxide, dimethyl disulphide and an oily yellow liquid which was deposited primarily about the entrance area of the inside of the reactor cell. The photo-excited mercaptan molecule forms a methyl thiyl radical which subsequently oxidizes or which may combine with another methyl thiyl to form dimethyl disulphide.

The quantum yield of decomposition of CH_3SH was found to be as shown in Table 5. Φ_{SO_2} = quantum yield of SO_2 appearance.

Table 5

Quantum Yields in CH_3SH Photolysis

$[CH_3SH]$ $\times 10^5$ M	$I_a \frac{\text{eins.}}{\text{l s}} \times 10^{10}$	Φ_{-SH}	σ	N	Φ_{SO_2}	Φ_{SS}
5.56	9.29	8.28	2.22	10	-	-
8.35	9.31	12.19	2.03	4	-	-
11.1	20.7	12.73	4.01	11	-	-
11.1	14.6	12.61	4.53	28	-	-
11.1	18.6	15.13	4.43	9	2.35	5.09
16.7	19.3	9.79	5.18	10	-	-
27.8	40.17	12.91	2.07	13	1.58	4.14
	Average	11.97	4.16	85		

A quantum yield in excess of 1 must involve a chain reaction mechanism to continue the reaction beyond the initial photo-excitation. Low pressure photolyses of CH_3SH in the absence of O_2 indicated a quantum yield of 1.7 when extrapolated to zero pressure (1, 18). When oxygen is present, it appears to be involved in the chain propagating sequence.

The reactions in Table 6 are proposed to explain the reaction of CH_3SH and the appearance of observed photoproducts. The proposed rates of reaction are based on a reaction taking place in air containing 20% O_2 (8.17×10^{-3} M). The sample concentration is chosen based on 150 µℓ of methyl mercaptan in a 40 ml reaction cell, which is equivalent to 1.53×10^{-4} M. Reactions involving atomic oxygen have been calculated assuming that the atomic oxygen concentration is 10^{-13} the concentration of molecular oxygen.

3.2.1.1 The Initiation Reactions

It is proposed that the initial reaction involves photolytic scission of methyl mercaptan (3-1, 3-2) into a methyl thiyl radical and hot hydrogen atom, or into a methyl radical and a mercaptan radical. These reactions have been well documented in the literature (1,2,3,4,5,6,7,10,11,14,15,16, 17,18,19,21,26,27,28). Reaction 3-1 has been found to predominate at the wavelengths of this investigation and greater than 90% of the initiation reactions may be expected to occur in this manner. Reaction 3-2 does occur, especially at shorter absorbed wavelengths. The photo-products of these initiating reactions provide the species to form a reaction chain which is responsible for further CH_3SH decompositions.

Table 6

Reactions involved in the Photolytic Oxidation of Methyl Mercaptan

		ΔHf_{298} kcal/mol.	Rate Constant	Relative Rate of Reaction
	INITIATION			
1.	$CH_3SH + h\nu \rightarrow CH_3S + H$		>.9	
2.	$CH_3SH + h\nu \rightarrow CH_3 + SH$			
	REACTIONS INVOLVING H ATOMS			
3.	$H + CH_3SH \rightarrow H_2 + CH_3S$	-18.5	$2.71 \times 10^{8}\ M^{-1}\ s^{-1}$	$R = 4.1 \times 10^{4}[H]\ s^{-1}$
4.	$H + O_2 + M \rightarrow HOO + M$	-47.	$1.99 \times 10^{10}\ M^{-2}\ s^{-1}$	$R = 6.65 \times 10^{6}\ [H]\ s^{-1}$
5.	$H + O + M \rightarrow HO + M$	-102.1	$7.24 \times 10^{9}\ M^{-2}\ s^{-1}$	R = low due to low [O] · [H] product
6.	$H + CH_3 \rightarrow CH_4$	-104.7	-	R = low due to low [H] · [CH_3] product
	REACTIONS INVOLVING THE CH_3S RADICAL			
7.	$CH_3S + O_2 \rightarrow CH_3O + SO$	-25.3	$8.39 \times 10^{2}\ M^{-1}\ s^{-1}$	$R = 6.86[CH_3S]\ s^{-1}$
8.	$CH_3S + O \rightarrow CH_3 + SO$	-53.6	$1.3 \times 10^{6}\ M^{-1}\ s^{-1}$	$R = 1. \times 10^{-9}\ [CH_3S]\ s^{-1}$
9.	$CH_3S + CH_3S + M \rightarrow CH_3SSCH_3 + M$		$2.5 \times 10^{10}\ M^{-1}\ s^{-1}$	$R = 2.5 \times 10^{10}\ [CH_3S]^2\ s^{-1}$
10.	$CH_3S + CH_3O \rightarrow CH_3SOCH_3$	-47.6	-	- low
11.	$CH_3S + CH_3OO \rightarrow CH_3SOOCH_3$		-	- low
	REACTIONS INVOLVING THE CH_3O AND CH_3OO RADICALS			
12.	$CH_3O + O_2 \rightarrow HCHO + HOO$	-26.2	$4.5 \times 10^{5}\ M^{-1}\ s^{-1}$	$R = 3.26 \times 10^{3}\ [CH_3O]\ s^{-1}$
13.	$CH_3O + CH_3SH \rightarrow CH_3OH + CH_3S$	-18.1	-	R = lower than 12 since $[CH_3SH] < [O_2]$
14.	$CH_3OO + CH_3SH \rightarrow CH_3OOH + CH_3S$		-	-
	REACTIONS INVOLVING HOO RADICALS			
15.	$HOO + CH_3SH \rightarrow HOOH + CH_3S$	- 3.36	$1.15 \times 10^{9}\ M^{-1}\ s^{-1}$	$R = 17.6\ [HOO]\ s^{-1}$
16.	$HOO + SO_2 \rightarrow SO_3 + HO$	-19.	$5.4 \times 10^{5}\ M^{-1}\ s^{-1}$	R = lower than 15 since $[SO_2] < [CH_3SH]$
	REACTIONS INVOLVING CH_3 RADICALS			
17.	$CH_3 + O_2 + M \rightarrow CH_3OO + M$		$1 \times 10^{9}\ M^{-1}\ s^{-1}$	$R = 8.17 \times 10^{6}\ [CH_3]\ s^{-1}$
18.	$CH_3 + O \rightarrow HCHO + H$	-70.	$6 \times 10^{10}\ M^{-1}\ s^{-1}$	$R = 4.9 \times 10^{-5}\ [CH_3]\ s^{-1}$
19.	$CH_3 + CH_3SH \rightarrow CH_4 + CH_3S$	-19.2	$1.8 \times 10^{4}\ M^{-1}\ s^{-1}$	$R = 2.75\ [CH_3]\ s^{-1}$
	REACTIONS INVOLVING ATOMIC O RADICALS			
20.	$O + CH_3SH \rightarrow CH_3S + OH$	-16.6	2×10^{7} to 9×10^{10} & $M^{-1}\ s^{-1}$	$R = 3.06 \times 10^{3}\ [O]$ to $1.37 \times 10^{7}\ [O]\ s^{-1}$
21.	$O + O + M \rightarrow O_2 + M$	-119.1	$3.8 \times 10^{8}\ M^{-2}\ s^{-1}$	R = low due to low $[O]^2$
22.	$O + O_2 + M \rightarrow O_3 + M$	-24.9	$1.96 \times 10^{8}\ M^{-2}\ s^{-1}$	$R = 6.54 \times 10^{4}\ [O]\ s^{-1}$
	REACTIONS INVOLVING SO RADICALS			
23.	$SO + O_2 \rightarrow SO_2 + O$	-13.03	$1.5 \times 10^{4}\ M^{-1}\ s^{-1}$	$R = 1.22 \times 10^{2}\ [SO]\ s^{-1}$
24.	$SO + O \rightarrow SO_2$	-59.72	no recommendation	-
	REACTIONS INVOLVING SH RADICALS			
25.	$SH + O_2 \rightarrow SO + OH$	-25.5	$< 6 \times 10^{7}\ M^{-1}\ s^{1}$	$R = 4.9 \times 10^{5}\ [SH]$
26.	$SH + O \rightarrow SO + H$	-40.5	$9.6 \times 10^{10}\ M^{-1}\ s^{-1}$	$R = 7.8 \times 10^{-8}\ [SH]$
	OTHER REACTIONS			
27.	$CH_3SSCH_3 + h\nu \rightarrow 2CH_3 + S_2$		-	-
28.	$OH + CH_3SH \rightarrow H_2O + CH_3S$		$1.0 \times 10^{10}\ M^{-1}\ s^{-1}$	
29.	$2\ HOO \rightarrow HOOH + O_2$		$2.0 \times 10^{9}\ M^{-1}\ s^{-1}$	

Basis: [M] = 4.09×10^{-2} M

$[CH_3SH]$ = 150 µℓ/cell

= 1.53×10^{-4} M

$[O_2]$ = .2 Atm = 8.17×10^{-3} M

$[O] = 1 \times 10^{-13}\ [O_2]$

3.2.1.2 Reactions Involving H Atoms

The hydrogen atom generated in 3-1 is a very reactive species. The atom will contain a great deal of kinetic energy for the first few collisions following lysis. The atom may react with CH_3SH, O_2, O or CH_3 in the reaction atmosphere. The abstraction of the sulphydryl hydrogen atom from methyl mercaptan (3-3) has been described in the literature (3,6,10,11, 15,17,18).

$$H + CH_3SH \rightarrow H_2 + CH_3S \qquad (3\text{-}3)$$

$$\Delta H_f = -18.5 \text{ kcal/mol}$$

Steer and Knight [10] found the abstraction rate to be independent of temperature. They photolysed CH_3SH in the presence of ethylene [10]. The hydrogen atom was found to add to ethylene as well as to enter into (3-3). The ratio of the metathesis to

$$H + C_2H_4 \rightarrow C_2H_5$$

$$k = 1.17 \times 10^8 \ M^{-1} \ s^{-1}$$

the addition, was found to be 2.32 ± .11. This ratio was found to be independent of ethylene pressure up to 200 torr. Pratt and Veltman (62) determined the rate constant for the reaction of hydrogen atoms with ethylene. At 295°K the rate constant was determined to be $1.17 \times 10^8 \ M^{-1} \ s^{-1}$. Thus the rate constant for (3-3) will be

$$k_3 = 2.32\ (1.17 \times 10^8) = 2.71 \times 10^8\ M^{-1}\ s^{-1}$$

This would imply a rate of reaction of

$$R_3 = 2.71 \times 10^8\ (1.53 \times 10^{-4}\ M)\ [H] = 4.14 \times 10^4\ [H]\ s^{-1}$$

The hydrogen atom is more likely to react with oxygen molecules in the atmosphere because of the high O_2 concentration.

$$H + O_2 + M \rightarrow HOO + M \qquad (3\text{-}4)$$

$$k = 1.99 \times 10^{10} \quad M^{-2}\ s^{-1}$$

Hampson and Garvin [52] suggest a bimolecular rate constant of $k = 6.42 \times 10^9\ M^{-2}\ s^{-1}$ measured in argon gas. They suggest that air ($O_2 + N_2$) is 3.1 times as efficient a medium for forming the HOO radical. Thus a reaction rate constant of $k = 1.99 \times 10^{10}\ \ell^2\ M^{-2}\ s^{-1}$ is suggested for air. Now this rate of reaction is governed by the concentrations of the reacting species and also of air.

$$R_4 = k_4\ [H]\ [O_2]\ [M]$$

We do not know the hydrogen atom concentration so it will be necessary to compare rates by factoring out the hydrogen atom concentration. Thus

$$R_4 = \left(1.99 \times 10^{10}\ \frac{}{M^2 s}\right)\left(8.179 \times 10^{-3}\ M\right)\left(4.09 \times 10^{-2}\ M\right)$$

$$= 6.65 \times 10^6\ [H]\ \frac{M}{s}$$

where $k_4 = 1.99 \times 10^{10}$ $M^{-2}\ s^{-1}$

$[O_2]$ = .2 atm @ 25°C = 8.179×10^{-3} M

[M] = 1 atm @ 25°C = 4.09×10^{-2} M

This rate is 2.64 times the rate for (3-3) which is a minimum since the rate of reaction (3-3) was established as an upper limit. The presence of a CH_3 group on the mercaptan would likely decrease the rate of (3-3) substantially.

The reaction of a hydrogen atom with atomic oxygen (3-5) is very exothermic (ΔH_f = -102.1 kcal/mol). The available data on this atomic reaction is based on temperatures in the range 1000 → 3000 °K [52].

$$H + O + M \rightarrow OH + M \qquad (3\text{-}5)$$

ΔH_f = -102.1 kcal/mol

$k \sim 7.24 \times 10^9$ $M^{-2}\ s^{-1}$ in Ar

This reaction is not a major sink for hydrogen atoms due to the low concentration of oxygen atoms which are in the atmosphere. The rate of this reaction may be estimated assuming an atomic oxygen concentration 10^{-5} that of molecular O_2.

$$R = k_5 [H] [O] [M]$$

$$= \left(7.24 \times 10^9 \ \frac{}{M^2 s}\right) \left(8.17 \times 10^{-8}\ M\right) \left(4.09 \times 10^{-2}\ M\right) [H]$$

$$= 2.4 \times 10^1 [H]$$

This rate is insignificant relative to other H atom reaction rates.

The reaction of atomic hydrogen with the methyl radical (3-6) is also very exothermic.

$$H + CH_3 \rightarrow CH_4 \qquad (3\text{-}6)$$

$$\Delta H_f = -104.7 \text{ kcal/mol}$$

There is no reaction rate data available for this reaction. The rate, however large the reaction rate constant, will depend upon the concentration product of two very low-concentration radicals. This is a factor which removes reaction (3-6) as a major sink for H atoms.

The major sink for hydrogen atoms is most likely reaction (3-4). This reaction generates the hydrogen peroxy radical which is a very reactive species. The HOO radical will react with reduced species in the reaction gas mixture.

3.2.1.3 Reactions Involving the Methyl Thiyl Radical

The methyl thiyl radical is the species most closely involved in the oxidation sequence of sulphur to SO_2. The oxidation reaction appears to occur in two steps. The first is the formation of SO after which the SO is more slowly oxidized to SO_2 [15,16]. Callear and Dickinson [5] showed that the presence of 10 torr O_2 suppressed the 215.8 nm absorption band of the CH_3S radical 5 micro-seconds after flashing the CH_3SH. They did not investigate the SO_2 bands, however this did indicate a rapid rate of reaction of the CH_3S radical with O_2 molecules. A two-step sequence for the oxidation of H_2S by flash photolysis has been suggested [35,36,38,40]. McGarvey and McGrath [35] observed the oxidation of H_2S under flash photolytic conditions. The

flash was found to rapidly produce SO absorption bands which were characterized by a broad-band absorption spectrum extending from 200 nm to 250 nm. A Lyman discharge was used as the source of background continuum for the absorption spectroscopy. After one millisecond, the broad bands of SO were still present and SO_2 absorption bands were beginning to appear. The long-lived nature of the SO absorption bands suggests a slow transition from the SO to the SO_2. Norrish and Zelenberg [40] found H_2S combustion to form S_2O_2 which was the stable form of SO at room temperature. The S_2O_2 later formed SO_2.

The sequential oxidation of the sulphur-containing species CH_3S and HS is therefore postulated for this photolytic oxidation.

Due to the high concentration of O_2, the majority of the oxidation reaction is accomplished by reaction (3-7).

$$CH_3S + O_2 \rightarrow CH_3O + SO \qquad (3\text{-}7)$$

$$\Delta H_f = -25.3 \text{ kcal/mol}$$

The oxidation rate constant for reaction (3-7) may be estimated by comparing the oxidation rate to the rate of recombination of CH_3S. By estimating the radical concentration from the known rate of CH_3SSCH_3 formation, and from the product balance (73% disulphide) the rate constant for CH_3S oxidation may be evaluated relative to the recombination rate constant. A detailed calculation may be found in Appendix H.

$$k_7 = 8.39 \times 10^2 \text{ M s}^{-1}$$

$$R_7 = (8.39 \times 10^2)\ (8.17 \times 10^{-3} \text{ M})\ [CH_3S]$$

$$= 6.86\ [CH_3S]$$

A secondary mechanism for sulphur oxidation is that due to atomic oxygen (3-8).

$$CH_3S + O \rightarrow CH_3 + SO \qquad (3\text{-}8)$$

$$\Delta H_f = -53.6 \text{ kcal/mol}$$

$$k_8 = 1.34 \times 10^6 \quad M^{-1} s^{-1}$$

There is no direct measurement for this reaction rate constant but the analogy may be made to the oxidation of HS:

$$HS + O \rightarrow H + SO$$

$$k = 9.63 \times 10^{10} \quad M^{-1} s^{-1} \text{ [52]}$$

The rate of the methyl sulphide oxidation may be slower by a ratio similar to the speed ratio of the molecular oxygen oxidation of CH_3S to that of HS. The ratio is 8.4×10^2 M s^{-1} (this work) to 6×10^7 M s^{-1} [52]. This would suggest a k_8 value of

$$\frac{8.4 \times 10^2}{6 \times 10^7} \left(9.6 \times 10^{10}\right) = 1.34 \times 10^6$$

from which for $[O] = 10^{-13} [O_2]$

$$R_8 = 1.0 \times 10^{-9} [CH_3S] \ s^{-1}$$

The methyl thiyl radical may escape oxidation temporarily by combining with another CH_3S to form CH_3SSCH_3.

$$CH_3S + CH_3S + M \rightarrow CH_3SSCH_3 + M \qquad (3\text{-}9)$$

$$k_9 = 2.5 \times 10^{10} \quad M^{-1}s^{-1}$$

Dimethyl disulphide is found as the major product and this reaction must have a very high rate constant considering the low concentration of the

CH_3S radical. A rate constant for sulphur atom recombination has been suggested by Hampson and Garvin [52]

$$S + S + M \rightarrow S_2 + M$$

we assume $k = 2.5 \times 10^{10}$ M s^{-1}

$k \simeq 4.09 \times 10^{10}$ M^{-1} s^{-1} in 1 atm. [M] [52]

This would appear to suggest a rate based on $[CH_3S]^2$ which would be quite small. The actual rate must be several times that of the oxidation reaction since a sulphur mass balance indicated that CH_3SSCH_3 accounted for 73% of the reacted CH_3SH sulphur atoms whereas 16.8% of the reacted sulphur atoms appeared as SO_2 (Table 11).

The CH_3S radical can react with either the methoxy or the methyl peroxy radical to form CH_3SOCH_3 and CH_3SOOCH_3 (3-10, 3-11).

$$CH_3S + CH_3O \rightarrow CH_3SOCH_3 \qquad (3\text{-}10)$$

$$CH_3S + CH_3OO \rightarrow CH_3SOOCH_3 \qquad (3\text{-}11)$$

The rate of formation of these compounds will undboutedly be low since it will be proportional to the product of two low reactive radical concentrations. Chromatographic analysis failed to show the presence of either of these compounds.

3.2.1.4 Reactions Involving the Methoxy and Methyl Peroxy Radicals

The methoxy radical is formed in the CH_3S oxidation (3-7) and by decay of the CH_3OO radical. The major source is (3-7). The CH_3O may react with either O_2 or CH_3SH - the molecules of greatest concentration (3-12, 3-13).

$$CH_3O + O_2 \rightarrow HCHO + HOO \qquad (3\text{-}12)$$

$$k_{12} = 4.0 \times 10^5 \quad M^{-1}\ s^{-1}\ [61]$$

$$CH_3O + CH_3SH \rightarrow CH_3OH + CH_3S \qquad (3\text{-}13)$$

$$\Delta H_f = -18.1\ \text{kcal/mol}$$

The rate constant of k_{12} 4.0×10^5 $M^{-1}\ s^{-1}$ was selected by Adachi and James [61] for reaction (3-12) at an oxygen pressure of one atmosphere. At an oxygen concentration in air of 8.17×10^{-3} M, the rate of reaction (3-12) may be expected to be 3.26×10^3 $[CH_3O]$ s^{-1}.

There is no data upon which to base a reaction rate estimate for (3-13). The reaction rate is likely lower than (3-12) because the concentration of CH_3SH is lower than that of O_2.

The methyl peroxy radical is formed from the oxidation of methyl radicals generated by reactions (3-2), (3-8) and (3-27). This CH_3OO radical may react with reduced species in the gaseous environment and is expected to react with CH_3SH as in (3-14).

$$CH_3OO + CH_3SH \rightarrow CH_3OOH + CH_3S \qquad (3\text{-}14)$$

The production of the CH_3S radical allows chain continuation by way of reaction (3-7).

3.2.1.5 Reactions Involving the Hydrogen Peroxy Radical

The hydrogen peroxy radical is generated by the reaction of molecular oxygen with the methoxy radical (3-12). The HOO radical may be expected to react with reduced species - in particular CH_3SH - and also with SO_2.

$$HOO + CH_3SH \rightarrow HOOH + CH_3S \qquad (3\text{-}15)$$

$$\Delta H_f = -3.36 \text{ kcal/mol}$$

$$k_{15} = 1.15 \times 10^5 \ M^{-1} \ s^1$$

$$HOO + SO_2 \rightarrow SO_3 + HO \qquad (3\text{-}16)$$

$$\Delta H_f = -19 \text{ kcal/mol}$$

$$k_{16} = 5.4 \times 10^5 \quad M^{-1} \ s^{-1} \ [52]$$

There is no measure of the rate of reaction (3-15) in the literature. The rate constant may be estimated by calculating a steady-state [HOO] as in Appendix H. The SO_2 oxidation by HOO (3-16) has been reported [52] to proceed with a rate constant of $k_{16} = 5.4 \times 10^5 \quad M^{-1} \ s^{-1}$. It is reasonable to expect that reaction (3-15) will proceed with a rate constant in excess of that for (3-16). The overall rate of reaction (3-15) is expected to be greatest due to the higher concentration of CH_3SH than of SO_2.

3.2.1.6 Reactions Involving Methyl Radicals

Methyl radicals are generated in the initial photolysis reaction (3-2) and during the oxidation of the CH_3S radical (3-7). An additional

minor source of CH_3 radicals is from the elimination of elemental sulphur from dimethyl disulphide (3-27). The methyl radical is an extremely reactive species and will react rapidly with the oxygen and sulphide species in the reaction matrix. Adachi and James [61] have investigated the reactions of methyl radicals in an oxygen-containing atmosphere. The major reaction of the CH_3 radical in an oxygen-containing atmosphere is to produce the methyl peroxy radical (3-17).

$$CH_3 + O_2 + M \rightarrow CH_3O_2 + M \qquad (3\text{-}17)$$

$$k_{17} = 1 \times 10^9 \quad M^{-1}\ s^{-1}$$

The rate constant k_{17} is suggested by Baulch *et al.* [52] whereas Adachi and James [61] used the value $k_{17} = 3.1 \times 10^8 \quad M^{-1}\ s^{-1}$ established by Basco (1972). The choice of a lower k_{17} value placed more severe restrictions on their calculation of the fraction of CH_3 radicals to form CH_3OO radicals and they chose the lower rate constant for that reason. Extending the Basco estimate to atmospheric O_2 concentrations suggests the rate of methyl radical oxidation to be $R_{17} = 8.17 \times 10^6\ [CH_3]\ s^{-1}$. The methyl peroxy radical can mutually interact with itself forming the methoxy radical and other products

$$2CH_3OO \rightarrow 2CH_3O + O_2$$

$$\rightarrow CH_3OH + HCHO + O_2$$

$$\rightarrow CH_3OOCH_3 + O_2$$

$$k = 3.5 \times 10^8 \quad M^{-1}\ s^{-1}\ [61]$$

Adachi and James developed a computer simulation of the methyl radical oxidation and concluded that, in a nitrogen-oxygen mixture, the CH_3OO radical is

the predominant species [61]. At a high O_2 concentration (79% vol; 3.23 x 10^{-2} M), 99.97% of available CH_3 radicals were converted to CH_3OO radicals within the first 50 μs after flash formation of the CH_3. The HOO concentration reached 12% of the initial concentration of CH_3OO at 1900 μs after the flash. When the oxygen concentration was lowered to 2.4% $\frac{V}{V}$ (1 x 10^{-3} M), 96.9% of the available CH_3 radicals formed CH_3OO and only 3.1% formed CH_3O. The HOO concentration was maximum at 3.1%, 4400 μs after initiation. It is apparent that the greatest portion of methyl groups which oxidize will form the methyl peroxy radical. A small portion of the methoxy groups will be formed from mutual interaction of the CH_3OO groups.

The methyl radical may also react with atomic oxygen as in (3-18).

$$CH_3 + O \rightarrow HCHO + H \qquad (3\text{-}18)$$

$$k_{18} = 6 \times 10^{10} \quad M^{-1}\ s^{-1}\ [52]$$

$$\Delta H_f = -70\ \text{kcal/mol}$$

This reaction is quite rapid but will play a small part in the oxidation of the methyl radical due to the low concentration product of two reactive radicals ($[CH_3]$ and $[O]$). Assuming an atomic oxygen concentration 10^{-13} that of molecular oxygen, the rate of oxidation may be expected to be $R = 4.9 \times 10^{-5}\,[CH_3]\ s^{-1}$.

An alternative to oxidation of the methyl radical is reaction with mercaptan to form methane (3-19)

$$CH_3 + CH_3SH \rightarrow CH_4 + CH_3S \qquad (3\text{-}19)$$

$$k_{19} = 1.8 \times 10^{4} \quad M^{-1}\ s^{-1}\ [54]$$

$$\Delta H_f = -19.2\ \text{kcal/mol}$$

This reaction rate constant is much lower than those of the competing reactions and thus is likely to contribute only slightly to the overall rate of removal of the methyl radical. Assuming an initial concentration of CH_3SH of 1.53 x 10^{-4} M. The relative reaction rate of (3-19) would be R = 2.75 $[CH_3]$. This relative rate is low enough to be disregarded.

3.2.1.7 Reactions Involving Atomic Oxygen Radicals

The atomic oxygen radical is generated during the oxidation of the SO radical (3-23). This highly reactive species may react with CH_3SH, O_2 or O itself. The reaction of CH_3SH and O will most likely oxidize the thiyl hydrogen atom as in (3-20).

$$O + CH_3SH \rightarrow CH_3S + OH \qquad (3\text{-}20)$$

$$\Delta H_f = -16.6 \text{ kcal/mol}$$

$$k_{20} = 2 \times 10^7 \text{ to } 9 \times 10^{10} \quad M^{-1} s^{-1} \text{ [52]}$$

The reaction rate constant for this reaction is estimated from data for the oxidation of HS ($k = 9 \times 10^{10}$ $M^{-1} s^{-1}$) and for the oxidation of H_2S ($k = 2.03 \times 10^7$ $M^{-1} s^{-1}$). The data for HS may represent the CH_3SH case more accurately since the sulphur group is the largest atom of the group and the H atom will represent a similar steric factor for both CH_3SH and SH. Assuming a CH_3SH concentration of 1.53 x 10^{-4} M, reaction rates will range from 3.06 x 10^3 $[O]$ s^{-1} to 1.37 x 10^7 $[O]$ s^{-1}.

Atomic oxygen may also combine to re-form molecular oxygen as in (3-21).

$$O + O + M \rightarrow O_2 + M \qquad (3\text{-}21)$$

$$k_{21} = 3.8 \times 10^8 \quad M^{-2}\ s^{-1}$$

$$\Delta H_f = -119.1 \text{ kcal/mol}$$

This reaction will have a relative rate of $1.5 \times 10^7\ [O]^2\ s^{-1}$ when in an air thermalizing medium. The expected concentration of O species is sufficiently low that the square reduces the expected rate of reaction (3-21) below the range of consideration.

Atomic and molecular oxygen may react to form ozone as in (3-22).

$$O + O_2 + M \rightarrow O_3 + M \qquad (3\text{-}22)$$

$$k_{22} = 1.96 \times 10^8 \quad M^{-2}\ s^{-1}$$

$$\Delta H_f = -24.9 \text{ kcal/mol}$$

At an oxygen concentration of 8.17×10^{-3} M (room air at 25°C), assuming O_2 and N_2 are equally good third bodies, the expected reaction rate would be $R = 6.54 \times 10^4\ [O]\ s^{-1}$.

The predicted rates of reaction for reactions (3-20), (3-21) and (3-22) suggest that the reactions with CH_3SH and with O_2 may be equally important as pathways for atomic oxygen reaction.

3.2.1.8 Reactions Involving Sulphur Monoxide Radicals

The rate of oxidation of SO radicals has been suggested as being slower than the reaction forming SO. The radical may be oxidized by either molecular or atomic oxygen as in reactions (3-23) and (3-24).

$$SO + O_2 \rightarrow SO_2 + O \qquad (3\text{-}23)$$

$$k_{23} = 1.5 \times 10^4 \quad M^{-1}\ s^{-1}$$

$$\Delta H_f = \text{-}13 \text{ kcal/mol}$$

$$SO + O \rightarrow SO_2 \qquad (3\text{-}24)$$

$$\Delta H_f = -59.7 \text{ kcal/mol}$$

The molecular reaction (3-23) will be the predominant reaction in an air environment due to the greater O_2 concentration. At prevailing O_2 concentrations a reaction rate of $R = 1.22 \times 10^2\ [SO]\ s^{-1}$ may be expected.

3.2.1.9 Reactions Involving Sulphydryl Radicals

The sulphydryl radical may react by oxidizing with either molecular or atomic oxygen; (3-25) or (3-26).

$$SH + O_2 \rightarrow SO + OH \qquad (3\text{-}25)$$

$$k_{25} < 6 \times 10^7 \quad M^{-1}\ s^{-1}\ [52]$$

$$\Delta H_f = -25.5 \text{ kcal/mol}$$

$$SH + O \rightarrow SO + H \qquad (3\text{-}26)$$

$$k_{26} = 9.6 \times 10^{10} \quad M^{-1}\ s^{-1}$$

$$\Delta H_f = -40.5 \text{ kcal/mol}$$

The molecular oxidation will proceed at a rate $R = 4.9 \times 10^5\ [SH]\ s^-$ for normal air concentrations of oxygen. The atomic oxidation (3-26) may be expected to proceed at a rate of $R = 7.8 \times 10^{-5}[SH]\ s^{-1}$ in air. The molecular oxidation is the most significant mechanism for removal of the SH radical.

3.2.1.10 Reactions Eliminating Elemental Sulphur

Photolysis of CH_3SSCH_3 has been suggested to directly expel elemental sulphur (3-27) [5].

$$CH_3SSCH_3 + h\nu \rightarrow 2CH_3 + S_2 \qquad (3\text{-}27)$$

Data upon the quantum yield of this reaction is lacking. The reaction may be involved in the production of the yellowish, oil deposit found on the inside of the cell walls. The deposit has also been noticed during reactions which do not involve CH_3SSCH_3 so that other reactions expelling S_2 must also be contributing. There is not sufficient evidence from this work to further speculate on the nature of these reactions.

3.2.2 The Chain Mechanism

The slope of the molecular reaction rate versus absorbed photon rate (Figure 22) indicates a quantum yield of 13.9 molecules decomposed per photon absorbed. For the quantum yield to exceed one, a chain mechanism must be in operation in order to propagate a free-radical chain of species which will react with other CH_3SH molecules in the surrounding atmosphere. Table 7 lists the major reactions which are involved in the chain propagating mechanism. The reaction is initiated by photon absorption and the subsequent lysis of the CH_3SH molecule into H, CH_3S, CH_3 and SH radicals. These four species are all very reactive and are capable of reacting with species in the reaction atmosphere in such a manner as to increase the number of chain carrying species. Each of the reactions included in the list of chain propagators is one in which the reacting radical produces another radical

Table 7

The Chain Mechanism

INITIATION REACTIONS

$CH_3SH + h\nu \rightarrow CH_3S + H$	(3-1)
$CH_3SH + h\nu \rightarrow CH_3 + SH$	(3-2)

CHAIN PROPAGATING REACTIONS

$CH_3S + O_2 \rightarrow CH_3O + SO$	(3-7)
$CH_3S + O \rightarrow CH_3 + SO$	(3-8)
$H + O_2 + M \rightarrow HOO + M$	(3-4)
$H + CH_3SH \rightarrow H_2 + CH_3S$	(3-3)
$CH_3 + O_2 + M \rightarrow CH_3OO + M$	(3-17)
$HOO + CH_3SH \rightarrow HOOH + CH_3S$	(3-15)
$SO + O_2 \rightarrow SO_2 + O$	(3-23)
$CH_3OO + CH_3SH \rightarrow CH_3OOH + CH_3S$	(3-14)
$CH_3O + CH_3SH \rightarrow CH_3OH + CH_3S$	(3-13)
$CH_3O + O_2 \rightarrow HCHO + HOO$	(3-12)
$SH + O_2 \rightarrow SO + OH$	(3-25)
$OH + CH_3SH \rightarrow H_2O + CH_3S$	(3-28)
	(3-29)

TERMINATING REACTIONS

$CH_3S + CH_3S + M \rightarrow CH_3SSCH_3 + M$	(3-9)
$CH_3S + CH_3O \rightarrow CH_3SOCH_3$	(3-10)
$CH_3S + CH_3OO \rightarrow CH_3SOOCH_3$	(3-11)
$2HOO \rightarrow HOOH + O_2$	(3-29)

which is capable of reacting in a manner which will ultimately react with another CH_3SH molecule. The species produced by the chain propagators are CH_3S, CH_3, CH_3O, CH_3OO, and HOO.

Perhaps the most important reactions in chain propagation are (3-4) and (3-7). The hydrogen atom reaction with molecular oxygen preserves the reactive radical as HOO. The HOO is able to react with CH_3SH to form HOOH (3-15) and a CH_3S radical which will oxidize and further supply chain carrying radicals. The methyl thiyl oxidation (3-7) is a reaction which produces two reactive radicals as products (CH_3O and SO). The oxidation of SO (3-23) produces an oxygen atom which continues the chain. The CH_3O radical reacts with O_2 to form a HOO radical (3-12). The O atom will react with CH_3SH (3-20) to continue the chain or will react with O_2 to form O_3 which itself is likely to react with CH_3SH. The HOO radical will react with CH_3SH (3-15) to remove a further CH_3SH and to release the CH_3S radical as a chain propagator.

The removal of the subsequent CH_3SH molecules creates reactive products which themselves continue the reaction. At the concentrations studied, the chain length has proven to be 13.9 reactions of CH_3SH.

The chain reaction is terminated by the quenching of reactive species primarily by recombination with other active species (3-9, 3-10, 3-11). The recombination of two CH_3S radicals (3-9), is responsible for the formation of CH_3SSCH_3 - a major reaction product. CH_3SOCH_3 is formed from the combination of CH_3O and CH_3S as in (3-10). CH_3SOOCH_3 is formed from recombination by CH_3S and CH_3OO radicals (3-11). These reactions account for the formation of compounds identified in the photolysis of CH_3SH and CH_3SCH_3. Recombinations of this sort are responsbile for terminating two chain sequences and do not produce radicals which continue the chain.

3.2.3 The Quantum Yield of CH_3SH Oxidation as a Function of Atmospheric Pressure

Table 8

The Effect of Atmospheric Pressure on the Quantum Yield of CH_3SH Decomposition

Concentration of CH_3SH and Pressure		Average Quantum Yield	σ	%	Number of Trials
2.55×10^{-4} M/ℓ	1 atm	12.9	2.07	16	13
2.55×10^{-4} M/ℓ	½ atm	6.4	4.0	62	17
2.55×10^{-4} M/ℓ	¼ atm	10.9	4.3	39	5

The quantum yields of CH_3SH removal at 1 atmosphere and at ¼ atmosphere are not significantly different. The yield at ¼ is not significantly different from that at ½ atmosphere. The yield at ½ atmosphere is only slightly signficantly different from that at 1 atmosphere. Thus it does not seem reasonable to conclude that the CH_3SH oxidation reaction is affected by atmospheric pressure as long as there is a large excess of oxygen.

3.2.4 The Quantum Yield of Dimethyl Sulphide Decomposition

The quantum yield of dimethyl sulphide oxidation was investigated at both atmospheric pressure and at ¼ atmosphere. The quantum yield of decomposition was found to increase significantly with decreasing pressure (Figure 23).

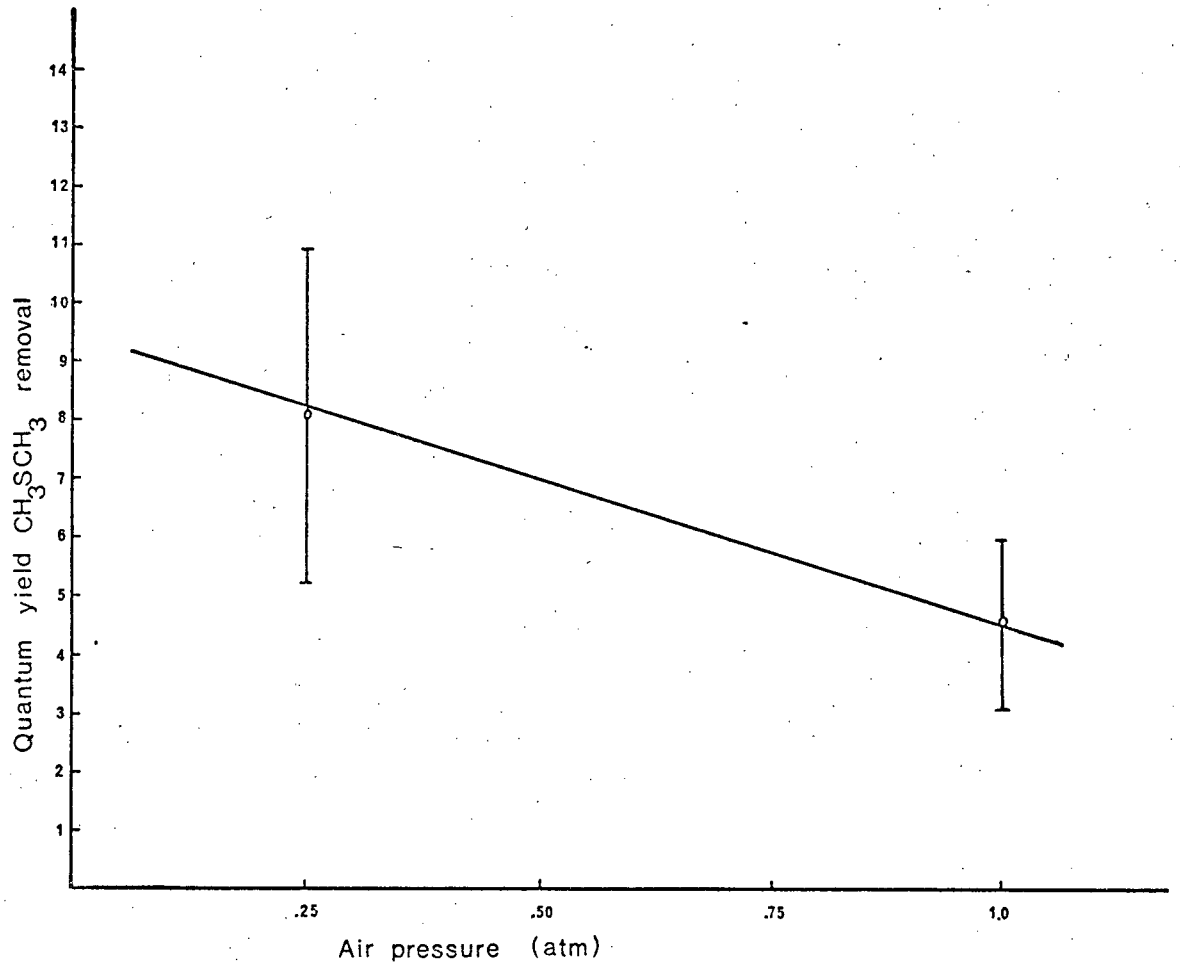

Figure 23. The quantum yield of CH_3SCH_3 decomposition vs. atmospheric pressure of air.

Table 9

The Quantum Yeild of Dimethyl Sulphide Decomposition

v.s. Atmospheric Pressure

$CH_3\ SCH_3$	Pressure Atm	Absorbed Photons	R x Rate	ϕ	σ	n
1.71×10^{-4} M	1	.04 (1.934×10^{18})	74.2×6^{-6} g/hr	4.07	1.6	10
1.71×10^{-4} M	¼	.04 (1.615×10^{18})	64.25×10^{-6} g/hr	8.02	2.9	6

The low rate of reaction of dimethyl sulphide is due to the fact that the compound absorbs only very short wavelength ultra-violet radiation (Figure 3). Most mercury discharge lamps provide only low levels of illumination in this region. The deuterium discharge provides extended short wavelength emission, however, ½ μℓ (ℓ) of CH_3SCH_3 in a 10 cm, 40 ml cell, absorbed only 4% of the incident energy below 300 nm.

3.2.5 The Quantum Yield of Dimethyl Disulphide Decomposition

Table 10

The Quantum Yield of Dimethyl Disulphide Decomposition

Disulphide Per Cell	Fractional Absorbance	Reaction Rate	Quantum Yield	No. Trials	σ
7.05×10^{-5} M	28.4%	93.6×10^{-6} g/hr	1.96	40	.94
14.10×10^{-5} M	42.8%	90.5×10^{-6} g/hr	1.27	7	.825

The quantum yield of dimethyl disulphide decomposition is not significantly affected by a change in reactant concentration (Figure 24). The average quantum yield of decomposition is 1.67. The low quantum yield suggests the presence of few successful chain carriers to continue the reactions initiated by the photochemical sequence. The low yield also suggests that CH_3O and HOO radicals, when produced by CH_3S oxidation, do not successfully attack the CH_3SSCH_3 molecule in a manner which would decompose the molecule.

The initial photochemical activation forms two methyl thiyl radicals from the disulphide [5, 8, 9, 20]. The low rate of decomposition indicates that the main fate of the CH_3S radicals is to recombine to reform disulphide. There was no evidence of CH_3SH formation during disulphide photolysis and SO_2 was the only detectable product.

The chain sequence is very short however there is the possibility that atomic oxygen formed from CH_3S oxidation contributes to the chain in the following manner:

$$CH_3SSCH_3 + h\nu \rightarrow 2CH_3S$$

$$CH_3S + O_2 \rightarrow CH_3O + SO$$

$$SO + O_2 \rightarrow SO_2 + O$$

$$O + CH_3SSCH_3 \rightarrow CH_3S + CH_3 + SO$$

The hydrogen peroxy radical may also participate; however, the interaction between HOO and CH_3SSCH_3 is not easily predictable.

$$CH_3S + O_2 \rightarrow CH_3O + SO$$

$$CH_3O + O_2 \rightarrow HCHO + HOO$$

$$HOO + CH_3SSCH_3 \rightarrow \text{products}$$

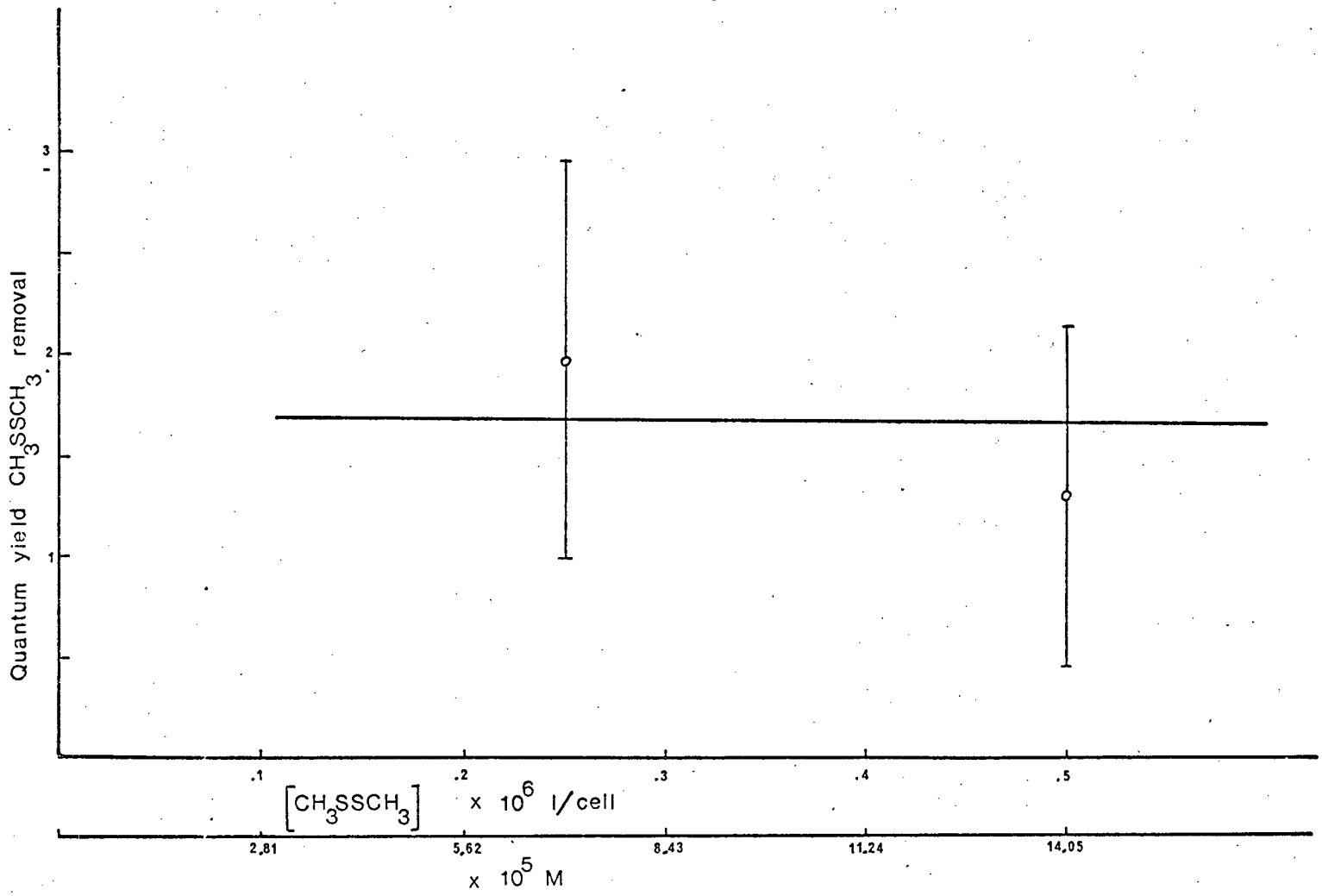

Figure 24. The quantum yield of CH_3SSCH_3 decomposition vs. concentration of sulphide.

3.3 Other Experimental Studies

3.3.1 The Effect of Added Sulphur Dioxide

Sulphur dioxide is a major reaction product of the CH_3SH oxidation and thus must be considered as a possible quencher or promoter of the oxidation reaction. Sulphur dioxide has a significant extinction coefficient in the wavelengths of interest for CH_3SH oxidation. It might therefore absorb light to form a photo-excited species which could transfer energy to other reacting species. The series of runs was done with 50 µℓ CH_3SH using 50 µℓ and 100 µℓ addends of SO_2 to the reaction cell.

Table 11

The effect of Added Sulphur Dioxide

CH_3SH	SO_2	SH Rate	% Absorbed Light	ϕ
50 µℓ	0 µℓ	53.05×10^{-6} g/hr	6.13%	8.24
50 µℓ	50 µℓ	57.2×10^{-6} g/hr	15.05%	3.61
50 µℓ	100 µℓ	53.5×10^{-6} g/hr	32.3%	1.57

Figure 25 shows the variation of CH_3SH oxidation rate with added SO_2. There is no significant effect on the mercaptan oxidation rate due to SO_2 addition for low total amounts of light absorbed by the reacting gas mixture. This indicates that there is no energy transfer from the photo-excited SO_2 species to the reacting mercaptan molecules. The SO_2 does absorb a significant amount of ultra-violet light which would otherwise not be absorbed by the CH_3SH-air mixture. Due to the increased absorption the effective quantum yield of CH_3SH decomposition becomes reduced. Figure 26

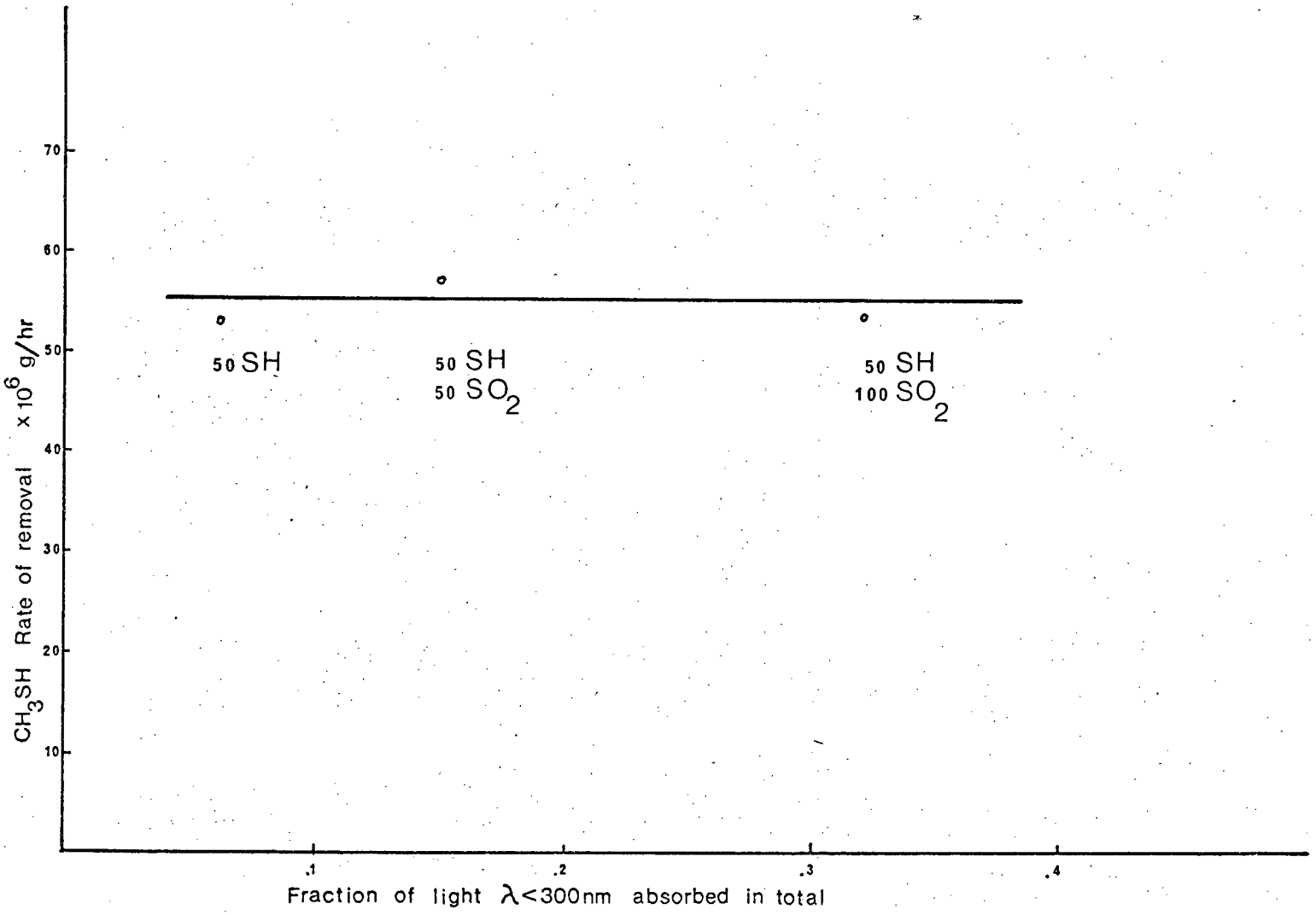

Figure 25. Reaction rate of CH_3SH vs. fraction of light absorbance with added SO_2.

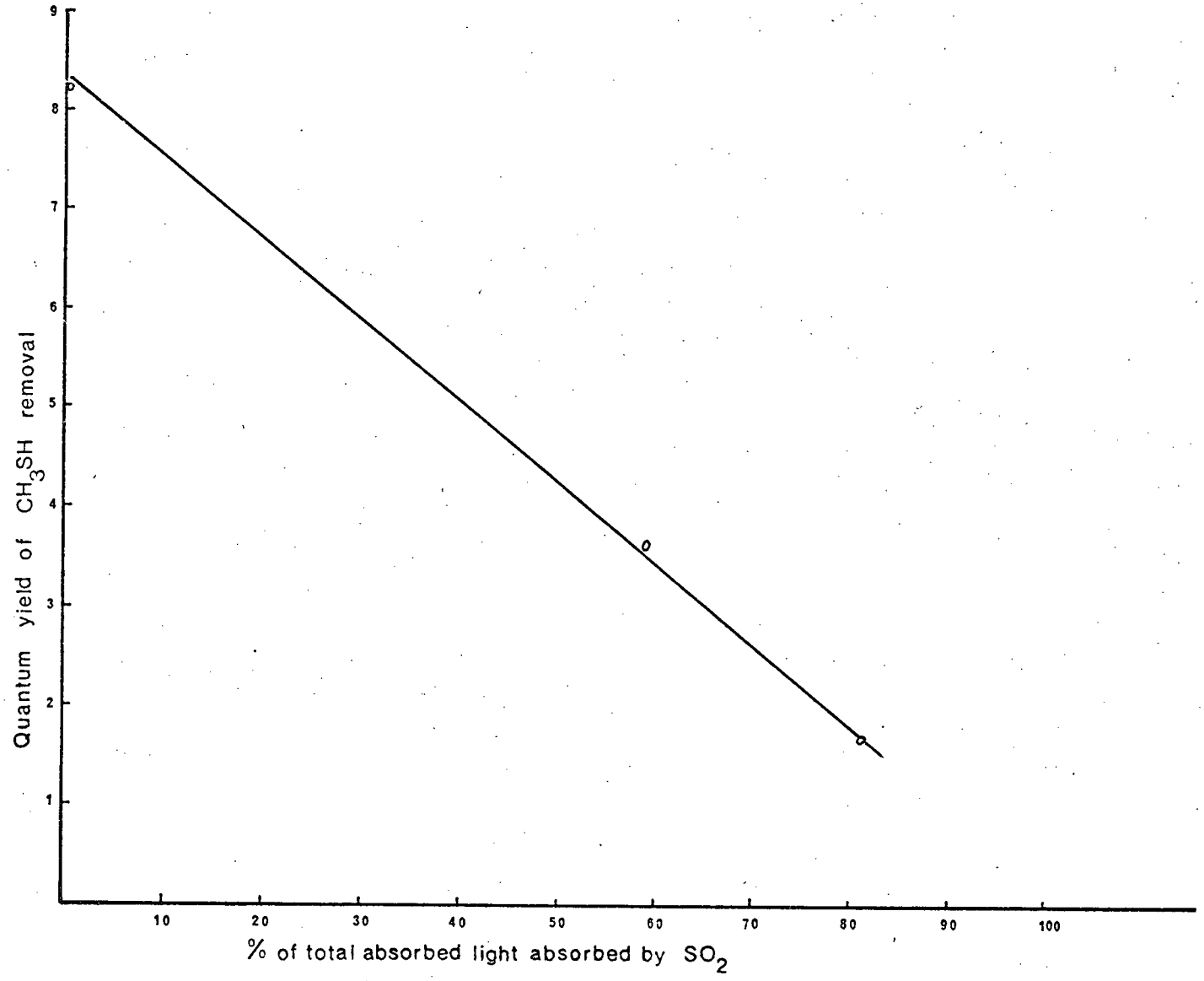

Figure 26. Quamtum yield of CH_2SH removal vs. % total of total light absorbed by SO_2.

indicates that the quantum yield is inversely proportional to the amount of light absorbed by the SO_2. Thus the major effect of the presence of SO_2 in the reaction atmosphere is to absorb light which would otherwise be available to initiate CH_3SH reaction.

3.3.2 A Sulphur Balance for Methyl Mercaptan Oxidation

The CH_3SH oxidation experiments were monitored both optically and chromatographically to determine the production of reaction products containing sulphur. The SO_2 production was most effectively monitored by gas chromatography. The optical absorbance at 290 nm was monitored during the reaction to follow the combined production of CH_3SSCH_3 and SO_2. The reaction showed a linear production rate of species absorbing at 290 nm.

The absorption coefficients for CH_3SH, SO_2 and CH_3SSCH_3 were determined by measuring known quantities of known gases in the cell. The absorption coefficients at 290 nm are shown in Table 12.

The total absorbance was considered to be the sum of that due to SO_2, CH_3SH and CH_3SSCH_3.

$$\log \frac{I}{I_0} = -(10 \text{ cm})\Big[(3.249 \times 10^3)[SO_2] + (18.304)[CH_3SH] + (1.390 \times 10^3)[CH_3SSCH_3]\Big]$$

The concentrations of CH_3SH and SO_2 were known chromatographically and that of CH_3SSCH_3 was found by difference from the total absorbance at 290 nm.

Table 12

The Absorption Coefficients for CH_3SH, SO_2, CH_3SCH_3 and CH_3SSCH_3

		This Work		Calvert & Pitts [59]		Deviation
CH_3SH	225 nm	147.1 $\frac{}{M\ cm}$	2.29 x 10^3 $\frac{cc}{g\ cm}$	165 $\frac{}{M\ cm}$	2.57 x 10^3 $\frac{cc}{g\ cm}$	+12.4%
CH_3SH	290 nm	-	18.3	-	-	-
SO_2	290 nm	207.9	3.24 x 10^3	228.6	3.57 x 10^3	+9.95%
CH_3SCH_3	215 nm	340	5.31 x 10^3	454	7.09 x 10^3	+33.5%
CH_3SSCH_3	250 nm	456	7.12 x 10^3	300	4.68 x 10^3	-34%
CH_3SSCH_3	290 nm	131	1.39 x 10^3	59	9.22 x 10^3	-55%

Table 13

A Sulphur Balance Based on 25 Minutes CH_3SH

Oxidation Per ml Reaction Volume

	100 µℓ Runs	250 µℓ Runs
S Atoms Lost as CH_3SH	2.712×10^{16} $\frac{\text{Atoms}}{\text{ml}}$	4.8449×10^{16} $\frac{\text{Atoms}}{\text{ml}}$
S Atoms Found as SO_2	$.458 \times 10^{16}$ "	$.5688 \times 10^{16}$ "
% of S lost	16.8%	11.7%
S Atoms Found as CH_3SSCH_3	1.981×10^{16} $\frac{\text{Atoms}}{\text{ml}}$	2.973×10^{16} $\frac{\text{Atoms}}{\text{ml}}$
% of S lost	73.04% "	60.8% "
TOTAL % FOUND	89.95%	73.1%

Experiments conducted at 100 µℓ per reaction cell were able to account for 89.9% of the sulphur reacted. Experiments conducted at 250 µℓ/cell were able to account for 73.1% of the sulphur atoms decomposed as CH_3SH.

A significant amount of sulphur also appeared as a pale yellow deposit on the inside of the reaction cell. The heaviest deposit occurred on the entrance window. The deposit was not large enough to analyze chemically but was examined under the optical microscope and under the scanning electron microscope. X-ray emission spectra from the deposit under electron bombardment confirmed the presence of sulphur in the deposit. The deposit was produced during both photolysis and light scattering studies of CH_3SH, CH_3SCH_3, CH_3SSCH_3 and SO_2. The deposit was not included in the sulphur balance.

3.3.3 The Quantum Yield of Product Formation for Sulphur Dioxide and Dimethyl Disulphide

The major products of the photo-oxidation of methyl mercaptan are sulphur dioxide and dimethyl disulphide. For the initial stages of the reaction, the product formation may be described in the form of a quantum yield of appearance based on the amount of light absorbed by the reacting compound, CH_3SH. The resulting quantum yields of product formation are shown in Table 14.

Table 14

The Quantum Yields of Product Formation

CH_3SH Level	100 μℓ/cell	250 μℓ/cell
ϕ SO_2 Formation	2.355	1.585
ϕ CH_3SSCH_3 Formation	5.096	4.144

The quantum yield of appearance of sulphur atoms should equal the yield of disappearance. Since dimethyl disulphide contains two sulphur atoms, then the atomic quantum yield balance should appear as:

$$\phi_{SH\ decomp.} = \phi_{SO_2} + 2\phi_{CH_3SSCH_3}$$

For the 100 μℓ runs using the average quantum yield of decomposition of 13.9:

$$13.9 \simeq 2.3 + 2(5.1) = 12.5$$

This agrees within 10% and suggests that some light produces products other than SO_2 and CH_3SSCH_3. The sulphur-containing cell deposit may account for the imbalance.

3.3.4 The Deposit on the Inside Cell Wall

Photolysis of the sulphur-containing compounds is accompanied by the appearance of a yellow deposit on the inside of the photolysis cell. The deposit is most heavily concentrated on the entrance window of the cell. The deposit has the appearance of droplets of an oily liquid of yellowish colour. The yellow liquid is not soluble in H_2O, CCl_4, $CHCl_3$, CH_3OH or acetone [58] but is reported to be soluble in carbon disulphide [41]. Chromatographic analysis was not possible due to the difficulty of collecting the sample and due to the lack of known standards.

The deposit was found to give off a background emission during emission runs which required occasional cleaning of the cell. Cell cleaning was accomplished by baking the cell overnight at 500 °C in air. A similar deposit has been reported by other investigators of sulphur compound photolysis and emission effects [1,5,12,16,41,42,48]. Kamra and White [16] found the deposit to disappear by heating an oxygen-filled cell to an unstated temperature until the deposit was gone. Mass spectral analysis of the gases revealed SO_2. The investigators suspected elemental sulphur and thioformaldehyde condensing on the side walls.

Rao and Knight [12] found mass spectral analysis of the deposit to suggest a molecular weight about 258 and that the compound contained CH_2S and CH_3S groups. Luria *et al.* [58] observed the appearance of a clear oil which turned brown with time. This deposit appeared on the inside cell wall

of the reaction vessel. Luria was photolysing a mixture of SO_2 and allene. An aerosol was found to form which was similar to the aerosol Heicklen found upon photolysis of SO_2-acetylene mixtures [58]. An elemental analysis was attempted but was not successful. The aerosol was found to grow in particle size throughout the run but did not grow in particle number. The aerosol was felt to deposit on the sides of the reaction vessel. The deposit, in my experiments, was responsible for a general decrease in short wavelength transmission of the reaction vessel. The transmission decrease was directly related to the amount of sulphur-containing gas which had been decomposed in the cell.

Photographs of the deposit with an optical microscope reveal a series of larger droplets surrounded by much smaller droplets (Figures 27, 28). The larger droplets may have been formed from the condensation of smaller droplets since there is a zone of clearing around each larger droplet.

Scanning electron microscope photographs reveal a more flat deposit which has decreased in diameter and moved to the side (Figure 29). A visible perimeter gives evidence of the original shape and location of the droplet (Figure 29c). The "change" of shape is a result of evaporation during the high-vacuum carbon evaporation cycle of scanning electron microscope sample preparation at which time the sample was rotated at 10^{-5} mm pressure to ensure a uniform carbon coating which provided electrical conductivity. The evaporation of deposit reveals that some of the deposit is volatile and some of the deposit is much less volatile. The less volatile portion of the deposit was found to blister and evaporate under 20 KeV electron bombardment (Figure 29d). The electron beam can be used to stimulate x-ray emission characteristic of atomic species and is able to detect sodium atoms and those of higher atomic

weight. An emission spectrum was run on the cell window and on the window plus deposit (Figure 30). The upper curve reveals the peak for silicon found in the glass window. No sodium is seen in the glass due to the sodium removal stages in preparing suprasil synthetic silica. The lower curve shows the characteristic sulphur peak at 2.31 KeV as well as a silicon peak which results from the underlying window.

Photographs of the sample and of the points of x-ray emission characteristic in energy for sulphur are superimposed in Figure 29d. The deposit is likely an organic polysulphide deposited from the molecular vapour state. Subsequent rephotolysis of the deposit on the surface likely results in long chain formation.

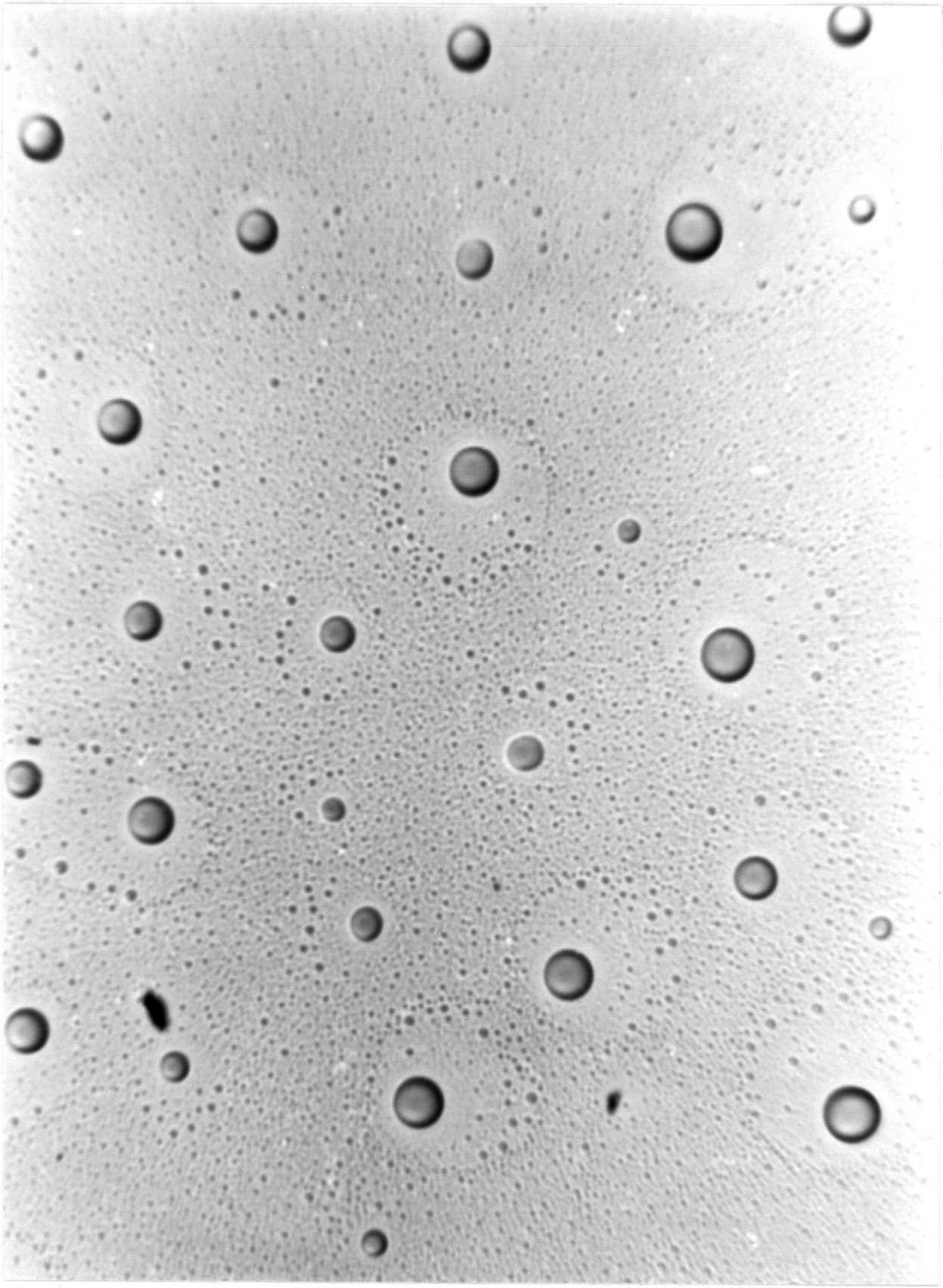

Figure 27. Photomicrograph of cell deposit.

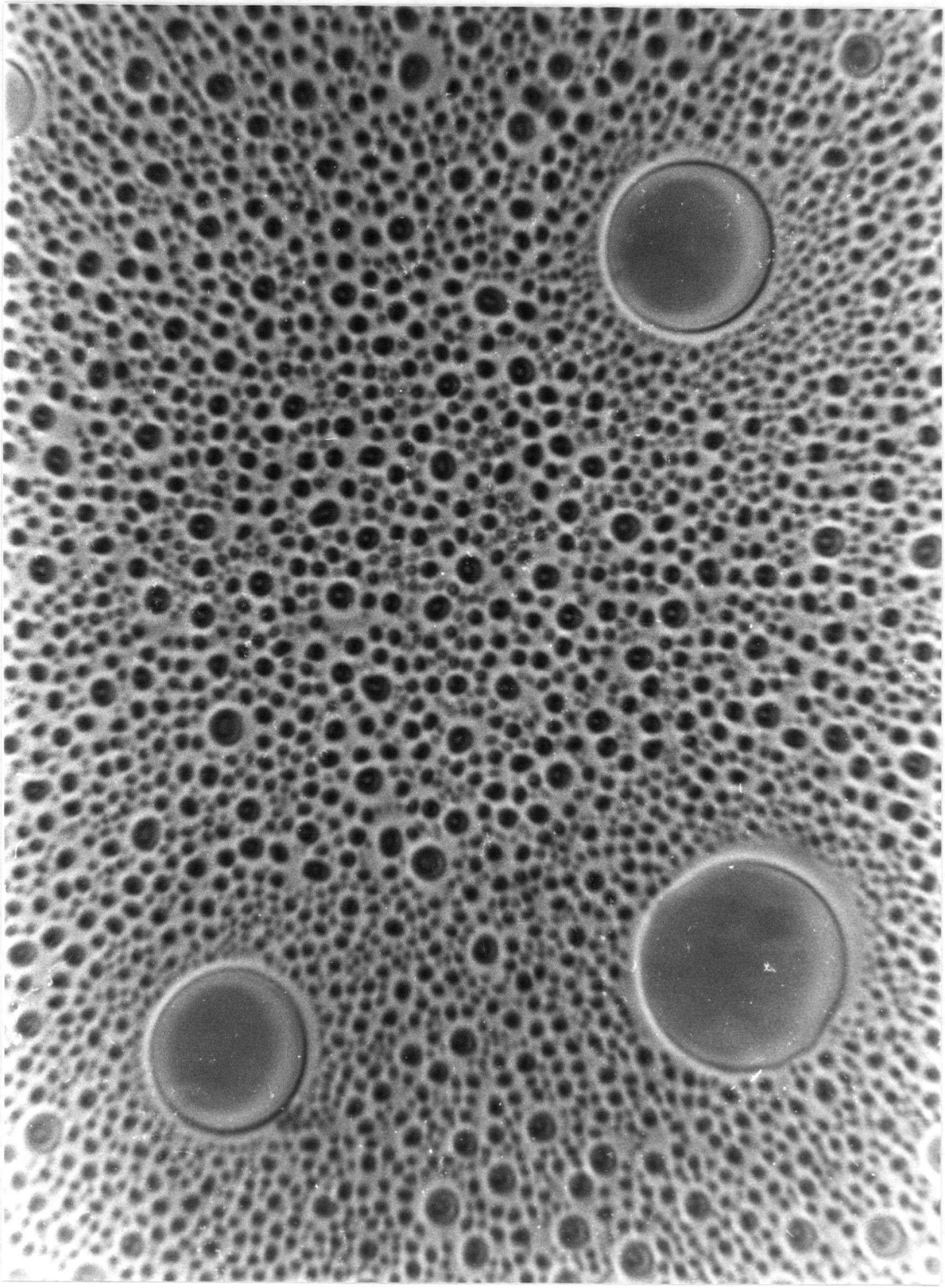

Figure 28. Photomicrograph of cell deposit.

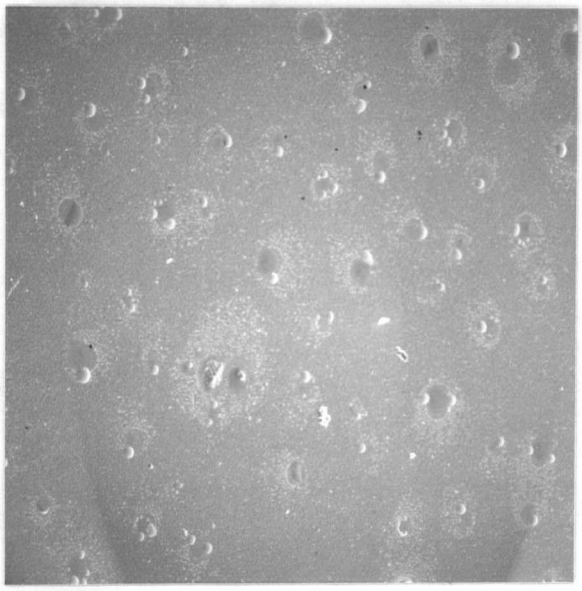

Figure 29a. Photolysis cell deposit x 100 • 10 KV.

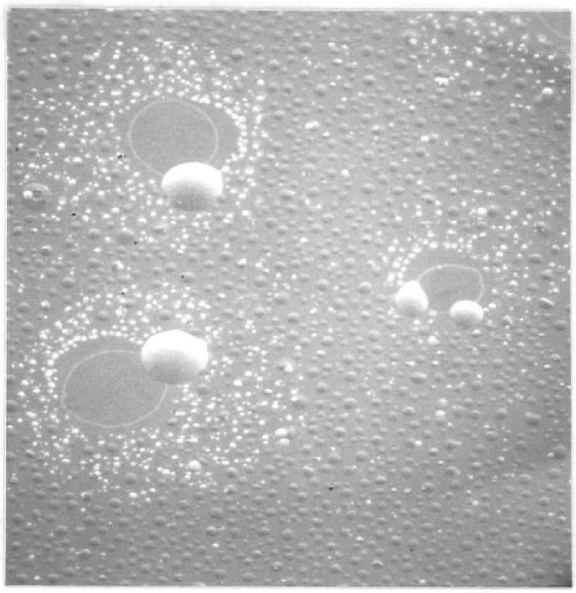

Figure 29b. Photolysis cell deposit x 400 • 20 KV.

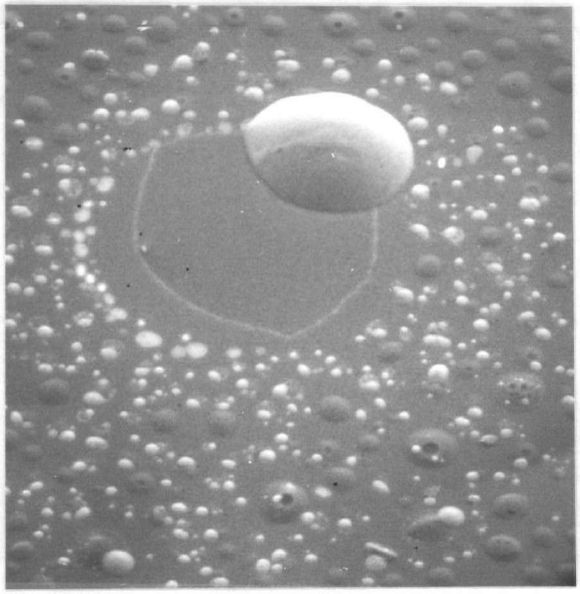

Figure 29c. Photolysis cell deposit x 1000 • 10 KV.

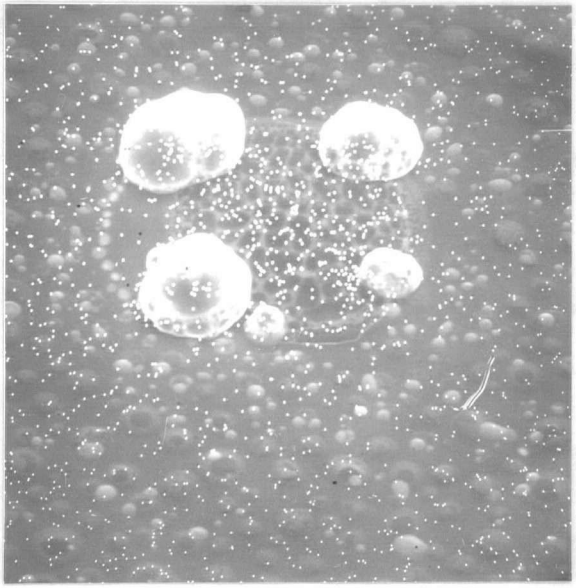

Figure 29d. Sulphur x-ray emission sources superimposed over the cell deposit x 1000 • 20 KV.

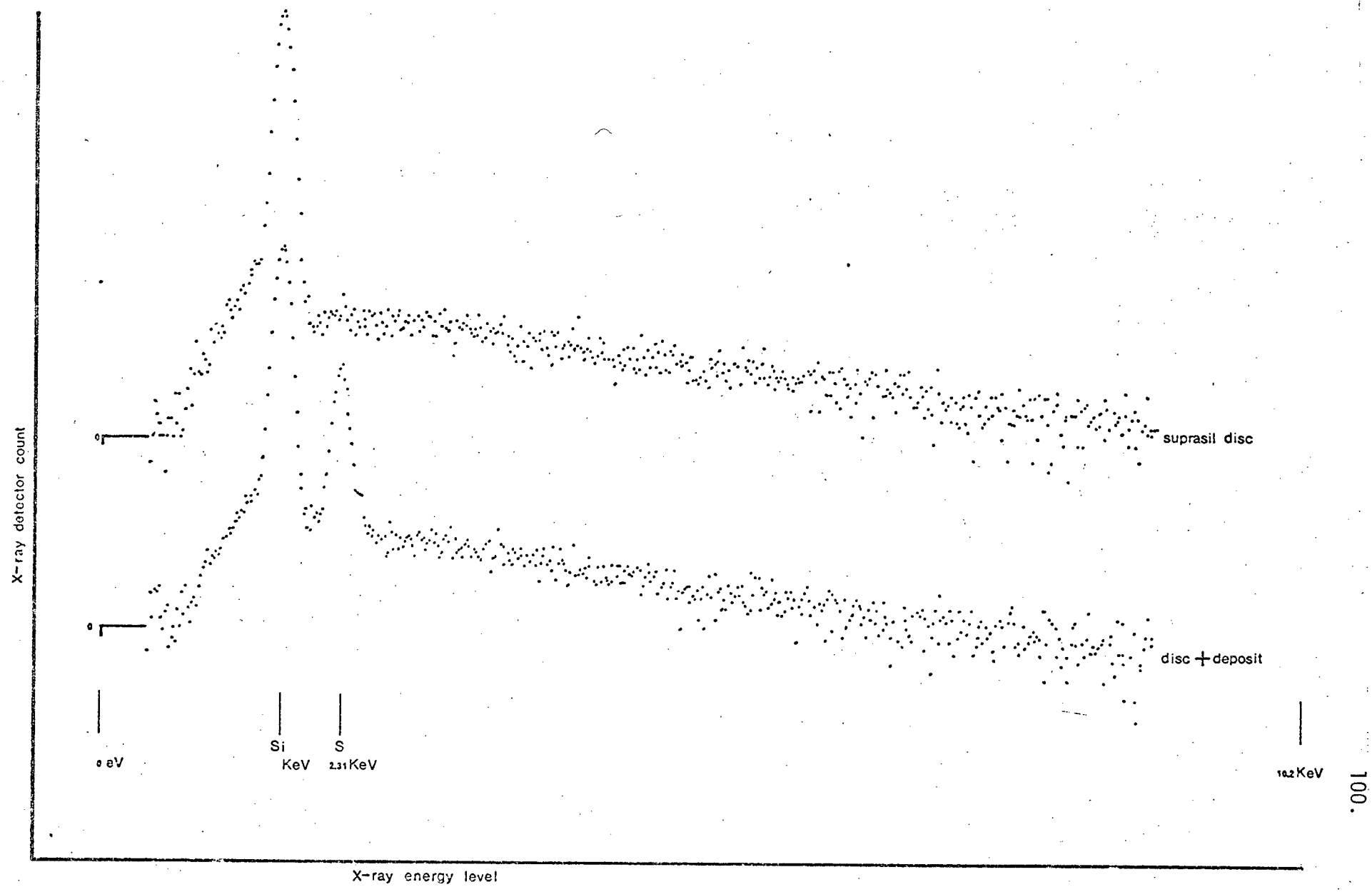

Figure 30. X-ray emission spectrum of cell wall deposit on end window of "zero" cell.

Chapter 4

LIGHT EMISSION FROM SULPHUR-CONTAINING ATMOSPHERES

4.1 Observation and Time Dependence

The reaction apparatus was modified from the form of a transmission spectrophotometer into a configuration which would allow photo-electric observation at 90° to the incident light path (Figure 11). This configuration was chosen in an attempt to detect light emission from the sulphur-containing gases as they underwent the photo-oxidation reaction. The arrangement was fully enclosed by a dark shroud and light reflection from the side of the containment vessel was eliminated by masking the entrance window so that the vessel sides were not illuminated. The gases CH_3SH, CH_3SCH_3, CH_3SSCH_3, H_2S and SO_2 were illuminated for five minutes in the polychromatic light beam and the spectrum of light emission was recorded with a 3.2 nm bandpass. Significant levels of light emission were recorded for H_2S, SO_2 and CH_3SCH_3 (Figure 31). The non-symmetrical sulphides CH_3SH and CH_3SSCH_3 did not emit significant levels of light (Figure 31). The spectrum of emission detected from the symmetrical sulphides was similar to the transmission spectrum in that the minimum at 280 nm in the SO_2 emission corresponded to the SO_2 absorption peak at 280 nm. The emission spectra begin at frequencies where the absorption coefficient for that particular gas is decreasing.

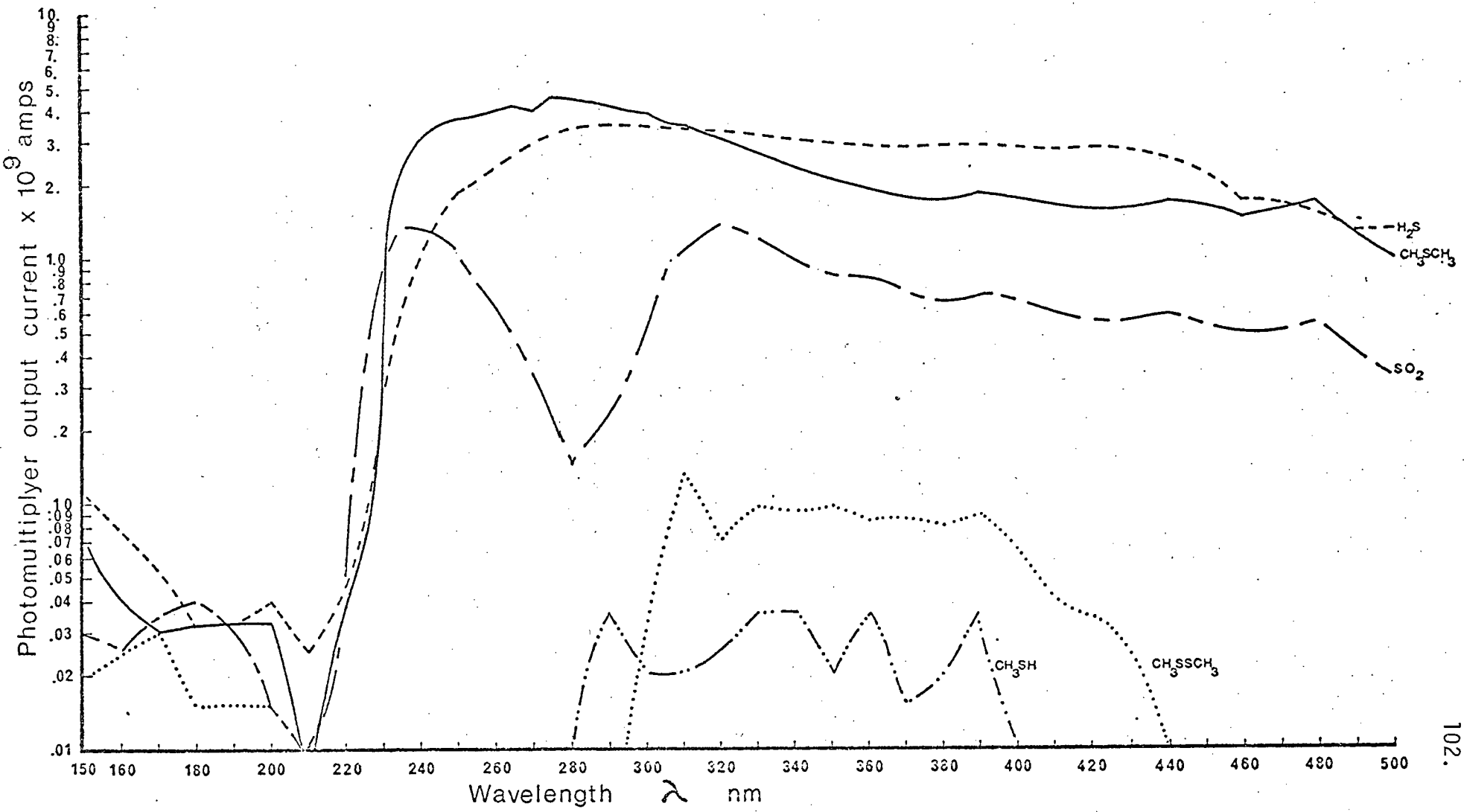

Figure 31. Emission intensity of sulphur-containing compounds under polychromatic illumination vs. wavelength.

During the course of other experiments the emission spectra were recorded at varying times after beginning illumination of the gas mixture. The intensity of the emitted light was found to vary depending on how long the gas mixture had been receiving illumination. In order to examine this apparent time-dependent behaviour, a series of experiments was performed at fixed wavelengths. The intensity of emission from a CH_3SCH_3-Air mixture was followed from the time of illumination using the 270 nm band. The time-dependent nature of the detected signal is shown in Figure 32. The emission slowly grew in intensity. After a period of six minutes the emission reached a maximum value and began a series of oscillations as the emitted intensity slowly decreased.

The same procedure was employed to examine the time-dependent behaviour of SO_2. The wavelengths of observation were chosen on either side of the 280 nm absorption peak of SO_2 so that a strong signal could be recorded. The results are shown in Figure 33a for the shorter wavelength 240 nm signal and in Figure 33b for the 320 nm signal. The initial level of emission develops as rapidly as can be measured by the recording equipment. This is a fluorescent emission from the excited SO_2 molecule. The initially low level increases until a plateau is reached after five or six minutes of illumination. Observation of the emission at 320 nm reveals somewhat different behaviour. The initial fluorescent emission is much stronger at 320 nm. The subsequent rise in emission intensity appears to experience a delay when monitored at the longer wavelength. The delay has exponential growth and suggests an initiating effect may be taking place and this initiation may be characterized by a wavelength dependence. The ultimate level of emission is established seven minutes after the start of illumination.

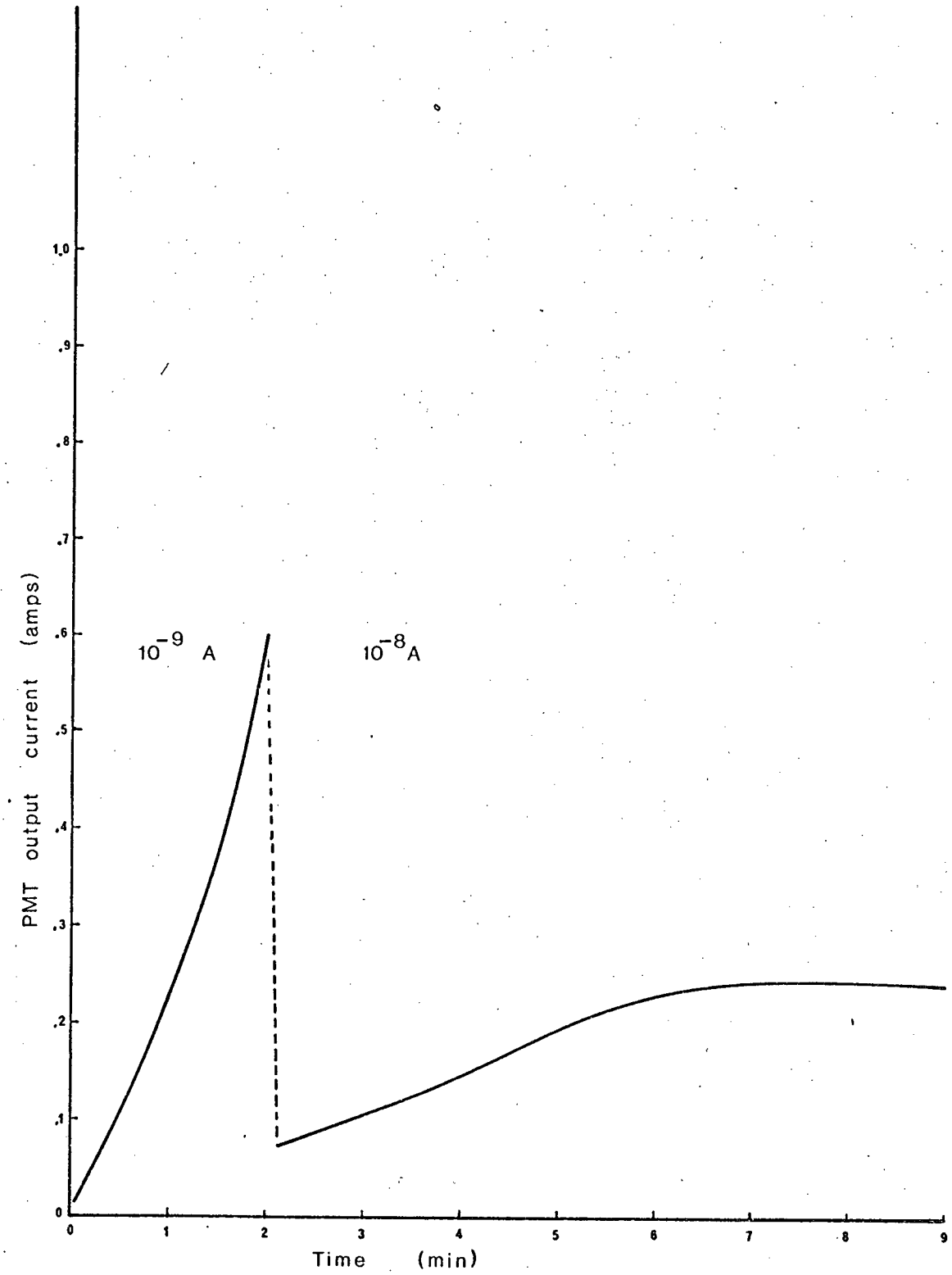

Figure 32. The time dependence of emission from CH_3SCH_3 in air (1 μℓ).

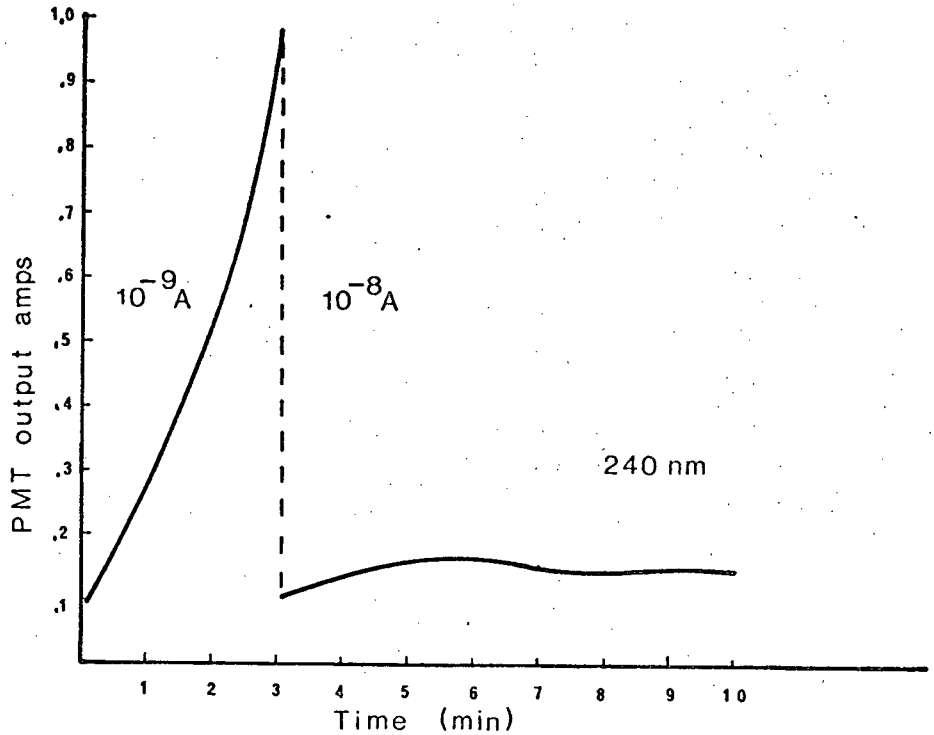

Figure 33a. The time dependence of SO_2 emission at 240 nm.

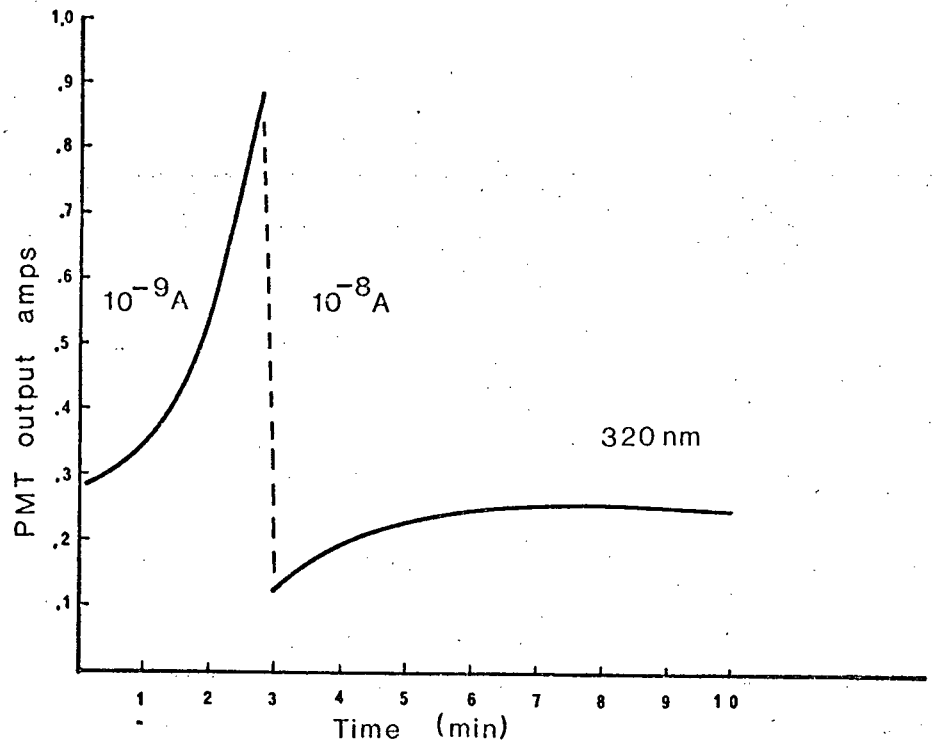

Figure 33b. The time dependence of SO_2 emission at 320 nm.

4.2 Possible Mechanisms to Describe the Delay of Emission

4.2.1 Fluorescence

The observation of a slow-developing component of emission required that the mechanism responsible for the emission be defined. Mechanisms which could have been involved include fluorescence and delayed fluorescence, chemiluminescence, impurity effects such as a reacting quenching agent and physical light scattering by possible aerosol formation. A fluorescent effect was not observed in the case of dimethyl sulphide. The emission did not display an instant level of emission and began the slow growth from a zero level of light emission (Figure 32). Fluorescence was noted for SO_2 at both 240 nm and 320 nm (Figure 33). The fluorescent component is much more significant at 320 nm (Figure 33b). The fluorescent component is a very small portion of the total emission even for SO_2 at 320 nm. A fluorescent emission occurs from the singlet photo-excited state and consequently is fully developed by the time the chart recorder records the initial emission level. Thus a fluorescent effect would not describe the slow-developing component of the emission.

4.2.2 Delayed Fluorescence

The phenomenon of delayed fluorescence involves a slow developing component of fluorescence which develops after the initial establishment of fluorescent emission. The slow component is due to thermal activation of the triplet pool to the first exicted singlet state from which fluorescence occurs. The E-type delayed fluorescence has been described by Parker [46] to occur as follows.

$A + h\nu \rightarrow A'$	activation
$Q + A' \rightarrow A + Q$	quenching
$A' \rightarrow A + h\nu$	fluorescence
$A' \rightarrow A^3$	inter-system-crossing
$A^3 \rightarrow A + h\nu$	phosphorescence
$A^3 + M \rightarrow A' \pm M$	energy absorption

A	ground state molecule
A'	singlet state molecule
A^3	triplet state molecule
M	atmospheric third body molecule

A delayed fluorescent effect would be expected to reach maximum intensity shortly after the triplet pool would reach its maximum population. This would be likely to occur very rapidly and a six minute time to maximum would be unlikely.

4.2.3 Chemiluminescence

The possibility that a chemiluminescent effect might be operating was investigated. The oxidation of the sulphur atom might have been responsible for the slow-developing emission component. This was tested by observing the emission curves when the experiment was performed in one atmosphere of dry N_2 instead of in air. The emission in a nitrogen atmosphere was identical to that from an air-containing system. Thus the sulphur oxidation reaction is not likely to be responsible for the slow-developing emission. One further reason to reject a chemiluminescent explanation is afforded by

the CH_3SH oxidation reaction. The photolytic oxidation of CH_3SH exhibits only a very low level of light emission. This reaction is also the one in which the formation of SO_2 from CH_3S is the most rapid. If the emission came from the sulphur oxidation reaction one would expect this reaction to exhibit the greatest level of light emission. Thus one must conclude that the reactions of oxidation of CH_3S to SO or of SO to SO_2 are not responsible for the slow-developing emission.

4.2.4 Presence of Quenching Impurity

A long delay in the establishment of emission could be caused by the presence of a quenching agent in the original gas mixture. If this quenching agent was to be slowly removed, a fluorescent emission would appear to be slowly growing. As the quenching agent was removed the emission would approach a plateau level which could be maintained. The quenching agent could be removed by reaction with the activated sulphide or might be deactivated due to photolysis of the quencher itself by direct absorption of ultra-violet light. This possibility was examined by interrupting the light beam for various lengths of time and examining the level of emission as the illumination was resumed. If there was a quenching agent present, and if it was consumed by reaction or photolysis, the emission should resume at the same level as when the beam was interrupted. If the quenching agent was regenerated in the dark, the emission should resume at a very low level after a sufficiently long dark period. The results of this examination are shown in Figures 34, 35 and 36.

The results are quite different for CH_3SCH_3 and SO_2. The dimethyl sulphide emission tends to resume at levels which are very similar to those

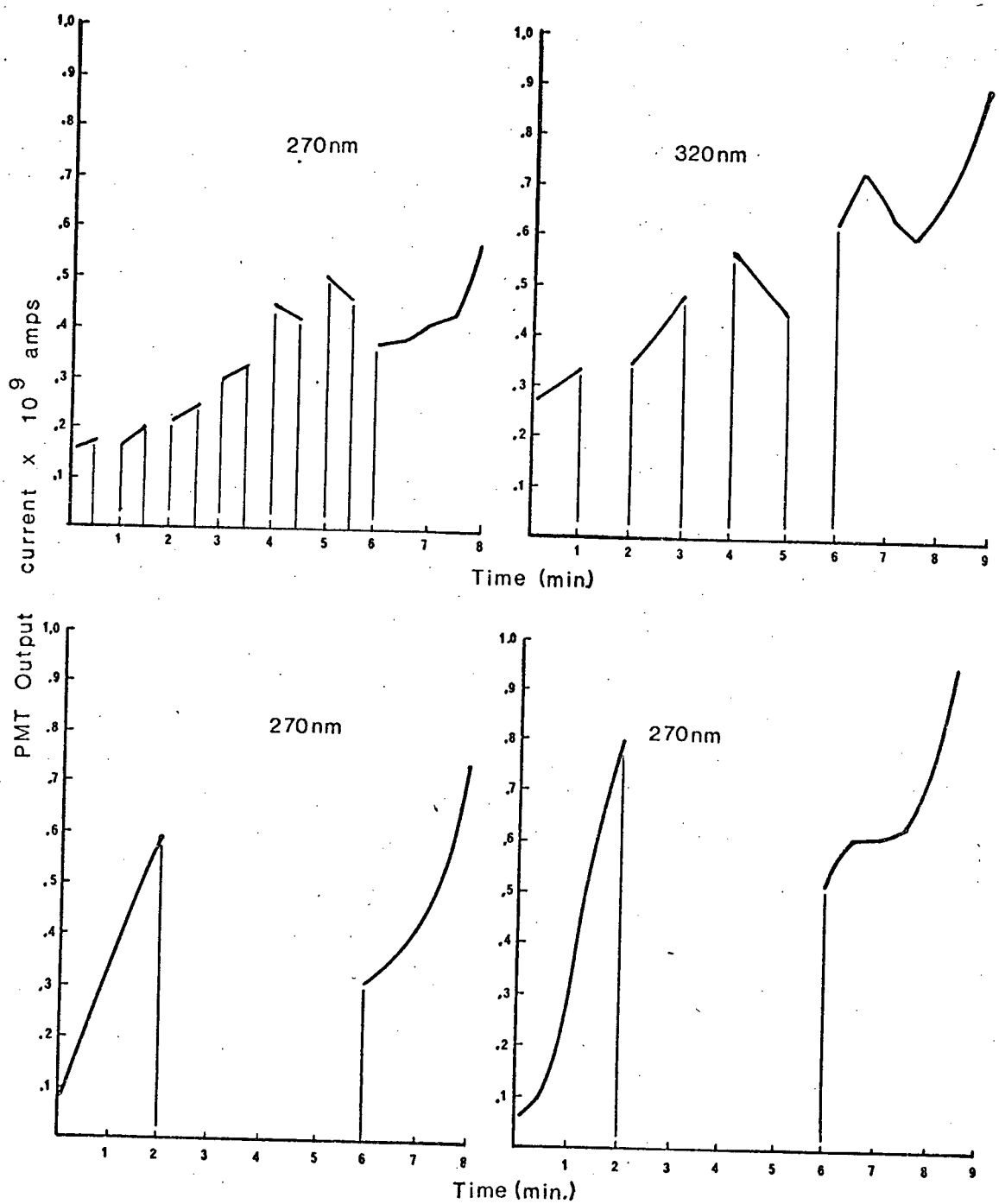

Figure 34. Emission behaviour during interrupted illumination of CH_3SCH_3.

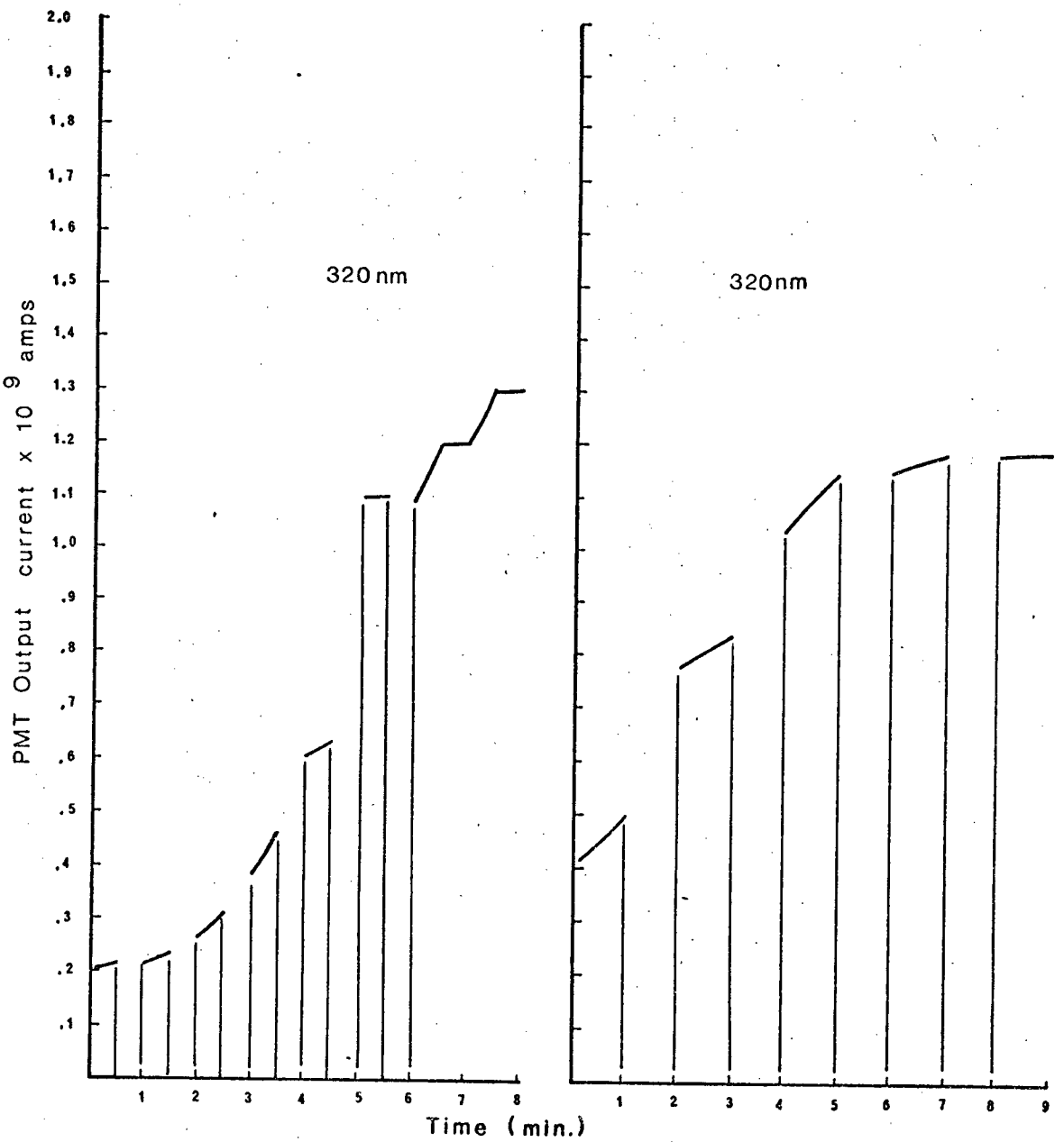

Figure 35. Emission behaviour during interrupted illumination of SO_2.

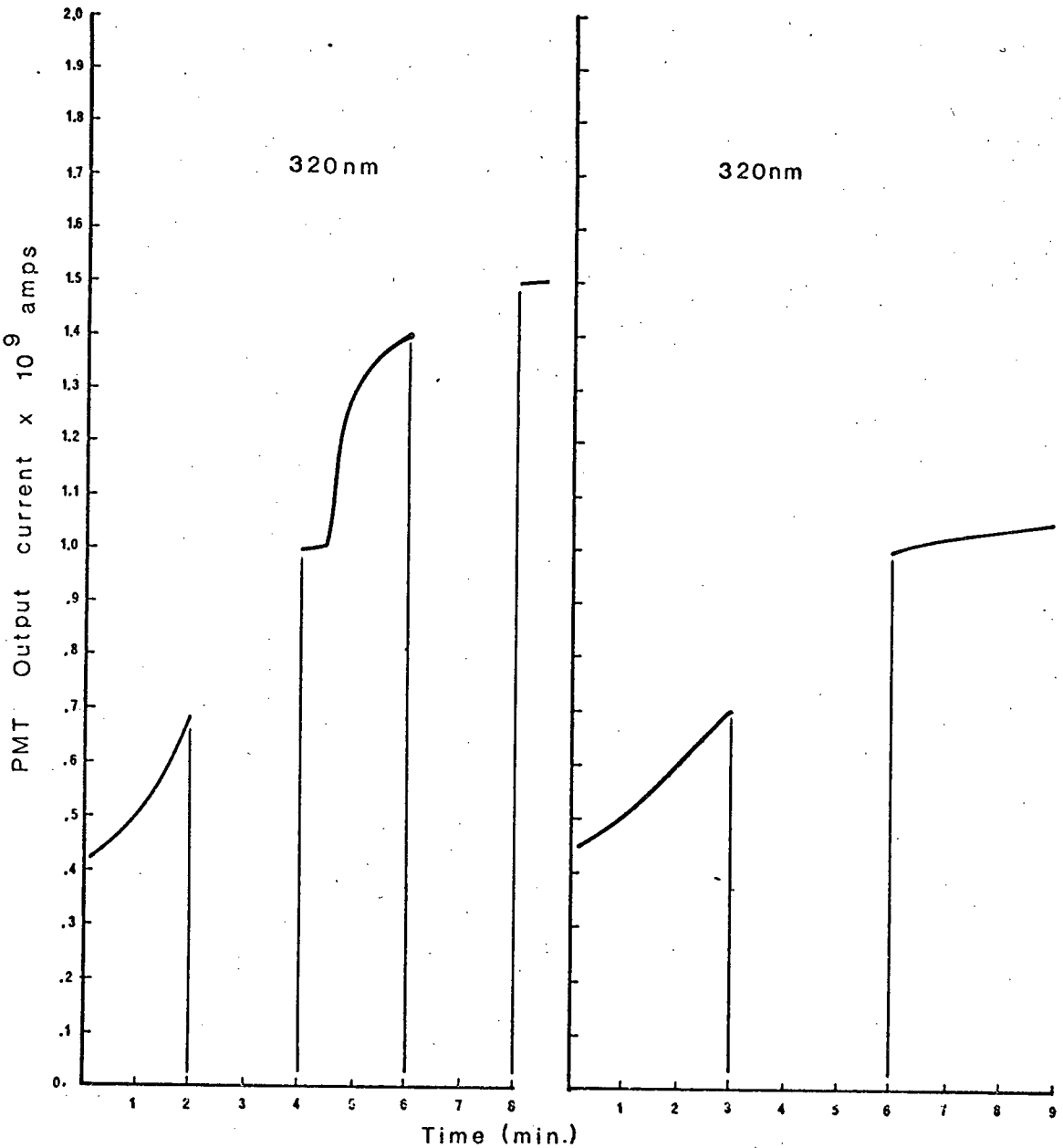

Figure 36. Emission behaviour during interrupted illumination of SO_2.

when illumination was suspended. Figures 34c and 34d demonstrate the resumption of emission at levels which are below those established when the light was first shut off. Thus a four-minute dark period appears to be a significant event to whatever mechanism is occurring in this delay of emission. A shorter period of illumination and dark results in a pattern which follows an interrupted, smooth curve. Figures 34a and 34b show some periods of anomalous emission weakening during illumination. The major trend is toward emission which resumes at the previous intensity level for periods of darkness less than four minutes. For longer periods of darkness (such as four minutes) the emission resumes at a level significantly below that of the first photoperiod. The growth of emission also shows a second induction period after the four minute dark period. This suggests that if a quenching agent was present, that a portion of it re-appears after a four minute period. One would expect that if a quenching agent was being photolysed by ultra-violet light or if it was reacting with CH_3SCH_3, the agent would be strongly altered and its reappearance after four minutes would be unlikely.

The behaviour of the SO_2 system is most different from that of the CH_3SCH_3. The SO_2 emission resumes at significantly higher levels of emission than at the end of the previous photoperiod. Figure 35 indicates that even for a 30 second photoperiod, the emission resumes at a level which appears to be unchanged by the dark period. For short photoperiods, the dark does not appear to interrupt the growth curve of the emission once a sufficient amount of light has been absorbed. The initial period of light absorption required to promote unaltered rate of growth appears to be about one minute. Thus the process appears to be initiated by one minute illumination and is able to continue throughout a short dark period. If this was a

quenching agent reacting, one would expect the reaction not to continue during a dark period. Photo-produced radicals should react sufficiently rapidly that the dark reaction should continue only a short time into the dark period. Thus one would not expect the large increase in emission found after a long dark period.

4.2.5 Photochemical Aerosol Formation

The remaining possibility that the emission might be due to physical scattering of the light by an aerosol suspension was investigated. In order to separate the physical scattering effect from an emission resulting from absorption of light, one must be able to eliminate absorbable wavelengths from the illumination envelope of wavelengths. If an emission persists at a wavelength which is illuminating the gas mixture but which is too long to be absorbed by the gas, then the cause is some physical scattering of the light beam. It is necessary, of course, to illuminate the mixture with polychromatic light for an initial period in order to build up the emissive effect. A borosilicate glass filter was used to cut off all wavelengths short enough to be absorbed by the sulphide. The emission spectrum was followed at 370 nm. This wavelength is efficiently passed by the borosilicate filter with only slight loss due to reflection. A 10% loss may be expected. Figure 37 demonstrates the effect of removing absorbable wavelengths from the light path while analysis was maintained at 370 nm. The emission was allowed to develop normally using polychromatic illumination. After a period when the emission was well formed, the borosilicate filter was inserted into the light path. An immediate decrease in emission intensity is caused by reflection losses of the borosilicate filter in the illuminating beam. The level of emission

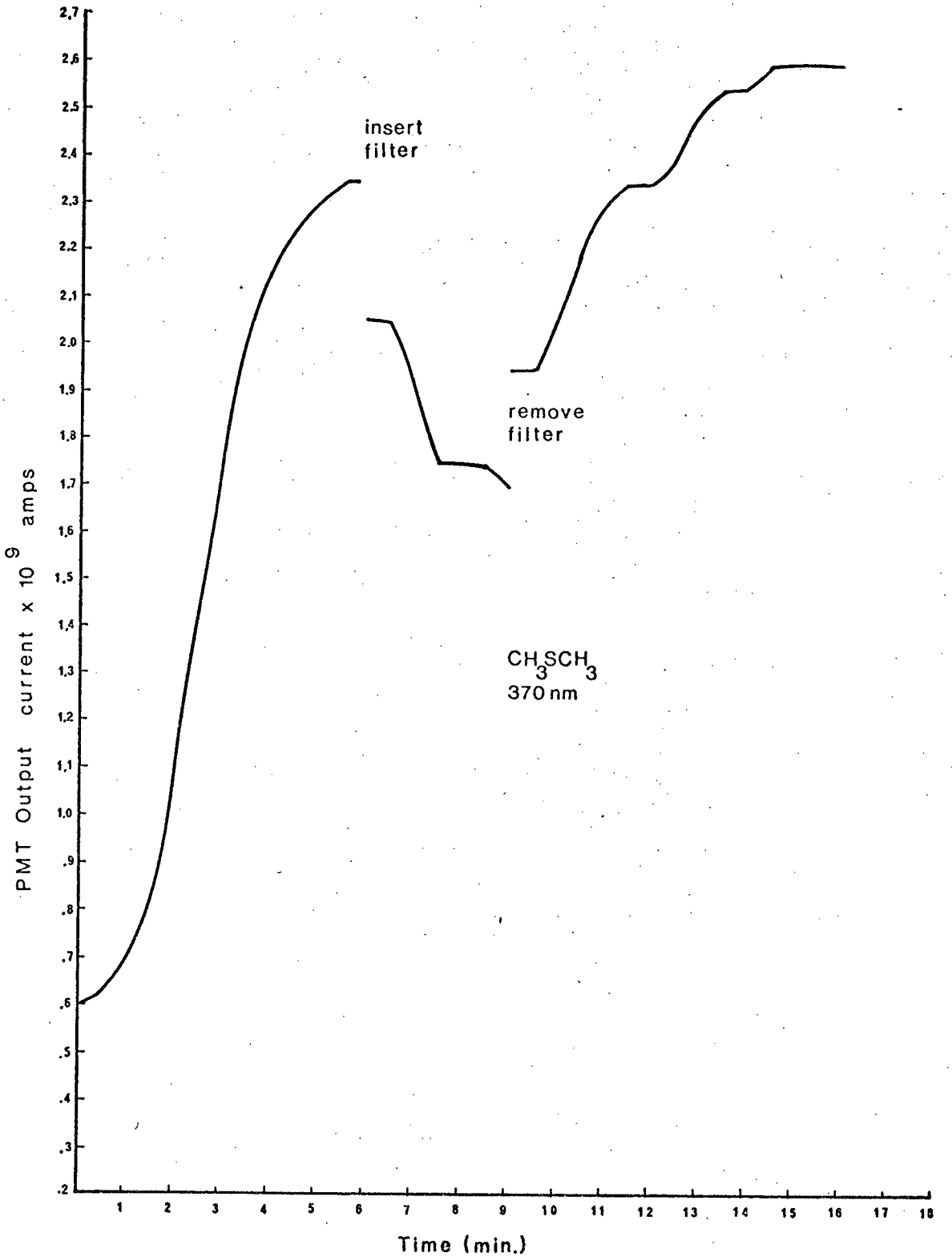

Figure 37. The CH_3SCH_3 emission at 370 nm with borosilicate glass filter.

maintains itself for 30 seconds and begins to decrease slowly for three minutes. This indicates that there is some photo-generated species in the reaction mixture that is capable of scattering light of many wavelengths. Removal of the filter at the nine minute point increases the light emission by regaining what was lost to reflection. Further illumination increases the emissive effect at a rate similar to that observed before filtration.

This experiment establishes that the emission observed is caused by a physical scattering of the light by particles which are produced under short wavelength ultra-violet radiation. The particles are very likely an aerosol. The emission must be due to a scattering since the emission is maintained even when all wavelengths which can be absorbed by CH_3SCH_3 are removed from the illumination beam. Thus the emission is not re-radiation of absorbed energy since energy cannot be absorbed by CH_3SCH_3 at wavelengths longer than 320 nm (Figure 3). Short wavelength ultra-violet illumination is required for the formation of the aerosol since the emission does not form at all during exposure to borosilicate filtered light. The emission also drops from its previous level of development when the filter is inserted into the light path. This indicates that the aerosol is not very stable since it decays significantly once the generating energy is removed. The aerosol is then regenerated by admitting the short wavelength light. The aerosol production mechanism seems the most successful in explaining the emission effect. The results will be discussed in terms of an aerosol mechanism in a later section.

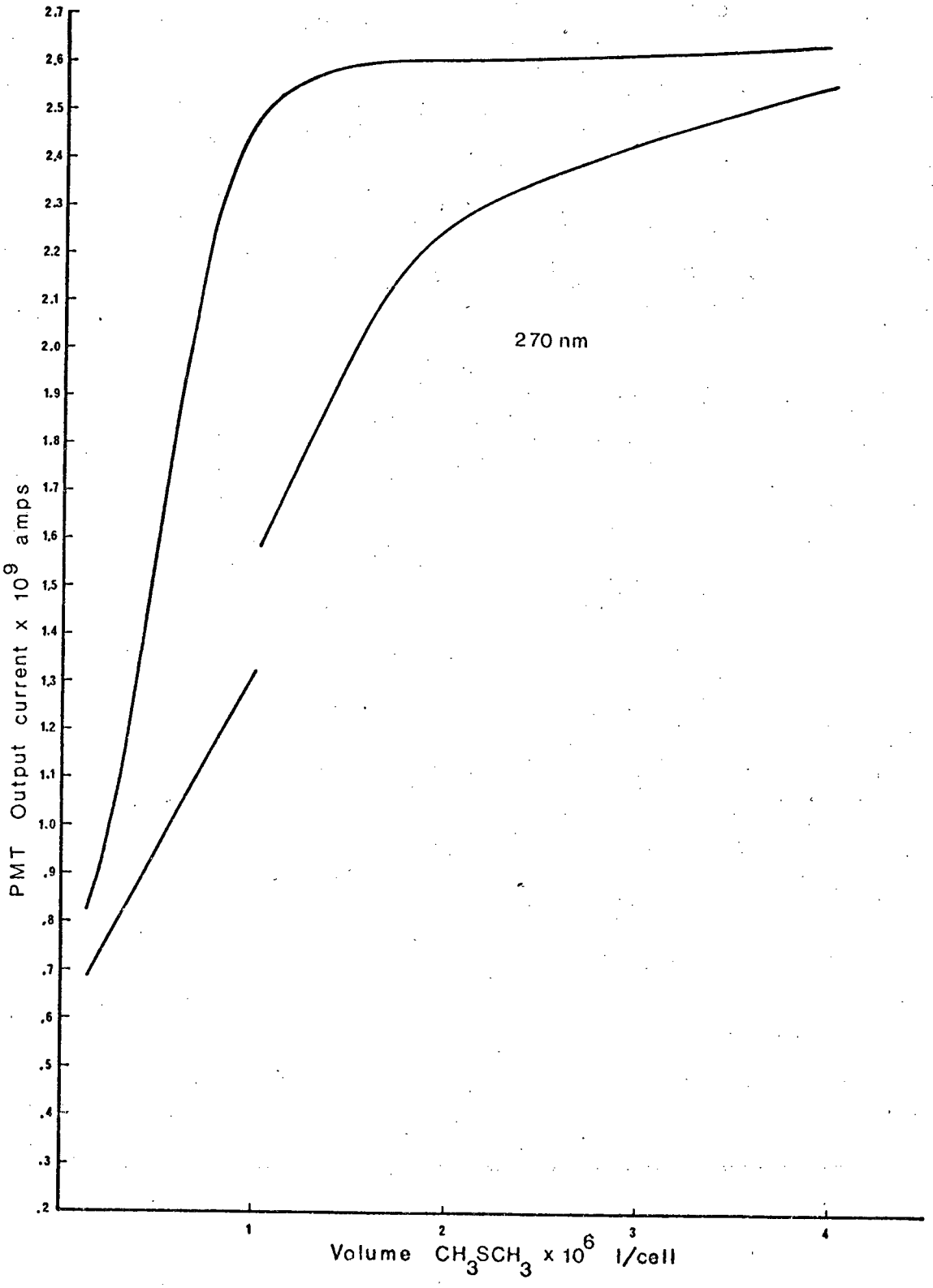

Figure 38. Emission of CH_3SCH_3 in air vs. volume of CH_3SCH_3 added.

4.3 Concentration Dependence of Emission

The emission was examined to observe a concentration dependence upon the amount of CH_3SCH_3 added. The ultimate intensity of emission at 270 nm was observed and recorded as a function of the volume of liquid CH_3SCH_3 added to the emission cell (Figure 38). The experiment, when performed on different days under apparently identical conditions, yields rather different results. The behaviour of emission for volumes of CH_3SCH_3 under 1 μℓ is quite linear. At these levels, the emission is most defintely a function of concentration. For sulphide additions greater than 1 μℓ the emission reaches a maximum and does not appear to increase above a certain level.

4.4 Pressure Dependence of Emission

The emission was also examined to determine any dependence upon the atmospheric pressure of molecules in the emitting mixture. The ultimate emission intensity was measured for a given concentration of sulphide in the emission cell. The cell was evacuated to 3/4, 1/2 and 1/4 atmosphere while maintaining the same partial pressure of sulphide. The results are shown in Figure 39. Each individual concentration level was measured on a different day and the deuterium lamp used for this set of trials was approaching the end of its useful life. For this reason, each individual day can be related but the results from different days cannot be related since the total light emitted from the deuterium lamp was rapidly decreasing. The emission is shown to be a strong function of atmospheric pressure. The possibility of an oxygen dependence in this set of experiments was examined by conducting the whole set with a new deuterium lamp using dry nitrogen gas as the reaction

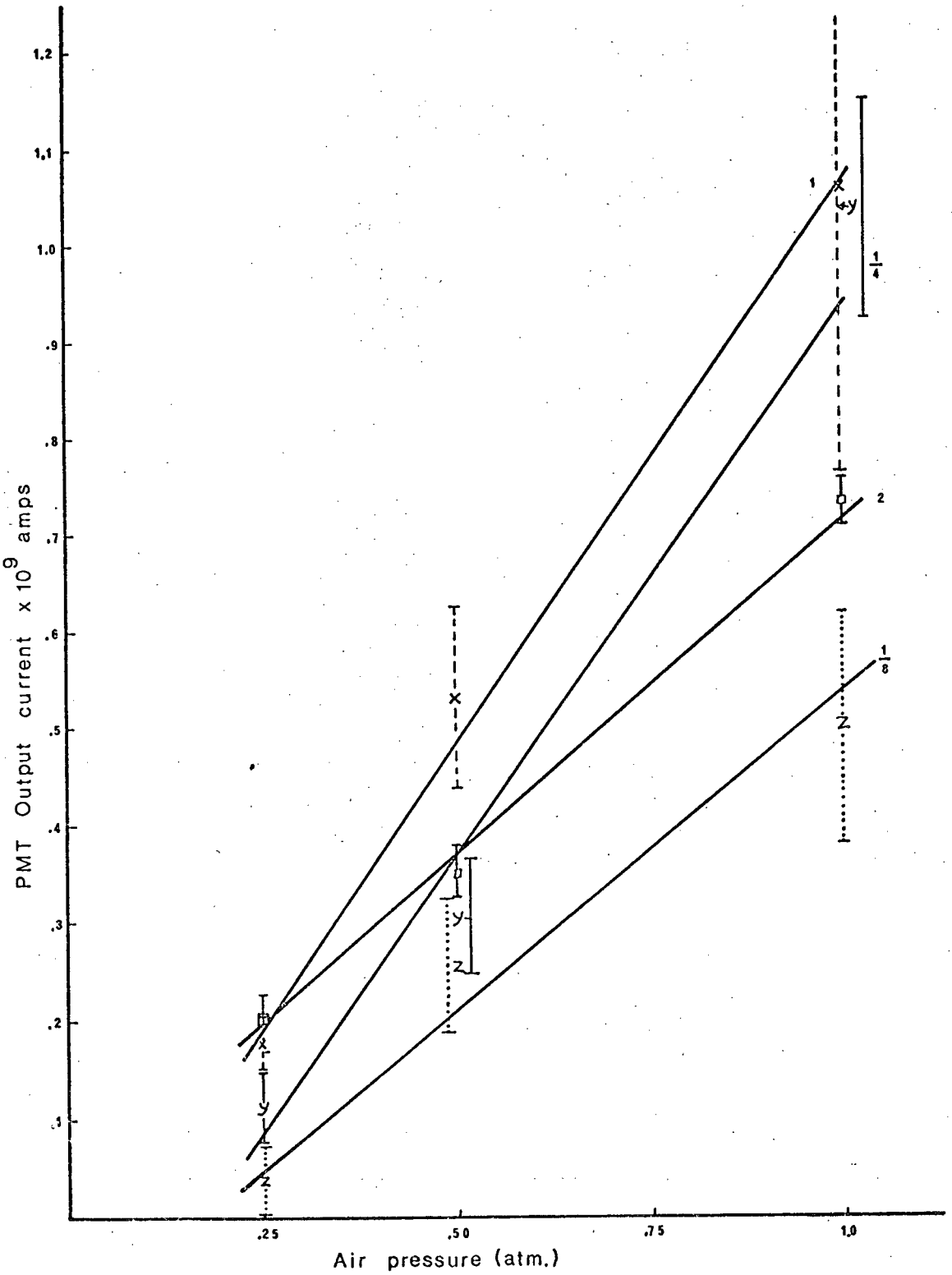

Figure 39. Emission from CH_3SCH_3 in air vs. air pressure.

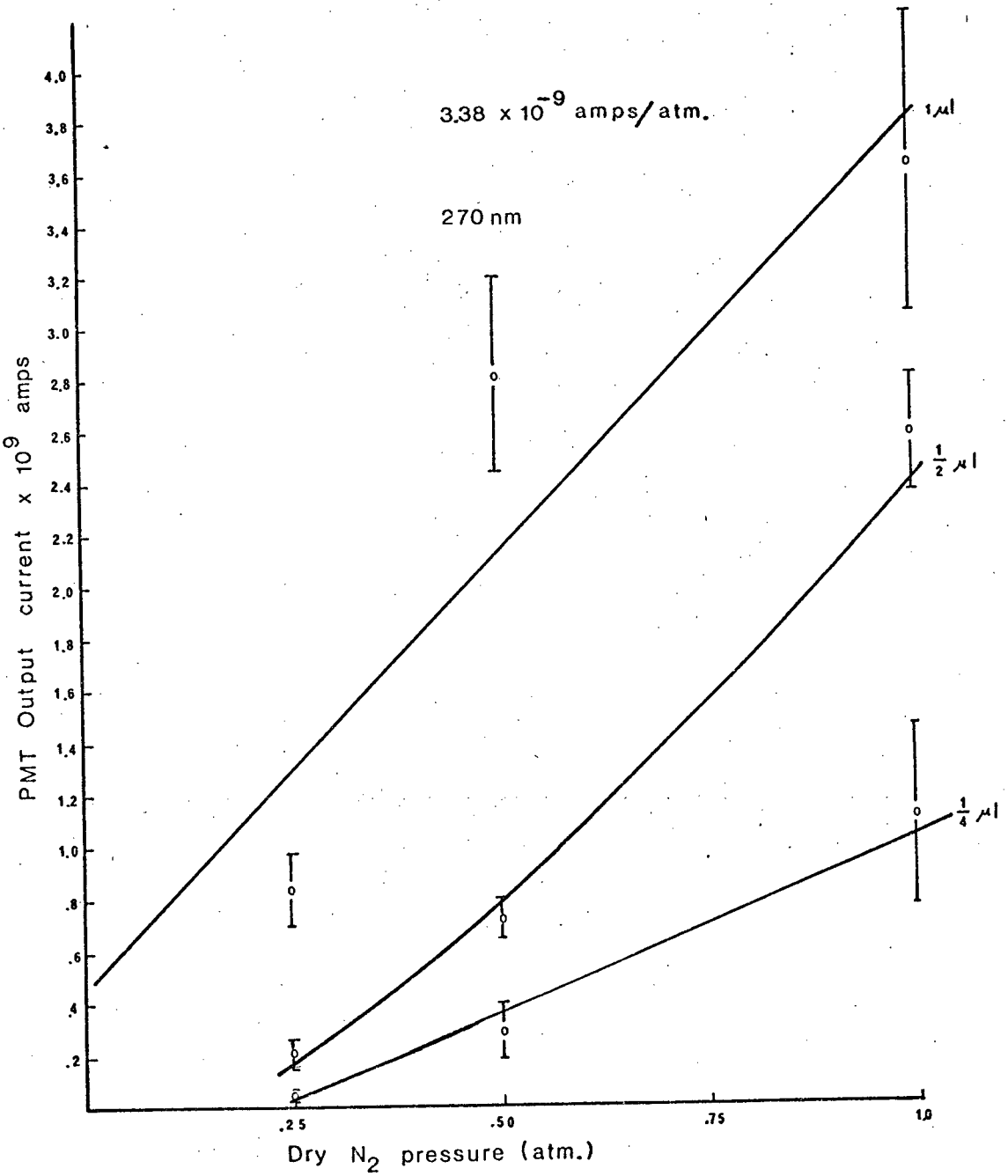

Figure 40. Emission from CH_3SCH_3 in dry nitrogen vs. pressure.

atmosphere (Figure 40). The level of emission was generally much greater with the new deuterium lamp. The emission revealed a similar pressure dependence to the air experiments. This allows one to rule out an oxygen concentration effect as the cause of the pressure dependence of the emission. In terms of aerosol formation, the aerosol appears to be pressure dependent with respect to the ultimate level of scattered light.

4.5 The Emission as an Aerosol Scattering Effect

4.5.1 Previous Work

A slow-developing emission has been observed previously by Lalo and Vermeil [42] in studies of SO_2 fluorescence. The emission was found to be greater for short-wavelength illumination than for long wavelengths. The emission was, at that time, attributed to the emission of the OH radical which was formed from the diluting H_2 gas and a postulated air leak into the static system. The emission was avoided by using a flowing gas system. Bentley and Douglass [37] reported an observable aerosol to be formed during CH_3SCH_3 photolysis studies using a high power xenon light source. The system contained measurable amounts of water vapour since the work was done using humid air. The high intensity work of Bentley and Douglass was carried to a high degree of completion and the product gases contained many sulphoxides and sulphones which may have played a part in aerosol formation. Luria *et al.* [58] observed the formation of an aerosol when SO_2 and allene were irradiated with wavelengths greater than 300 nm. A similar effect was noticed by the same authors upon irradiation of a SO_2-acetylene mixture. No aerosol formation was mentioned when SO_2 was photolysed without added

hydrocarbon. The photolysis of a SO_2-C_2H_2 mixture was found to produce a solid aerosol which was analysed to have the composition of a $C_3H_4S_2O_3$ trimer [58]. Luria *et al.* were unsuccessful in their attempts to isolate and analyze the aerosol oil in the SO_2-C_3H_4 photolysis. A partial molecular analysis indicated a carbon-to-sulphur ratio of 4.85. The number of particles was measured using two counting devices. Particles larger than 100 nm were counted in a thermal diffusion chamber. Particles larger than 25 nm were measured in an "Environment One Condensation Nuclei Counter."

The production of particles was found to commence after a short induction time (45 sec.) and the number of particles was found to reach a maximum which would subsequently decrease slowly. Particle production was found to be essentially complete within 10 minutes. The size of the particles was found to increase with time. The number of particles greater than 2.5 nm was found to rapidly approach the number of particles of size greater than 100 nm. Two reasons were suggested to explain the maximum in the number of particles. The first was that particle production stopped after a period of photolysis. The second was that the particle production rate was offset by a particle removal process. The sequence of events appears to be photochemical production of a SO_2-C_3H_4 polymer which eventually nucleates to form particles. The particles condense and reach a maximum in number after which they grow in size by accumulating further photoproduced polymer. The particle count was checked by filtering the aerosol on a filter and examining the filter under a scanning electron microscope. The particles produced were sufficiently large and were stable enough to withstand the evaporative sample preparation steps without evaporating themselves. The filter count method was found to correlate well with the particle counting devices.

4.5.2 Discussion of Results as a Particle Effect

The emission of light from the H_2S, SO_2 and CH_3SCH_3 systems can best be described in terms of light scattering from a slowly growing aerosol which is formed by photochemical reaction. The aerosol appears to be the result of condensation of a super-saturated solution of oil molecules which are produced photochemically. The droplets form and subsequently increase in size by agglomerating molecules from the photochemical reaction atmosphere. Continued irradiation results in the continued growth of the aerosol. The growth of aerosol particle size results in a light scattering effect which is characteristic of particles in varying scattering regimes.

The particle size of an aerosol is often characterized by the size of the particle relative to the wavelength of light used to observe the particle. For a given size, shorter wavelengths of light are scattered more than long wavelengths. The dimensionless optical particle size parameter x is used to describe the diameter-wavelength relationship:

$$x = \frac{\pi d_p}{\lambda}$$

d_p = particle diameter

λ = observing wavelength

For very small particles where $x < .3$, scattering follows the Rayleigh model in which light is scattered symmetrically both forward and back. As the dimensionless particle diameter increases beyond $x = .3$, the scattering follows the Mie theory. Mie theory holds for particles of diameter between x values of .3 and 3. As the diameter increases, the scattered light develops a foreward directed symmetry which has a maximum within 45° of the illuminating beam.

The extinction coefficient described by Mie is composed of two factors: absorption and scattering. For particles of carbon, the absorption and scattering effects have been separated [60]. Figure 41 shows the part played by scattering in the Mie-theory extinction of transmitted light by carbon particles [60]. The scattering of light becomes a significant factor as the dimensionless diameter approaches 0.6. As the particle grows the scattering increases rapidly until the particle approaches x = 1.6. Beyond a particle diameter of 1.6 the scattering becomes much less dependent upon particle diameter and approaches a plateau level. The sum of absorption and scattering has been calculated for organic liquids of refractive index m = 1.5 [60] (Figure 42). The total of scattering and absorption reaches a maximum at x = 4 and subsequently decreases in an oscillatory fashion to approach the value two at large particle diameters. The extinction coefficient is defined by the Bouguer law which is a modification of Beer's law.

$$\frac{I}{I_0} = e^{-naK\ell}$$

n = number of particles per unit volume

a = mean projected particle area

K = extinction coefficient

ℓ = path length

This limitation on the value of the extinction coefficient results in a limit on the intensity of light scattering such that a particle may continue to grow in size but the light scattered from it will no longer be increasing in intensity. Such behaviour is likely responsible for the plateau effect

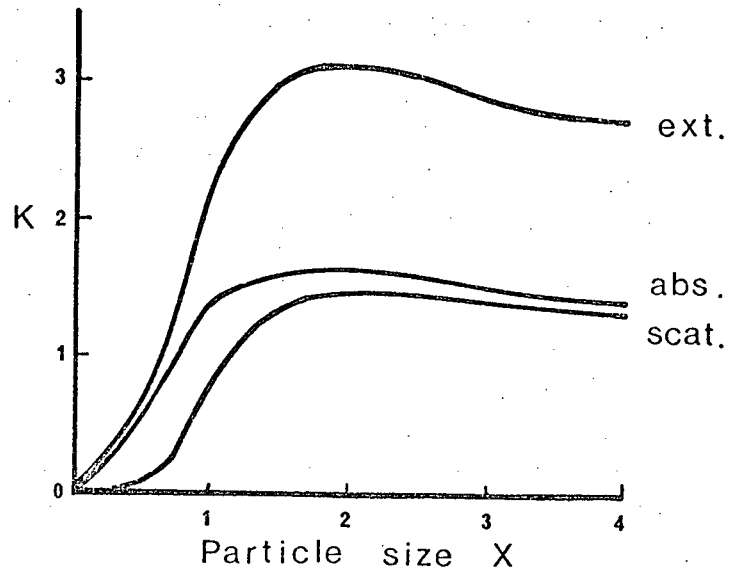

Figure 41. Relative importance of absorption and scattering to extinction coefficient for carbon particles.

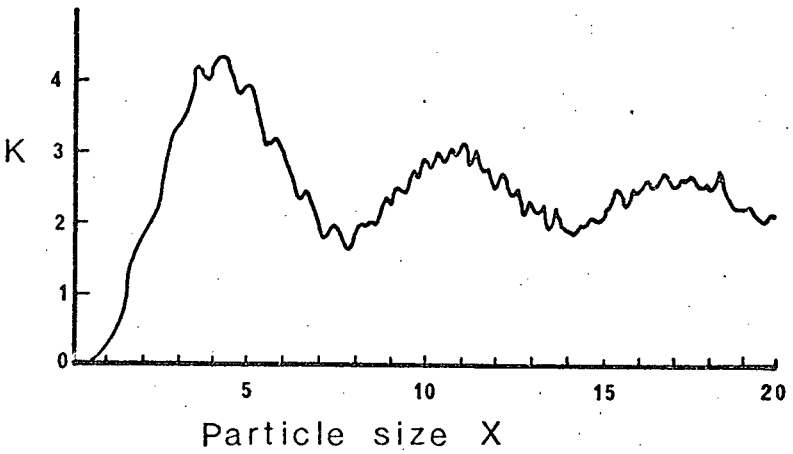

Figure 42. Extinction curve for the theory of Mie for particles of refractive index m = 1.5.

evident in Figure 32. When observed at 270 nm, the scattered light grows in intensity quite linearly for five minutes before the emission reaches a plateau. At this point the dimensionless particle diameter has likely reached a value close to 5. This would correspond to an actual particle diameter of 429 nm. Figure 33 reveals another feature characteristic of particle growth. The SO_2 emission was followed at 240 nm and at 320 nm under otherwise similar conditions. At the longer wavelength, there is a significantly longer nucleation period before a linear emission growth is observed Figure 33.b). This period is the time taken to nucleate the particle and to achieve a dimensionless diameter where $x \simeq .60$. As may be seen from Figure 41 the scattering may be considered to begin about $x \simeq .60$. The longer nucleation period is required due to the longer wavelength of observation which requires a larger particle diameter before appreciable scattering takes place.

4.5.3 Stability of the Aerosol

The stability of the aerosol formed appears to vary with the parent compound. Figures 34, 35 and 36 indicate the behaviour of the CH_3SCH_3 and SO_2 aerosol systems under discontinuous radiation. The CH_3SCH_3 system is seen to resume emission at a lower level after a dark period of four minutes (Figure 34). This behaviour was investigated by observing the scattered light intensity as the borosilicate filter is inserted into the optical path (Figure 37). The loss of wavelengths below 320 nm eliminates energy absorption by the sulphide. The generating mechanism is stopped and the stability of the aerosol may be investigated by observing the scattering at 370 nm. After insertion of the filter at the six minute mark, the emission is seen to decrease after a 30 second period of stability. The decrease is a

significant lowering of intensity. This gradual decrease is likely the result of the agglomeration of aerosol particles into a smaller number of large particles. The size increase of the particles does not result in the increase of emission which one might expect because the particles are already near the size limit ($x \simeq 2$) where the scattered intensity is more a function of number than size. As a result of the agglomeration, the emission is reduced. The decrease in emission shortly after short wavelength elimination suggests that the CH_3SCH_3 aerosol does not arise from a highly super-saturated gas mixture.

The aerosol generated from SO_2 appears to be a more stable phenomenon. Figure 43 is the result of examining the SO_2 aerosol under conditions similar to the above. As the energizing illumination is removed at 3 3/4 minutes, the emission drops due to reflection from the filter slide. The emission continues to grow for one minute after the energizing radiation is removed. The rate of decay of the emission is much slower than that shown by CH_3SCH_3. The continued growth shown in Figure 43 confirms the behaviour noted in Figures 35 and 36. The emission resumed at significantly higher levels for two and three minute dark periods. This behaviour requires that the particles continue to grow in size even after the activating energy is filtered out. This also requires a growth rate greater than the agglomeration effect which is responsible for the decay of the scattered illumination. Such continued growth must be the result of a super-saturated reaction-gas solution which continues to condense upon the aerosol and increase its size for a period of time after the short wavelength light is stopped. The aerosol appears to be more stable with respect to agglomeration than is that from the CH_3SCH_3 reaction.

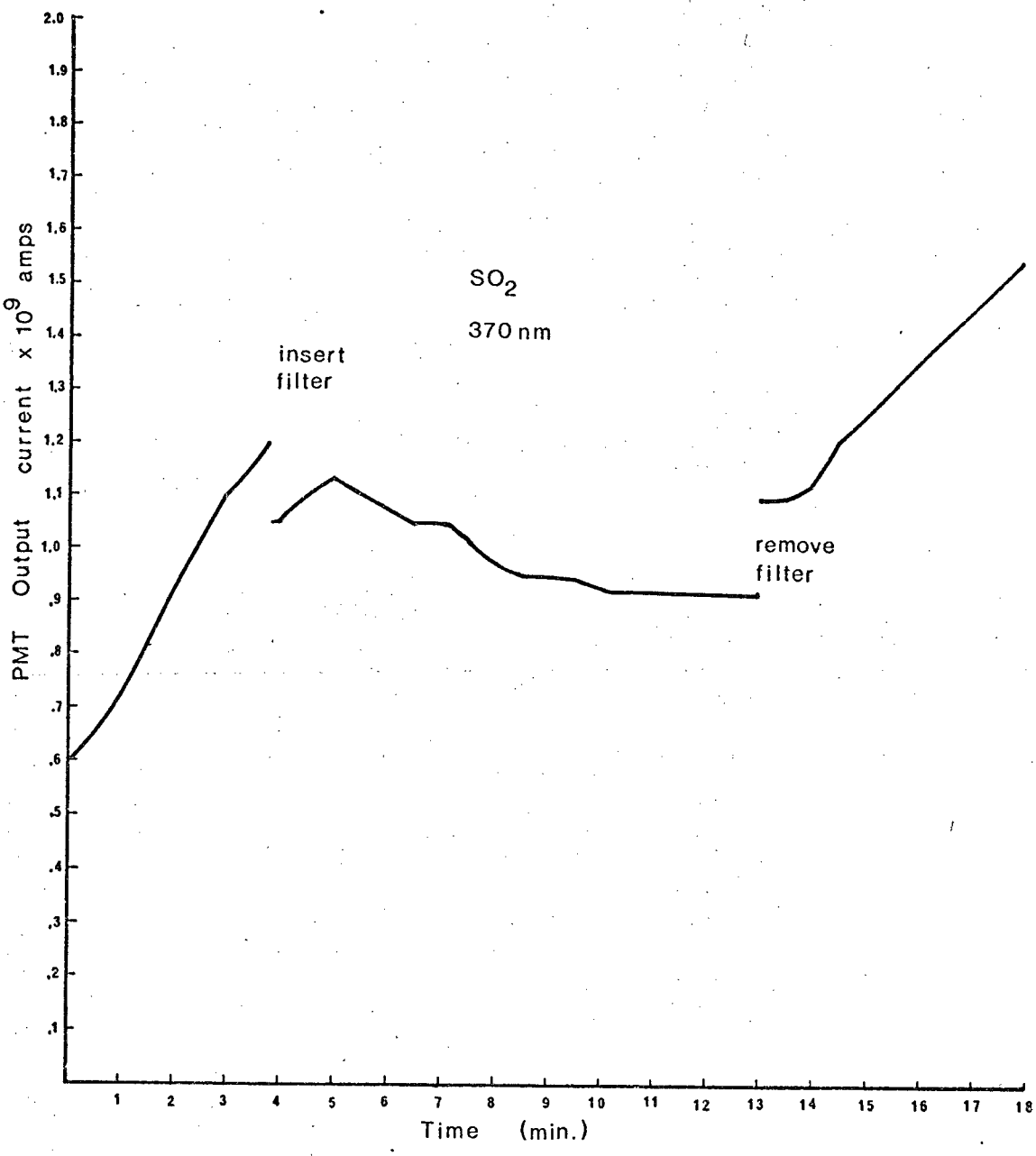

Figure 43. Behaviour of the 370 nm emission during interrupted short wavelength illumination of SO_2.

4.5.4 Concentration Dependence of the Aerosol

The dependence of the emission intensity upon the added volume of CH_3SCH_3 suggests that the number of particles generated in the nucleation stage depends upon the concentration of CH_3SCH_3 initially present (Figure 38). At levels of CH_3SCH_3 addition greater than 1 µℓ per 53.91 ml cell the dependence drops off. This plateau suggests that for higher concentrations the number of particles formed reaches a maximum and is not increased beyond that number. For large levels of CH_3SCH_3 addition, the particle size may increase to much larger diameters; however this does not increase the level of scattered light as the dimensionless diameter exceeds $x \approx 2$. Low levels of CH_3SCH_3 added never reach the emission levels ultimately attained by greater addend amounts. This effect is not varied by time and is thus independent of the ultimate size of the aerosol particle which must be assumed to be continuously growing. The low levels of CH_3SCH_3 addition must be producing a lower number of particles which grow by the condensation process. Each particle behaves as outlined previously and the emission grows until $x \approx 2$. at which time the emission reaches its ultimate intensity. The number of particles formed is thus a function of the starting concentration of CH_3SCH_3 in the reaction gas matrix.

4.5.5 Pressure Dependence of the Emission

The ultimate level of emission for any one fixed concentration of CH_3SCH_3 was found also to be a function of atmospheric pressure. The dependence did not differ between N_2 and air (Figures 39, 40). The effect of the size of the particles is removed from consideration by examining for the ultimate level of emission which occurs at an average particle size

where $x \simeq 2$. Thus the number of particles appears to be a function of atmospheric pressure. The number formed must be a function of a third body nucleation process in which an O_2 or N_2 molecule can serve as a third body to stabilize formation of the aerosol particle. The greater collision frequency due to higher pressures, nucleates a greater number of aerosol particles which grow to form an increased ultimate emission intensity.

4.6 The Number of Particles Formed

The number of particles formed by the nucleation of the sulphide is dependent upon both atmospheric pressure and the amount of sulphide initially present. The dependence upon sulphide concentration is related to the number of photo-activated sulphide molecules which are available within a certain critical volume to aggomerate and form an aerosol particle. There is also a critical level of sulphide concentration above which larger numbers of particles are not formed. This suggests that when sufficient quantities of activated sulphide are available, this quantity is no longer the controlling factor as to the number of particles formed. At lower sulphide concentrations, the concentration of photo-activated species is responsible for determining the number of particles to nucleate at a constant atmospheric pressure. The atmospheric pressure exerts its effect by means of third body collision frequency which defines a volume within which a particle is likely to form. At higher pressures, this volume decreases in size and results in a larger number of particles to be formed from a given volume of reaction. This volume may be considered as a nucleation volume and is related to the mean free path of the N_2-CH_3SCH_3 mixture. At lower pressures the mean free path is larger and within a given volume, fewer particles nucleate. This may

also be considered as the volume of reaction gas which is swept by N_2 molecules to form one aerosol particle.

For concentrations of CH_3SCH_3 lower than 1 µℓ per 53.9 ml both dependencies can be related in a manner which involves proportionality to both sulphide concentration and to atmospheric pressure. With respect to sulphide concentration for the results of Figure 38.

$$I_s = (Vol_{msm}) \frac{1.8 \times 10^{-9} A}{\mu\ell \text{ msm}}$$

I_s = scattered intensity A = Amps

With respect to atmospheric pressure from Figure 40 for a 1 µℓ addend.

$$I_s = 3.38 \times 10^{-9} \frac{A}{Atm} \cdot \left(P_{N_2}\right)$$

P_{N_2} = atmospheric pressure of N_2

Combining both proportionalities

$$I_s \propto \left(\frac{1.8 \times 10^{-9} A}{\mu\ell} \cdot [MSM]\right) \cdot \left(\frac{3.38 \times 10^{-9} A}{Atm}\right) \cdot P_{N_2}$$

Now the number of particles is proportional to the scattered intensity when $x>2$, therefore:

$$N_p \propto \left(1.8 \times 10^{-9} \frac{A}{\mu\ell} [MSM]\right) \cdot \left(3.38 \times 10^{-9} \frac{A}{Atm}\right)\left(P_{N_2}\right)$$

4.6.1 Attempted Optical Verification of Particle Size and Number

An attempt to measure the number of particles was made. This involved generation of the aerosol and confirmation by emission intensity growth. At varying times in the reaction the cell was removed and placed on the vacuum manifold. A Nucleopore filter was placed on the outlet of the emission cell and numerous cell volumes of dry N_2 were swept through the filter. The filter pores were 0.1 μ in diameter. Samples were taken from newly generated aerosols at 0, 2, 5 and 10 minutes intervals. The filters were examined under a scanning electron microscope in a manner similar to Luria *et al*. Very few particles were found on any filter. The reason for the lack of confirmation of particle production by the reaction lies in the sample preparation stages for the electron microscopy. In order to attract the electron beam to the mylar filter target, the filter surface and adherent particles must be covered by a conductive film of gold. This film is evaporated onto the sample under high vacuum. The aerosol is not likely stable to such low pressures and most probably evaporated at this time. As a result only a few particles were found on each filter and these could not be considered to be representative of the aerosol.

Chapter 5

CONCLUSIONS

A. 1. CH_3SH oxidation is initiated through photon absorption by CH_3SH.

2. The quantum yield of CH_3SH decomposition is 13.9.

3. The quantum yield of CH_3SH is not affected by atmospheric pressure.

4. Air containing water vapour retards the reaction.

5. Oxygen concentration greater than that of air does not increase the quantum yield.

6. Added SO_2 does not increase the quantum yield of CH_3SH decomposition and is responsible for a decrease in effective overall quantum yield.

B. 1. The quantum yield of CH_3SCH_3 decomposition is 4 ± 1.6 at atmospheric pressure.

2. The quantum yield of CH_3SCH_3 decomposition increases to 8 ± 2.9 at one-quarter atmosphere of air.

C. The quantum yield of CH_3SSCH_3 decomposition is 1.96 ± .94 at concentrations of 7.0×10^{-5} M.

D. 1. An aerosol has been found to be formed from ultra-violet illumination of H_2S, SO_2 and CH_3SCH_3.

2. The intensity of light scattered from the aerosol is dependent upon the atmospheric pressure of third body molecules in the environment.

3. The scattered intensity is concentration dependent up to a limit of $\frac{1\ \mu\ell}{53.9 ml}$ of CH_3SCH_3 (2.58×10^{-4} M).

E. The reaction scheme would be a suitable sequence for computer modeling. This would yield information about reactive radical species in the reaction atmosphere.

BIBLIOGRAPHY

[1] Skerrett, N.P. and N.W. Thompson, The Photolysis of Mercaptans, Trans. Faraday Soc., 37, 81 (1951).

[2] Ueno, Tamotsu and Yoshimasa Takezaki, Some Observations on the Photolysis of Dimethyl Disulphide, Kyoto University Institute Chemical Research Bulletin, 36, 19 (1958).

[3] Inaba, T. and B. de B. Darwent, The Photolysis of Methyl Mercaptan, Journal of Physical Chemistry, 64, 1431 (1960).

[4] Milligan, B., D.E. Rivett and W.E. Savige, The Photolysis of Dialkyl Sulphides, Disulphides, and Trisulphides, Aust. J. Chem, 16, 1020 (1963).

[5] Callear, A.B. and D.R. Dickson, Transient Spectra and Primary Processes in the Flash Photolysis of CH_3SSCH_3; CH_3SCH_3; CH_3SH and C_2H_5SH Trans. Far. Soc., 66, 1907 (1970).

[6] Skelton, J. and F.C. Adam, The Photolysis and Radiolysis of Simple Mercaptans in Dilute Glassy Matrices, Can. J. Chem. 49, 3536 (1971).

[7] Steer, R.P., B.L. Kalra, A.R. Knight, Reactions of Thiyl Radicals I: Methylthiyl Recombination and Thionitrite Formation in the Photolysis of Methane Thiol, J. Phys. Chem., 71, 783 (1967).

[8] Rao, P.M., J.A. Copeck, A.R. Knight, Reactions of Thiyl Radicals II: The Photolysis of Methyl Disulphde Vapour, Can. J. Chem., 45, 1369 (1967).

[9] Sayamol, K. and A.R. Knight, Reactions of Thiyl Radicals III: Photochemical Equilibrium in the Photolysis of Liquid Disulphide Mixtures, Can. J. Chem. 46, 999 (1968).

[10] Steer, R.P., A.R. Knight, Reactions of Thiyl Radicals IV: Photolysis of Methanethiol, J. Phys. Chem. 72, 2145 (1968).

[11] Steer, R.P. and A.R. Knight, Reactions of Thiyl Radicals VI: Photolysis of Ethane Thiol, Can. J. Chem., 47, 1335 (1969).

[12] Rao, P.M. and A.R. Knight, Reactions of Thiyl Radicals VII: Photolysis of Methyl Sulfide Vapor, Can. J. Chem. 50, 844 (1972).

[13] Tycholiz, D.R. and A.R. Knight, Reactions of Thiyl Radicals VIII: Photolysis of Methyl Ethyl Sulfide Vapor, Can. J. Chem 50, 1734 (1972).

[14] Hemphill, G.L and J.M. White, Photochemistry of Ethanethiol at 254 & 214 nm, Lamar Bridges, J. Phys. Chem, 76, 2668 (1972).

[15] Bridges, L and J.M. White, Photochemistry of Methanethiol at 254 and 214 nm, J. Phys. Chem., 77, 295 (1973).

[16] Kamra D. and J.M. White, On the Photolysis of Methanethiol and Ethanethiol at 185 nm, Journal of Photochemistry, 4, 361 (1975).

[17] Dzantiev, B.G. and A.V. Shishkov, Hydrogen Formation in the Photolysis of Mercaptans, Khimiya Vysokikh Energii, Vol. 2, No. 2, p. 119 (1968).

[18] Dzantiev, G.B., A.V. Shishkov and M.S. Unukovich, The Photolysis of Mercaptans. Reactions of Excited Thiyl Radicals, Khimiya Vysokikh Énergii, Vol. 3, No. 2, p. 111 (1969).

[19] Dzantiev, B.G., A.V. Shishkov and M.S. Unukovich, Energy Transfer in the Radiolysis of Mixtures of Hydrogen Sulfide and Ethylene, Khimiya Vysokikh Énergii, Vol. 5, No. 2, p. 172 (1971).

[20] Rao, P.M. and A.R. Knight, Reactions of Thiyl Radicals V. The Gas Phase Photolysis of Methyl Disulphide and Ethyl Disulphide in the presence of Ethylene, Can. J. Chem. 46, 2462 (1968).

[21] Dzantiev, B.G., O.S. Shimchuk and A.V. Shishkov, Photolysis of Hydrogen Sulfide, Effect of Added Inert Gases, Khimiya Vysokikh Énergii, Vol. 4, No. 4, 361 (1970).

[22] Dzantiev, B.G., A.D. Pershin, O.S. Shimchuk, A.V. Shishkov and L.L. Yasina, The Photoylsis of Hydrogen Sulfide. The Hydrogen Removal Action by Hot H° Atoms from Deutero Compounds, Khimiya Vysokikh Énergii, Vol. 4, No. 6, 545 (1970).

[23] Dzantiev, B.G. and A.V. Shishkov, Photolysis of Hydrogen Sulphide. Influence of Additions of Ethylene, Khimiya Vysohikh Énergii, Vol. 1, No. 3, 192 (1967).

[24] White, J.M., R.L. Johnson Jr., D. Bacon, Energy Disposal in the Photodissociation of Ethanethiol, J. Chem. Phys., 52, 5212 (1970).

[25] White, J.M. and R.L. Johnson Jr., Energy Disposal in the Photodissociation of Ethanethiol, J. Chem. Phys., 56, 3787 (1972).

[26] Sturm, G.P. and J.H. White, Photodissociation of Hydrogen Sulfide and Methanethiol. Wavelength Dependence of the Distribution of Energy of the Primary Products, J. Chem. Phys., 50, 5035 (1969).

[27] White, J.M. and G.P. Sturm, Photochemical Decomposition of Methanethiol II. The Wavelength Dependence of the H Atom Energy, Can. J. Chem., 47, 357 (1969).

[28] Sturm, G.P. and J.M. White, The Photochemical Decomposition of Methanethiol. Hot Hydrogen Atoms Reaction with Deuterium, J. Phys. Chem., 72, 3679 (1968).

[29] Bridges, L. and J.M. White, Reaction of Hot Hydrogen Atoms with Methanethiol, J. Chem. Phys., 59, 2148 (1973).

[30] Su, H.Y., J.M. White, L.M, Raff, and D.L. Thompson, Abstraction Versus Exchange in the Reaction of H with DBr, J. Chem. Phys., 62, 1435, 1975.

[31] Oldershaw, G.A. and D.A. Porter, Reaction of Hot Hydrogen Atoms with COS, J. of Chem. Soc., Faraday Trans. I, v. 68, 709, Pt. 4 (1972).

[32] Rayner, H.B. and F.E. Murray, The Photolytic Oxidation of Methyl Mercaptan and Dimethyl Disulphide, Pulp and Paper Magazine of Canada, Vol. 71, 75 (1970).

[33] Murray, R.W. and S.L. Jindal, Photosensitized Oxidation of Dialkyl Disulphides, J. Org. Chem, Vol. 37, 3516 (1972).

[34] Graham, D.M. and Billy K.T. Sie, Sulfur Dioxide Formation in the Photo-Oxidation of Methanethiol, Can. J. Chem., 49, 3895 (1971).

[35] McGarvey, J.J. and W.D. McGrath, Kinetic Spectroscopy in the Vacuum Ultra-Violet Region I. The Dissociation Energy of SO and the Combustion of Hydrogen Sulphide, Carbon Disulphide and Carbonyl Sulphide, Proc. Roy. Soc. (London), A 278, 490 (1964).

[36] Wood, W.P. and J. Heicklen, The Photooxidation of CS_2 at 2139 Å, J. Photochem., 2, 173 (1973).

[37] Bentley, M.A., I.B. Douglass, J.A. Lacadie, and D.R. Whittier, The Photolysis of Dimethyl Sulfide in Air, Air Pollution Control Association, 64th Meeting, June 27, 1971.

[38] Gunning, H.E. and O.P. Strausz, The Reactions of Sulfur Atoms, Vol. 4, Noyes, Hammond, Pitts, Wiley Interscience.

[39] Becker, K.H. and D. Haaks, Lifetime Measurements on Excited SH (A^2) Radicals, Journal of Photochemistry, 1, 177 (1972/73).

[40] Norrish, R.G.W. and A.P. Zeelenberg, The Combustion of Hydrogen Sulphide Studied by Flash Photolysis and Kinetic Spectroscopy, Proc. Roy. Soc., A240, 293 (1957).

[41] Lalo, C. and C. Vermeil, Photolysis of SO_2 at 123.6 nm in the Presence of H_2, J. Photochem. 1, 321 (1972/73).

[42] Lalo, C. and C. Vermeil, Photochemistry of SO_2 in the Vacuum - U.V. II Luminescence Studies, J. Photochem. 3, 441 (1974/5).

[43] Stockburger, L. III, S. Braslavsky, J. Heicklen, J. Photochem. 2, 15 (1973/4).

[44] Cehelnik, E. J. Heicklen, S. Braslavsky, L. Stockburger III, E. Mathias, Photolysis of SO_2 in the Presence of Foreign Gases IV Wavelength and Temperature Effects with CO, J. Photochem. 2, 31 (1973/4).

[45] Wilkinson, f., Electronic Energy Transfer, Advances in Photochemistry, Vol. 3, Noyes, Hammond, Pitts (eds.), Wiley Interscience, p. 251.

[46] Parker, C.A., Phosphorescence and Delayed Fluorescence from Solutions, Advances in Photochemistry, Vol. 2, Noyes, Hammond Pitts (eds.), Wiley Interscience, p. 305.

[47] Williams, R., Delayed Fluorescence of Complex Moleclues in the Vapor Phase, J. Chem. Phys., 28, 577 (1958).

[48] Mackle, H., Tetrahedron, 19, 1159 (1963).

[49] Calvert and Pitts, Photochemistry, Wiley and Sons Inc., New York.

[50] Hatchard, C.G., and C.A. Parker, A New Sensitive Chemical Actinometer II. Postassium Ferrioxalate as a Standard Chemical Actinometer, Proc. Roy. Soc. (London), A. 235, 518 (1956).

[51] Baulch, D.L. and D.D. Drysdale, Evaluated Kinetic Data for High Temperature Reactions, Vol. 3, Homogenious Gas Phase Reactions of the O_2-O_3 System, CO-O_2-H_2 System and of Sulphur Containing Species, Butterworths, London, (1976).

[52] Hampson, R.F. Jr. and D. Garvin (eds.), Reaction Rate and Photochemical Data for Atmospheric Chemistry - 1977, National Bureau of Standards Special Publication #513.

[53] Kondratiev, V.N., Rate Constants of Gas Phase Reactions, U.S. Department of Commerce, National Bureau of Standards (1972).

[54] Ratajczak, E. and A.F. Trotman-Dickenson, Supplementary Tables of Bimolecular Gas Reactions, Office for Scientific and Technical Information, Department of Education and Science, London.

[55] Kelly, N., J.F. Meagher, J. Heicklen, The Photolysis of SO_2 in the Presence of Foreign Gases VIII: Excitation of SO_2 at 3600 to 4100 Å in the Presence of Acetylene, J. Photochemistry, vol. 6, No. 3, (1977), p. 157.

[56] Luria, M. and J. Heicklen, The Photolysis of SO_2 in the Presence of Foreign Gases VI: Acetylene and Allene, Can. J. Chem., 52, 3451.

[57] Partymiller, K. and J. Heicklen, The Photolysis of SO_2 in the Presence of Foreign Gases XI: The Photolysis of SO_2 at 313 nm in the Presence of Allene and O_2, J. Photochem., 8, 167 (1978).

[58] Luria, M., K.J. Olszyna, R.G. de Pena, S. Heicklen, Kinetics of Particle Growth-V: Particle Formation in the Photolysis of SO_2-Allene Mixtures, J. Aerosol Sci., 5, 435 (1975).

[59] Calvert, J.G. and J.N. Pitts, Photochemistry, John Wiley & Sons Inc., New York (1966).

[60] Friedlander, S.K., Smoke, Dust and Haze, Fundamentals of Aerosol Behaviour, John Wiley and Sons, New York, London, Sydney, Toronto, p. 130.

[61] Adachi, H. and D.E.L. James, Kinetic Spectroscopic Studies of Alkyl, Alkylperoxy and acetyl radicals, Ph.D. Thesis, Department of Chemistry, The University of British Columbia.

[62] Pratt G.and I.Veltman,Kinetics of Reaction of Hydrogen Atoms with Ethylene. J.Chem. soc. Far.I,72,1733(1976)

APPENDIX A

CH_3SH Reaction Data

Date-Cell	[SH]/Cell x 10^{-6} ℓ	Rx Rate x 10^{-6} g hr^{-1}	Light #	Photon Flux Photons hr^{-1}	% Abs. %	R_{SO_2} x 10^{-6} g hr^{-1}	ϕ_{SH}
Dec. 10 1974	50	57.6	1	1.317 x 10^{18}	4.94	-	
11	50	46.4	1	1.317	13.2	-	
13	50	40.1	1	1.317	-	-	
16	50	37	1	1.317	-	-	
19	50	52	1	1.317	3.5	-	
March 10 1975	50	88.8	1	1.317	-	-	
11	50	56.7	1	1.317	2.9	-	
17	50	45.4	1	1.317	4.6	-	
20	50	53.9	1	1.317	-	-	
24	50	52.6	1	1.317	7.6	-	
		AVG. 53.05					8.24
July 16 1973	75	100.2	1	1.317	-	-	
17	75	80.4	1	1.317	-	-	
17	75	67.5	1	1.317	-	-	
18	75	92	1	1.317	-	-	
		AVG. 85.02			Calc. 6.13		12.19
Oct. 4 1974	100 Wet	22.6	1	1.317	-	-	2.48
7	100	102.8	1	1.317	-	-	11.29
8	100	83.9	1	1.317	-	-	9.21
8	100	97.1	1	1.317	-	-	10.66
9	100	101.6	1	1.317	-	-	11.15
9	100	105	1	1.317	-	-	11.5
10	100	105	1	1.317	-	-	11.5
10	100	115.4	1	1.317	-	-	12.6
10	100	123.5	1	1.317	-	-	13.56
17	100	220	1	1.317	-	-	24.16
18	100 No O_2	41	1	1.317	-	-	4.5
Nov. 14 1974	100	97	1	1.317	15.8	-	10.65
20	100	117	1	1.317	15.3	-	12.85

Date-Cell	[SH]/Cell x 10^{-6} ℓ	Rx Rate x 10^{-6} g hr^{-1}	Light #	Photon Flux x 10^{18} phot. hr^{-1}	% Abs. %	R_{SO_2} x 10^{-6} g hr^{-1}	ϕ_{SH}
Nov. 27 1974	100 Pure O_2	48.5	1	1.317	-	-	5.32
28	100 Pure O_2	79.5	1	1.317	9.6	-	8.73
Dec. 2	100 Pure O_2	103	1	1.317	17.2	-	11.3
3	100 Pure O_2	79	1	1.317	6.25	-	8.67
Sept. 20 1976 V	100	184	2 late	1.739	-	-	15.3
20 O	100	121	2 L	1.739	-	-	10.06
21 V	100	231	2 L	1.739	-	-	19.2
27 V	100	78.5	2 L	1.739	-	-	6.5
27 O	100	115.4	2 L	1.739	-	-	9.59
29 V	100	122.3	2 L	1.739	-	-	10.17
29 O	100	96.1	2 L	1.739	-	-	7.99
Oct. 4 1976 V	100	85.9	2 L	1.739	11.16	-	7.14
4 O	100	202	2 L	1.739	6.2	-	16.8
16 V	100	224	2 L	1.739	6.46	-	18.6
19 V	100	92.5	2 L	1.739	7.3	-	7.69
19 O	100	89.7	2 L	1.739	8.42	-	7.46
20 V	100	138	2 L	1.739	-	-	11.47
20 O	100	153.9	2 L	1.739	9.7	-	12.8
Nov. 2 1976 V	100	76	2 L	1.739	6.1	-	6.3
2 O	100	109	2 L	1.739	7.9	-	9.06
2 V	100	152	2 L	1.739	5.1	-	12.6
2 O	100	182	2 L	1.739	3.7	-	15.13
3 V	100	205	2 L	1.739	7.8	-	17.05
3 O	100	166	2 L	1.739	6.7	-	13.8
4 V	100	252	2 L	1.739	11.8	-	20.9
4 O	100	76.9	2 L	1.739	7.7	-	6.39
8 V	100	168	2 L	1.739	7.9	-	13.97
8 O	100	186	2 L	1.739	-	-	15.47
8 N	100	112	2 L	1.739	7.3	-	9.31
9 V	100	165	2 L	1.739	-	-	13.72

Date-Cell	[SH]/Cell x 10^{-6} ℓ	Rx Rate x 10^{-6} g hr^{-1}	Light #	Photon Flux x 10^{18} phot. hr^{-1}	% Abs. %	R_{SO_2} x 10^{-6} g hr^{-1}	ϕ_{SH}
Nov. 9 1976 O	100	237	2L	1.739	10.5	-	19.7
9 N	100	224	2L	1.739	3.7	-	18.63
Dec. 8 1976 V	100	158.7	3	2.2154	-	49.6	12.8
8 O	100	359	3	2.2154	-	49.7	17.01
8 N	100	179.3	3	2.2154	-	58.4	10.9
18 V	100	198.3	3	1.9147	-	41.7	20.5
18 O	100	298.2	3	2.1125	-	41.7	19.6
18 N	100	240.5	3	2.095	-	45.46	14.2
19 V	100	198	3	2.1968	-	45.5	11.5
19 N	100	166.5	3	2.2154	-	48	11.16
19 O	100	230.8	3	2.2154	-	45.7	11.16
						Avg.	12.72
July 4 1973	150	50.1	1	1.317	12.71	-	3.75
5	150	118	1	1.317	Avg.	-	8.8
9	150	300	1	1.317	Calc.	-	22.4
10	150	167	1	1.317	-	-	12.5
12	150	170	1	1.317	-	-	12.7
13	150	121	1	1.317	-	-	9.06
15	150	87.4	1	1.317	-	-	6.5
16	150	92.5	1	1.317	-	-	6.9
17	150	104	1	1.317	-	-	7.79
18	150	97.9	1	1.317	-	-	7.34
						Avg.	9.79
Dec. 21 1976 V	250	487.7	3	2.2129	8.75	66.12	15.4
22 N	250	432	3	2.2154	19.19	62.04	12.7
22 O	250	424	3	2.2154	20.8	60.1	11.54
22 V	250	288	3	2.2154	20.07	61.9	10.94
Jan. 11 V	250	280.2	3	1.9879	16.24	57.8	14.76
11 O	250	368	3	2.0854	16.57	64.1	13.35
11 N	250	304	3	2.0196	16.3	56.0	11.59

Date-Cell	[SH]/Cell x 10^{-6} ℓ	Rx Rate x 10^{-6} g hr^{-1}	Light #	Photon Flux x 10^{18} phot. hr^{-1}	% Abs. %	R_{SO_2} x 10^{-6} g hr^{-1}	ϕ_{SH}
Jan. 11 1977 V	250	297	3	1.8824	16.25	51.6	12.17
11 O	250	240	3	1.979	14.42	50	10.5
12 V	250	314	3	1.9153	16.61	55.8	12.4
12 N	250	304	3	2.1075	16.18	54	10.76
12 O	250	328	3	-	-	50.1	-
Dec. 21 1976 O	250	464	3	2.2154	18.46	68	14.2
21 N	250	488	3	2.20	15.84	66	17.56
						Avg.	12.91
Feb. 23 1977 O	250 ½ Atm.	116.9	3	1.741	18.5	-	4.55
23 V	250 ½ Atm.	119	3	1.420	14.1	-	7.45
23 N	250 ½ Atm.	168	3	1.42	15.1	-	9.79
25 V	250 ½ Atm.	82.6	3	1.42	16.8	-	4.34
25 N	250 ½ Atm.	111	3	1.412	15.4	-	6.4
25 N	250 ½ Atm.	-	3	-	15.4	-	-
26 O	250 ½ Atm.	112	3	1.530	15.2	-	6.04
July 11 1977 Z	250 ½ Atm.	152.3	4	2.197		50.1	5.41
11 V	250 ½ Atm.	169	4	2.208		40.3	5.37
12 V	250 ½ Atm.	202	4	2.059		45.4	6.31
12 Z	250 ½ Atm.	184	4	2.1533		47.1	5.37
13 Z	250 ½ Atm.	180	4	2.02		49	5.37
13 V	250 ½ Atm.	194	4	2.01		43.3	6.72
14 V	250 ½ Atm.	438	4	1.91		33	16.79
14 Z	250 ½ Atm.	408	4	1.934		34	13.91
						Avg.	6.40

CONTINUED

Date-Cell	[SH]/Cell x 10^{-6} ℓ	Rx Rate x 10^{-6} g hr^{-1}	Light #	Photon Flux x 10^{18} phot. hr^{-1}	% Abs. %	R_{SO_2} x 10^{-6} g hr^{-1}	ϕ_{SH}
Feb. 28 1977 N	250 ¼ Atm.	254	3	1.433	13.7		16.23
28 O	250 ¼ Atm.	308	3	1.570	17.4		14.14
Mar. 1 N	250 ¼ Atm.	144	3	1.545	19.1		6.12
1 O	250 ¼ Atm.	168	3	1.723	16.7		7.32
3 O	250 ¼ Atm.	240	3	1.559	17.4		11.09
3 N	250 ¼ Atm.	-	3	-	8.5		-
						Avg.	10.98
Jan. 11 1975	50 SH-50 SO_2	57.6	1	1.317	14.6		
11 1975	50 SH 50 SO_2	50.6	1	1.317	14.6		
12 1975	50 SH-50 SO_2	63.4	1	1.317	15.5	Avg.	3.61
13 1975	50 SH-100 SO_2	55.6	1	1.317	32.3		
13 1975	50 SH-100 SO_2	51.4	1	1.317	32.3	Avg.	1.57

APPENDIX B

CH_3SSCH_3 REACTION DATA

Date	[SS]/Cell x 10^{-6} ℓ	Rate SS x 10^{-6} g hr^{-1}	Photon Flux x 10^{18} Phot. hr^{-1}	% Abs. %	ϕ_{ss}
Apr. 3 1975	.25 liquid	55.9	1.317	13.6	1.46
	.25	36.5	1.317	13.6	.77
June 20 1975	.25	72.4	.9104	30.2	1.38
	.25	65.8	.9104	30.2	1.18
24 1975	.25	36.2	.9104	30.5	.49
	.25	82.2	.9104	30.5	1.55
25	.25	69.1	.9104	30.9	1.23
	.25	58.15	.9104	30.9	.984
27 1975	.25	82.3	.9104	28.45	1.66
	.25	74	.9104	28.45	1.46
Sept. 17 1975	.25	119	.9104	30.49	2.39
	.25	82.3	.9104	30.49	1.55
18 1975	.25	92.17	.9104	30.5	1.78
	.25	69.13	.9104	30.5	1.25
Oct. 2 1975	.25	125	.9104	27.6	2.80
	.25	68	.9104	27.6	1.35
7 1975	.25	59.2	.9104	29.0	1.07
	.25	102	.9104	30.9	1.98
	.25	70.7	.9104	30.9	1.27
8 1975	.25	128	.9104	27.8	2.85
9 1975	.25	49.3	.9104	20.46	1.18
	.25	77.3	.9104	20.46	2.14
15 1975	.25	118	.9104	27.4	2.64
	.25	74.1	.9104	27.4	1.52
16 1975	.25	148	.9104	32.9	2.84
	.25	106	.9104	32.9	1.95
Oct. 20 1975	.25	88.8	.9104	27.3	1.90
	.25	69.13	.9104	27.3	1.39
21 1975	.25	158	.9104	28.45	3.53
	.25	92	.9104	28.45	1.91
22 1975	.25	88.6	.9104	25.2	2.06
	.25	60.9	.9104	25.2	1.28
23 1975	.25	82.3	.9104	25.5	1.86
	.25	65.4	.9104	25.5	1.39
25 1975	.25	190.9	.9104	28.4	4.35
	.25	119.2	.9104	28.4	2.58
28 1975	.25	223.8	.9104	28.4	5.15
	.25	156.3	.9104	28.4	3.49
29 1975	.25	131.6	.9104	28.45	2.88
	.25	97.1	.9104	28.45	2.03
May 13 1975	.5	37.8	.9104	47	.34

CONTINUED

Date	[SS]/Cell x 10^{-6} ℓ	Rate SS x 10^{-6} g hr^{-1}	Photon Flux x 10^{18} phot. hr^{-1}	% Abs. %	ϕ_{ss}
June 3 1975	.5	164	.9104	44.3	2.36
	.5	128	.9104	44.3	1.79
4 1975	.5	52.6	.9104	44.6	.59
	.5	35.5	.9104	44.6	.33
5 1975	.5	111.9	.9104	37.5	1.81
	.5	103.7	.9104	37.5	1.65
leak tests	.25	14.8 x 10^{-6}g over 4 hours			

APPENDIX C

CH_3SCH_3 REACTION DATA

Date		[MSM]/Cell x 10^{-6} ℓ $Cell^{-1}$	R_{-s} x 10^{-6} g hr^{-1}	Photon Flux x 10^{18} phot. hr^{-1}	% Abs. %	R_{SO} x 10^{-6} g hr^{-1}	ϕ_s
July 20 1977	N	.5 1 atm.	64.04	2.170	4	-	3.54
20	V	.5 1 atm.	49.6	1.938	4	-	3.44
21	N	.5 1 atm.	116	2.189	4	30	3.35
21	Z	.5 1 atm.	96	2.029	4	35	4.94
21	V	.5 1 atm.	103	1.844	4	36	5.75
22	V	.5 1 atm.	119	1.82	4	25.8	7.05
22	Z	.5 1 atm.	86	1.954	4	25	4.74
29	N	.5 1 atm.	60	2.1	4	-	3.96
29	V	.5 1 atm.	20	1.55	4	-	1.78
29	Z	.5 1 atm.	28	1.75	4	-	2.22
							Avg. 4.07
24	V	.5 ¼ atm.	78.5	1.5703	4	24.7	10.4
24	Z	.5 ¼ atm.	76	1.7015	4	25	8.36
25	V	.5 ¼ atm.	66	1.7621	4	31	4.97
	Z	.5 ¼ atm.	48	1.7510	4	30	4.43
26	V	.5 ¼ atm.	61	1.4499	4	25.8	8.06
	Z	.5 ¼ atm.	56	1.5119	4	23	11.9
							Avg. 8.02

APPENDIX D

SULPHUR BALANCE DATA

Date-Cell	[SH] Start x 10^{-6} g ml^{-1}	[SH] End x 10^{-6} g ml^{-1}	[SO_2] End x 10^{-6} g ml^{-1}	I/I_0 290 nm at End	[SS] End x 10^{-7} g ml^{-1}	% S Found
Dec. 8 1976 V	5.12	3.2	.599	.962	10.66	
8 O	5.6	3.2	.620	.948	15.9	
8 N	-	-	.729	-	-	
18 V	5.6	3.2	.504	.956	11.78	
18 O	6.6	2.88	.520	.940	18.08	
18 N	5.92	2.92	.567	.967	9.12	
19 V	5.52	3.12	.55	.926	22.69	
19 O	5.2	3.12	.60	.934	19.88	89.9
19 N	5.76	2.88	.570	.944	16.63	
21 N	13.8	7.7	.824	.925	22.33	
21 V	13.8	7.9	.799	.918	24.82	
21 O	14	8.2	.848	.916	25.32	
22 N	15.6	10.2	.775	.925	22.27	
22 V	14.8	10.1	.749	.920	24.17	
22 O	14.4	9.1	.749	.944	16.13	
Jan. 11 1977 O	14.4	9.4	.799	.898	31.62	
11 V	14.4	9.8	.699	.918	24.96	
11 N	13.8	10.0	.699	.939	17.89	
11 N	11.8	8.8	.625	.928	21.77	
11 O	-	-	-	.920	-	
11 V	11.8	8.2	.62	.922	23.81	
12 N	14	10.2	.674	.925	22.78	
12 V	14	10.2	.675	.924	22.91	
12 O	12.5	8.4	.625	.919	24.85	73.1
13 N	20.8	18.5	1.074	.908	27.46	
13 V	20.7	-	-	-	-	
13 O	21	18	.998	.902	29.65	

CONTINUED

Date-Cell	[SH] Start x 10^{-6} g ml^{-1}	[SH] End x 10^{-6} g ml^{-1}	[SO_2] End x 10^{-6} g ml^{-1}	I/I_0 290 nm at End	[SS] End x 10^{-7} g ml^{-1}	% S Found
Feb. 1 1977 V	25.4	15	2.19	.59	159.5	
2 V	23.2	15	3.1	.622	140.9	
2 O	22.6	15	3.3	.553	177.2	
3 V	23.4	15.2	3.0	.645	129.9	
3 N	23.6	14.8	3.4	.576	164.2	
5 N	25.4	17	2.8	.60	152.8	95.2

APPENDIX E

Concentration Dependence of Emission From Dimethyl Sulphide Aerosol

[MSM]/Cell x 10^{-6} ℓ per cell	Time to Max. Emission	Intensity of Max. Emission
4	12 min.	2.64 x 10^{-9} A
2	12	2.59
1	11	2.49
1/2	10	1.59
1/4	10	.94
1/8	17	.835
1	5	1.39 x 10^{-9} A
1/2	4	.945
1/4	14.2	.97
1/8	21	.67
1		1.58 x 10^{-9} A
2		2.27
4		2.52

APPENDIX F

DEPENDENCE OF INTENSITY OF EMISSION FROM DIMETHYL SULPHIDE AEROSOL UPON ATMOSPHERIC PRESSURE OF AIR

[MSM]/Cell x 10^{-6} ℓ/Cell	Atmospheric Pressure	Intensity of Max. Emission
4	1 atm.	.067 x 10^{-8} A
4	1 atm.	.072
4	1 atm.	.052
4	1 atm.	.067
4	1 atm.	.065
		avg. .646 x 10^{-9} A
4	1/2 atm.	.32 x 10^{-9} A
4	1/2 atm.	.32
		avg. .32 x 10^{-9} A
4	1/4 atm.	.18 x 10^{-9} A
4	1/4 atm.	.16
		avg. .17 x 10^{-9} A
2	1 atm.	.75 x 10^{-9} A
2	1 atm.	.72
		avg. .735 x 10^{-9} A
2	1/2 atm.	.37 x 10^{-9} A
2	1/2 atm.	.32
2	1/2 atm.	.36
		avg. .35 x 10^{-9} A
2	1/4 atm.	.18 x 10^{-9} A
2	1/4 atm.	.2
2	1/4 atm.	.23
		avg. .203 x 10^{-9} A

CONTINUED

[MSM]/Cell x 10^{-6} ℓ/Cell	Atmospheric Pressure	Intensity of Max. Emission
1	1 atm.	1.65 x 10^{-9} A
1	1 atm.	1.0
1	1 atm.	.8
1	1 atm.	1.1
1	1 atm.	1.05
1	1 atm.	.8
		avg. 1.066 x 10^{-9} A
1	1/2 atm.	.55 x 10^{-9} A
1	1/2 atm.	.42
1	1/2 atm.	.62
1	1/2 atm.	.645
1	1/2 atm.	.54
1	1/2 atm.	.39
1	1/2 atm.	.56
		avg. .532 x 10^{-9} A
1	1/4 atm.	.2 x 10^{-9} A
1	1/4 atm.	.16
1	1/4 atm.	.2
1	1/4 atm.	.12
		avg. .17 x 10^{-9} A
1/2	1 atm.	.62 x 10^{-9} A
1/2	1 atm.	1.05
1/2	1 atm.	1.5
1/2	1 atm.	1.325
1/2	1 atm.	1.3
1/2	1 atm.	1.15
		avg. 1.15 x 10^{-9} A
1/2	1/2 atm.	.63 x 10^{-9} A
1/2	1/2 atm.	.9
1/2	1/2 atm.	.87
		avg. .80 x 10^{-9} A
1/2	1/4 atm.	.305 x 10^{-9} A
1/2	1/4 atm.	.265
1/2	1/4 atm.	.29
		avg. .286 x 10^{-9} A

[MSM]/Cell x 10^{-6} ℓ/Cell	Atmospheric Pressure	Intensity of Max. Emission
1/4	1 atm.	.9 x 10^{-9} A
1/4	1 atm.	1.11
1/4	1 atm.	1.0
1/4	1 atm.	1.16
		avg. 1.04 x 10^{-9} A
1/4	1/2 atm.	.38 x 10^{-9} A
1/4	1/2 atm.	.29
1/4	1/2 atm.	.25
		avg. .306 x 10^{-9}A
1/4	1/4 atm.	.08 x 10^{-9} A
1/4	1/4 atm.	.08
1/4	1/4 atm.	.18
1/4	1/4 atm.	.12
1/4	1/4 atm.	.08
1/4	1/4 atm.	.14
		avg. .113 x 10^{-9}A
1/8	1 atm.	.47 x 10^{-9} A
1/8	1 atm.	.42
1/8	1 atm.	.61
1/8	1 atm.	.35
1/8	1 atm.	.40
		avg. .505 x 10^{-9} A
1/8	1/2 atm.	.22 x 10^{-9} A
1/8	1/2 atm.	.24
1/8	1/2 atm.	.36
1/8	1/2 atm.	.20
		.255 x 10^{-9} A
1/8	1/4 atm.	.00
1/8	1/4 atm.	.05 x 10^{-9} A
1/8	1/4 atm.	.08
1/8	1/4 atm.	.10
1/8	1/4 atm.	.00
1/8	1/4 atm.	.00
		avg. .0383 x 10^{-9}A

APPENDIX G

DEPENDENCE OF INTENSITY OF EMISSION FROM DIMETHYL SULPHIDE AEROSOL UPON ATMOSPHERIC PRESSURE OF DRY NITROGEN

[MSM]/Cell x 10^{-6} ℓ/Cell	Atmospheric Pressure (N_2)	Intensity of Max. Emission
1	1 atm.	3.51 x 10^{-9} A
1	1 atm.	3.85
1	1 atm.	2.40
1	1 atm.	2.05
1	1 atm.	4.45
1	1 atm.	2.45
1	1 atm.	3.9
1	1 atm.	2.95
1	1 atm.	4.15
1	1 atm.	3.35
1	1 atm.	2.85
		avg. 3.26 x 10^{-9} A
1	1/2 atm.	2.23 x 10^{-9} A
1	1/2 atm.	3.4
1	1/2 atm.	2.68
1	1/2 atm.	2.78
1	1/2 atm.	2.88
		avg. 2.81 x 10^{-9} A
1	1/4 atm.	.98 x 10^{-9} A
1	1/4 atm.	.93
1	1/4 atm.	.73
1	1/4 atm.	.73
		avg. .84 x 10^{-9} A
1/2	1 atm.	2.8 x 10^{-9} A
1/2	1 atm.	2.43
1/2	1 atm.	2.74
1/2	1 atm.	2.35
		avg. 2.58 x 10^{-9} A

[MSM/Cell x 10^{-6} ℓ/Cell	Atmospheric Pressure (N_2)	Intensity of Max. Emission
1/2	1/2 atm.	.73 x 10^{-9} A
1/2	1/2 atm.	.69
1/2	1/2 atm.	.85
1/2	1/2 atm.	.68
		avg. .737 x 10^{-9}A
1/2	1/4 atm.	.16 x 10^{-9} A
1/2	1/4 atm.	.26
1/2	1/4 atm.	.17
1/2	1/4 atm.	.28
		avg. .217 x 10^{-9}A
1/4	1 atm.	1.45 x 10^{-9} A
1/4	1 atm.	1.52
1/4	1 atm.	.79
1/4	1 atm.	1.04
1/4	1 atm.	.76
		avg. 1.112 x 10^{-9}A
1/4	1/2 atm.	.21 x 10^{-9} A
1/4	1/2 atm.	.475
1/4	1/2 atm.	.35
1/4	1/2 atm.	.20
1/4	1/2 atm.	.18
		avg. .283 x 10^{-9}A
1/4	1/4 atm.	.04 x 10^{-9}
1/4	1/4 atm.	.03
		avg. .035 x 10^{-9}A
1/8	1/4 atm.	.02 x 10^{-9} A

APPENDIX H

ESTIMATION OF RATE CONSTANTS FOR REACTIONS (3-7) AND (3-15)

(A) Estimation of the CH_3S Oxidation Rate Constant

The oxidation rate constant for reaction (3-7) may be estimated relative to the rate constant for recombination of the CH_3S radical (3-9).

From experiment 73% of sulphur atoms formed disulphide and 16.8% oxidized. Thus the recombination proceeds at a rate 4.3 that of oxidation.

Now $R_c = k_c [CH_3S]^2$ molecules disulphide produced

$= 2k_c [CH_3S]^2$ radicals CH_3S reacted

$R_{ox} = k_{ox} [CH_3S] [O_2]$

and $R_c = 4.3 R_{ox}$

$k_c = 2.5 \times 10^{10} M^{-1} s^{-1}$

Thus

$$2 k_c [CH_3S]^2 = 4.3 k_{ox} [CH_3S] [O_2]$$

$$k_{ox} = \frac{2k_c[CH_3S]}{4.3[O_2]}$$

The rate of combination of methyl thiyl radicals is also known from which we may calculate the concentration of methyl thiyl species in the reaction atmosphere.

R_c = 73% of CH_3S produced from CH_3SH from Figure 22 for a photon absorption rate of 3×10^{17} photons $\cdot$ hr^{-1}.

Then

$$\frac{d[CH_3SH]}{dt} = 4.17 \times 10^{18} \text{ molecules} \cdot hr^{-1}$$

Thus $$\frac{d[CH_3SSCH_3]}{dt} = \frac{3 \times 10^{18}}{2} \text{ molecules} \cdot hr^{-1}$$

$$= \frac{3 \times 10^{18}}{(2)(6.02 \times 10^{23})} \quad \frac{10^3}{40} \quad \frac{1}{3600} \; M\, s^{-1}$$

$$= 1.755 \times 10^{-8} \; M\, s^{-1}$$

Now $$R_c = 2k_c[CH_3S]^2 = 1.755 \times 10^{-8} \; M\, s^{-1}$$

Thus

$$[CH_3S] = \sqrt{\frac{R_c}{2k_c}}$$

$$= \sqrt{\frac{1.755 \times 10^{-8}}{2(2.5 \times 10^{10})}}$$

$$= 5.9 \times 10^{-10} \; M$$

Then $$k_{ox} = \frac{2\ k_c\ [CH_3S]}{4.3\ [O_2]}$$

$$= \frac{2(2.5 \times 10^{10})\ (5.9 \times 10^{-10})}{4.3\ (8.17 \times 10^{-3})}$$

$$= 8.39 \times 10^{2}\ M\ s^{-1}$$

(B) Estimation of the Metathetical Rate Constant for Reaction (3-15)

If reaction (3-15) is to occur, it must proceed at a rate greater than the mutual interaction of HOO ($k_d = 1.5 \times 10^{9}\ M^{-1}\ s^{-1}$). If the metathesis did not occur, the HOO is produced by CH_3S at one radical per absorbed photon (via reactions 3-1, 3-7, 3-12). For an absorbed photon rate of 3×10^{17} photon $\cdot\ hr^{-1}$

$$R_d = 2\ k_d\ [HOO]^2 = I_a = \frac{3 \times 10^{17}}{6.02 \times 10^{23}} \cdot \frac{10^3}{40} \cdot \frac{1}{3600}$$

$$= 3.46 \times 10^{-9}\ \text{ein}\ \ell^{-1}\ s^{-1}$$

Thus $$[HOO] = \sqrt{\frac{3.46 \times 10^{-9}\ M\ s^{-1}}{3 \times 10^{9}\ M^{-1}s^{-1}}} = 1.07 \times 10^{-9}\ M$$

Now if we assume the metathesis to be a factor of 10 greater than the mutual interaction then $R_m = 10\ R_d$.

So $$\frac{R_m}{R_d} = \frac{k_m [HOO] [CH_3SH]}{2 k_d [HOO]^2} = 10$$

Thus

$$k_m = \frac{20 k_d [HOO]}{[CH_3SH]}$$

Now when $I_a = 3 \times 10^{17}$

$[CH_3SH] = 250$ µl/cell

$= 13.4 \times 10^{-6}$ g/ml

$= 2.79 \times 10^{-4}$ M

Thus $$k_m = \frac{20(1.5 \times 10^9)(1.07 \times 10^{-9})}{[2.79 \times 10^{-4})}$$

$= 1.15 \times 10^5 \ M^{-1} \ s^{-1}$

For $[CH_3SH] = 1.53 \times 10^{-4}$ M

Then $R_{15} = (1.15 \times 10^5 \ M^{-1} \ s^{-1})(1.53 \times 10^{-4} \ M) \ [HOO]$

$= 17.5 \ [HOO] \ s^{-1}$